Structural and biophysical characterization of FKBP51/52 and their binding partners

Dissertation

Technische Universität München
Fakultät für Chemie
Lehrstuhl für Biotechnologie

Wolfgang Sebastian Draxler

Technische Universität München
Fakultät für Chemie
Lehrstuhl für Biotechnologie

Structural and biophysical characterization of FKBP51/52 and their binding partners

Wolfgang Sebastian Draxler

Vollständiger Abdruck der von der Fakultät für Chemie der Technischen Universität München zur Erlangung des akademischen Grades eines Doktors der Naturwissenschaften genehmigten Dissertation.

Vorsitzender: Prof. Dr. Matthias J. Feige

Prüfer der Dissertation:
1. Prof. Dr. Johannes Buchner
2. Prof. Dr. Michael Sattler

Die Dissertation wurde am 13.07.2020 bei der Technischen Universität München eingereicht und durch die Fakultät für Chemie am 19.10.2020 angenommen.

Abstract

The glucocorticoid receptor (GR) depends on the interaction with heat shock protein 90 (Hsp90), a chaperone, to function *in vivo*. This requires collaboration with a subset of the many Hsp90 co-chaperones. The peptidyl-prolyl isomerases (PPIases) FK506-binding protein 51 (FKBP51) and FKBP52 are co-chaperones of Hsp90 and found in complex with Hsp90 and GR. While FKBP51 and FKBP52 share high sequence identity, it is believed that they play different roles in GR signaling and act sequentially during the Hsp90 cycle. The overexpression of FKBP51 negatively affects GR signaling and is associated with neuropsychiatric disorders. Studies in *Saccharomyces cerevisiae* showed that FKBP52 potentiates the GR response. However, the biophysical and structural mechanism of the FKBP51/52 regulation of GR signaling in Hsp90 complexes is not understood.

In this thesis, the complexes formed by FKBP51/52 and Hsp90 as well as their impact on hormone binding to a stabilized ligand binding domain (LBDm) of GR were characterized. Different truncation constructs of Hsp90α/β and FKBP51/52 were recombinantly expressed and purified. Isothermal titration calorimetry experiments showed that the FK1-FK2 domains of the FKBPs do not interact alone with Hsp90 and that the PPIases do not distinguish between both human Hsp90 isoforms. The high affinity interaction of FKBP51 and FKBP52 with Hsp90α/β is driven by the tetratricopeptide repeat domain of the FKBPs and the C-terminal domain of Hsp90. Structural information on Hsp90α:FKBP51 and Hsp90α:FKBP52 complexes generated with small-angle X-ray scattering revealed that both PPIases have different interaction patterns with Hsp90α.

A hormone binding assay surprisingly showed that FKBP51 and FKBP52 prolong hormone association to GR *in vitro* and the FK1 domain is essential to mediate this effect. The effects of the FK1 inhibitors Rapamycin and SAFit2 suggest that FKBP51 and FKBP52 address different mechanisms to slow down hormone association. Furthermore, FKBP51 and FKBP52 accelerated the Hsp90α ATPase activity in the presence of GR-LBDm. This indicates that the PPIases induce conformational changes in either Hsp90 or GR-LBDm that prevent inhibition of ATPase activity by GR. The addition of the co-chaperone p23 accelerated hormone association to GR-LBDm in the presence of Hsp90 and the PPIases. Analytical ultracentrifugation experiments revealed that FKBP51/52 and p23 can bind simultaneously to Hsp90:GR complexes.

In the context of depression and neuropsychiatric disorders that are associated with the overexpression of FKBP51, the findings might provide a new perspective on potential intervention opportunities. In conclusion, the new data on the Hsp90:GR:FKBP51/52 complex provide a better understanding of this sophisticated system, which remains an important target for drug discovery.

Contents

List of Figures

List of Tables

Abbreviations

4E-BP1	Eukaryotic initiation factor 4E binding protein
Å	Angström
Aβ	Amyloid-β
ADP	Adenosine diphosphate
AF-1	Activation function-1 in GR-LBD
AF-2	Activation function-2 in GR-LBD
Aha1	Activator of Hsp90 ATPase
ALL	Acute lymphoblastic leukemia
AMP-PNP	Adenosine 5′-(β,γ-imido)triphosphate
AR	Androgen receptor
ATP	Adenosine triphosphate
ATPγS	Adenosine 5′-(γ-thio)triphosphate
AUC	Analytical ultracentrifugation
BSA	Bovine serum albumine
Cdc37	Cell division cycle 37 homolog
CHIP	Carboxyl terminus of Hsc70-interacting protein
Co-IP	Co-immunoprecipitation
cryo-EM	Cryogenic electron microscopy
CTD	Hsp90 C-terminal dimerization domain
CV	Column volume
Cyp	Cyclophilin
DBD	DNA binding domain
DEX	Dexamethasone
$\mathbf{D_{max}}$	Maximum dimension
DMSO	Dimethyl sulfoxide
DSF	Differential Scanning Fluorimetry
DTT	1,4-Dithithreitol
E. coli	*Escherichia coli*
EDTA	Ethylenediaminetetraacetic acid
ER	Estrogen receptor
ESI	Electrospray ionization
F-DEX	Dexamethasone Fluorescein
FL	Full-length
FRET	Förster resonance energy transfer
FXa	Factor Xa protease
FKBP	FK506-binding protein
FP	Fluorescence polarization
GC	Glucocorticoid

GHKL	Gyrase, Hsp90, Histidine Kinase, MutL
GR	Glucocorticoid receptor
GRE	Glucocorticoid response element
GR-LBD	Ligand binding domain of the GR
GR-LBDm	Ligand binding domain of the GR with five mutations (F602S, A605V, V702A, E705G, M752T)
GST	Glutathione S-transferase
HEPES	4-(2-hydroxyethyl)-1-piperazineethanesulfonic acid
Hip	Hsc70-interacting protein
Hop	Hsp70-Hsp90 organizing protein
HPA	Hypothalamic-pituitary-adrenal
HPLC	High-performance liquid chromatography
Hsc70	Heat shock cognate protein 70
Hsp	Heat shock protein
Hsp70	Heat shock protein 70
Hsp90	Heat shock protein 90
HTS	High-throughput screening
IKKα	Inhibitor of NF-κB kinase subunit α
IL-2	Interleukin-2
IMAC	Immobilized metal ion affinity chromatography
IPTG	Isopropyl-β-D-1-thiogalactopyranoside
k_{cat}	Catalytic rate constant
K_D	Dissociation constant
k_{obs}	Observed association rate constant
LB	Luria broth
LBD	Ligand binding domain
LC	Liquid chromatography
LDH	Lactate dehydrogenase
MD	Hsp90 middle domain
MES	2-(*N*-morpholino)ethanesulfonic acid
MR	Mineralcorticoid receptor
MS	Mass spectrometry
mTORC1/2	Mammalian target of rapamycin complex 1/2
M_W	Molecular weight
MWCO	Molecular weight cut-off
NES	Nuclear export signal
NFAT	Nuclear factor of activated T cells
NF-κB	Nuclear factor κ-light-chain-enhancer of activated B cells
NHS	N-Hydroxysuccinimide

NLS	Nuclear localization sequence
NRS	Nuclear retention signal
NTA	Nitrilotriacetic acid
NTD	Hsp90 N-terminal nucleotide-binding domain
OD	Optical density
P(r)	Inter-atomic distance distribution function
PAGE	Polyacrylamide gel electrophoresis
PDK1	Pyruvate dehydrogenase kinase isozyme 1
PEP	Phosphoenolpyruvate
PHLPP	PH domain and leucine-rich repeat protein phosphatase
pI	Isoelectric point
PK	Pyruvate kinase
PP2A	Protein phosphatase 2
PPIase	Peptidyl-prolyl isomerase
PR	Progesterone receptor
PTM	Post-translational modification
R_g	Radius of gyration
RPM	Rotations per minute
RT	Room temperature
S6K1	S6 kinase 1
S. cerevisiae	*Saccharomyces cerevisiae*
SAFit	Selective antagonist against FKBP51 by induced fit
SAXS	Small-angle X-ray scattering
SBDD	Structure-based drug design
SDS	Sodium dodecyl sulfate
SEC	Size-exclusion chromatography
SHR	Steroid hormone receptor
sHsp	Small heat shock protein
SNP	Single nucleotide polymorphism
SOC	Super optimal broth
SPR	Surface Plasmon Resonance
Sti1	Stress inducible 1
T-TBS	Tris-buffered saline with Tween 20
TBS	Tris-buffered saline
TCEP	Tris(2-carboxyethyl)phosphine
TEV	Tobacco etch virus
TOF	Time of flight
TPR	Tetratricopeptide repeat
TRIS	Tris(hydroxymethyl)aminomethane
v-Src	Viral Src kinase

1 Introduction

1.1 Heat shock protein 90 - a molecular chaperone

Protein misfolding and aggregation in the cell is prevented by evolutionary conserved families of molecular chaperones (Balchin et al., 2016). These molecular chaperones not only support newly synthesized proteins and stabilize partially folded intermediates, they also play a role in protein degradation (Hartl and Hayer-Hartl, 2009; McClellan et al., 2005; Balchin et al., 2016; Dahiya and Buchner, 2019). They were first discovered due to their increased expression levels as a response to heat shock or stress and are referred to as heat shock proteins (Hsps) (Georgopoulos and Welch, 1993). Molecular chaperones are classified according to their molecular weight as Hsp40, Hsp60, Hsp70, Hsp90, Hsp100, and the small Hsp (sHsp). The larger Hsps (Hsp60 - Hsp100) promote folding and refolding in an ATP-dependent manner and are also called foldases. In contrast, sHsps function in an ATP-independent manner and are called holdases (Haslbeck et al., 2005). Holdases and foldases may functionally cooperate together.

Heat shock protein 90 (Hsp90) is one of the most abundant proteins in cells with up to 1-2 % of all proteins even in an unstressed state (Lai et al., 1984). In eukaryotes, different, highly homologous Hsp90 isoforms are expressed. In mammals, the isoforms Hsp90α and Hsp90β are localized in the cytosol. Hsp82 and Hsc82 are the corresponding yeast homologs. The cytosolic mammalian Hsp90 isoforms can be further distinguished in a stress-inducible isoform (Hsp90α) and a constitutively expressed isoform (Hsp90β) (Pratt et al., 2004; Hickey et al., 1989). In addition, Hsp90 isoforms can be found in different cellular compartments: Grp94 in the endoplasmic reticulum, TRAP1 in mitrochondria, and Hsp90C in plastids (Johnson, 2012; Felts et al., 2000; Willmund and Schroda, 2005). A small fraction of the cytosolic Hsp90 is found in the nucleus and Hsp90α is also found extracellular (Langer et al., 2003; Eustace et al., 2004). Hsp90 regulates a plethora of functions from cell cycle control, cell survival, hormone signaling, and response to cellular stress (Echeverria et al., 2011). These processes are regulated by acting on different classes of client proteins (Boczek et al., 2015; Ding et al., 2016; Lorenz et al., 2014). Hsp90 can either help in folding a specific, active conformation of kinases, promoting the formation of multiprotein complexes or stabilizing clients to allow ligand binding in case of steroid receptors (Boczek et al., 2015; Lorenz et al., 2014; Zhao et al., 2008). Co-chaperones interact with Hsp90 depending on specific conformational states and the loaded client protein (Schopf et al., 2017; Zuehlke and Johnson, 2010).

1.1.1 Structure and conformational dynamics

Hsp90 belongs to the GHKL (gyrase, Hsp90, histidine kinase, and MutL) superfamily (Dutta and Inouye, 2000). The dimerization of Hsp90 is essential for its *in vivo* function (Mayer and Le Breton, 2015; Wayne and Bolon, 2007). Each monomer is composed of three conserved domains: the N-terminal nucleotide-binding domain (NTD), the middle domain (MD), and the C-terminal dimerization domain (CTD) (Ali et al., 2006; Prodromou et al., 1997). The

NTD can bind and hydrolyze ATP and is connected to the MD by a long and highly charged linker region (Prodromou et al., 1997; Pearl and Prodromou, 2000). N-terminal inhibitors such as Radicicol and Geldanamycin bind to the ATP-binding pocket and inhibit Hsp90 (Schulte et al., 1998; Whitesell et al., 1994; Stebbins et al., 1997). The charged linker has been shown to modulate NTD-MD contacts, play a role in client binding, and affect Hsp90 function (Hainzl et al., 2009; Jahn et al., 2014; Tsutsumi et al., 2012; Zuehlke and Johnson, 2012). The CTD ends with an MEEVD motif that is important for the binding of tetratricopeptide repeat (TPR) motif containing co-chaperones (Scheufler et al., 2000). In addition, the CTD promotes dimerization via a dimer interface (Minami et al., 1994).

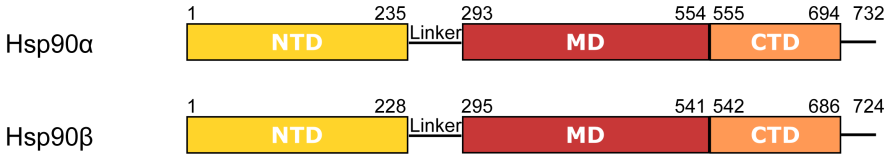

Figure 1: Schematic depiction of human Hsp90α and Hsp90β. Domain boundaries are indicated by numbers. NTD, MD, and CTD are colored in yellow, red, and orange, respectively.

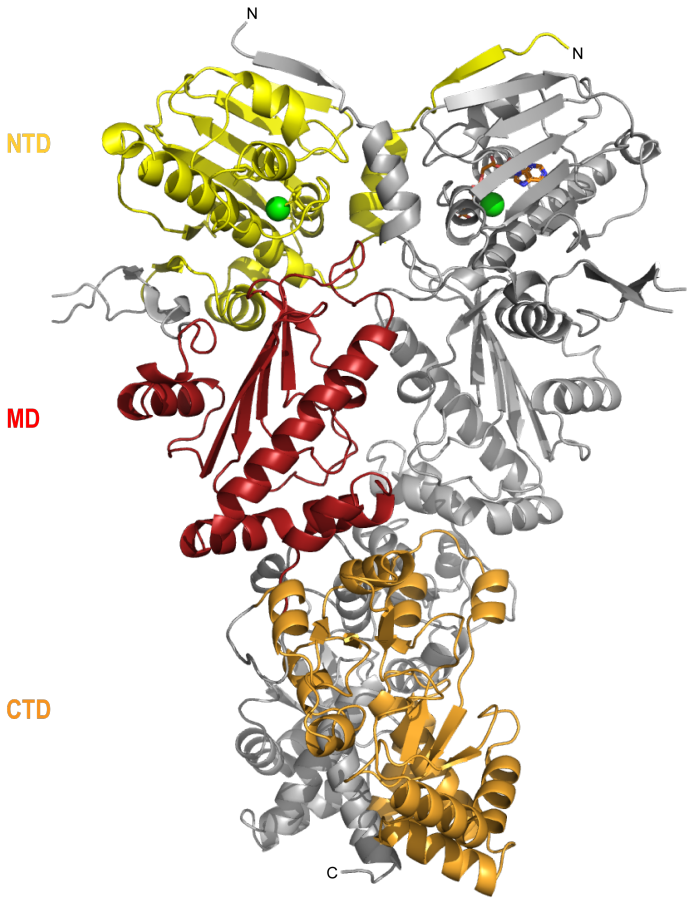

Figure 2: Three-dimensional structure of a human Hsp90β dimer (PDB ID 5FWK) showing the N-terminal ATPase domain (NTD), the middle domain (MD), and C-terminal dimerization domain (CTD) in yellow, red, and orange, respectively (Verba et al., 2016). Bound Mg^{2+} ions are shown as green spheres and bound ATP is shown in sticks.

Hsp90 undergoes several conformational changes that are driven by ATP binding and hydrolysis. In the absence of ATP, the C-terminally dimerized Hsp90 adopts a V-shaped open conformation (Fig. 3) (Shiau et al., 2006; Dollins et al., 2007; Krukenberg et al., 2009). Hsp90 transitions to a closed, compact conformation upon binding of ATP via intermediate steps (Fig. 3) (Verba et al., 2016; Hellenkamp et al., 2017). The so-called lid segment in the NTD closes over the nucleotide binding site in the presence of ATP. Structural rearrangements first promote the dimerization of the NTD and subsequently the association with the MD (Hessling et al., 2009). These rearrangements allow a catalytic arginine residue in the MD to access the ATP-binding sites. Both steps are necessary for ATP hydrolysis (Cunningham et al., 2008; Prodromou, 2012). After ATP hydrolysis, the NTDs dissociate and ADP and inorganic phosphate are released. The Hsp90 dimer adopts an open conformation again.

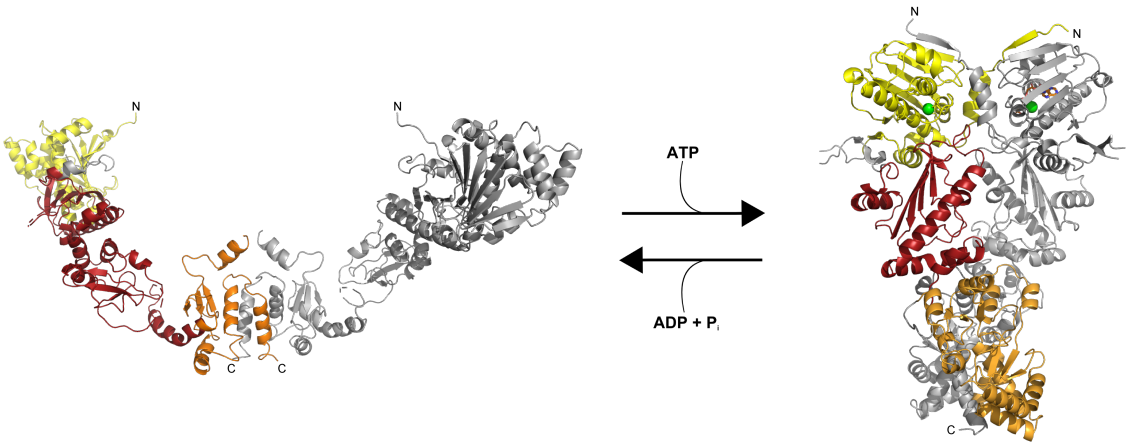

Figure 3: Hsp90 shifts from an open to a closed conformation upon ATP binding. The binding of ATP leads to NTD dimerization and structural rearrangements to shift from a V-shaped open conformation to a closed conformation (PDB ID 5FWK) (Krukenberg et al., 2009; Verba et al., 2016). ATP hydrolysis leads to NTD dissociation and Hsp90 moves back into an open conformation. Bound Mg^{2+} ions are shown as green spheres and bound ATP is shown in sticks.

The ATPase activity of human Hsp90 is extremely slow. Yeast Hsp90 hydrolyses ATP with a rate of $1\,min^{-1}$, while that of the human Hsp90 is tenfold slower (Panaretou et al., 1998; Richter et al., 2008). The rate-limiting step is not the hydrolysis reaction itself but the conformational changes that lead to the closed state (Hessling et al., 2009).

1.1.2 The Hsp90 chaperone cycle

Hsp90 achieves the maturation of client proteins with the support of co-chaperones. These co-chaperones bind to specific conformations of Hsp90. Reconstitution experiments and functional studies have shown that co-chaperones bind in a sequential manner to yield asymmetric complexes to drive the chaperone cycle of Hsp90 (Li et al., 2011; Kirschke et al., 2014; Ebong et al., 2016).

Many co-chaperones contain TPR motifs to interact with the C-terminal tail of Hsp90. The TPR motif consists of tandem repeats of 34 amino acids (Sikorski et al., 1990). The

consensus sequence adopts a helix-turn-helix arrangement and three of these motifs stack on each other to yield seven anti-parallel α-helices which bind to the C-terminal MEEVD (Hsp90) and/or EEVD (Hsp70) motifs (Scheufler et al., 2000; D'Andrea and Regan, 2003).

The adaptor protein Hop/Sti1 (Hsp70-Hsp90 organizing protein/stress inducible 1) facilitates client recruiting to Hsp90. It is composed of three TPR domains and two aspartate-proline rich (DP) domains. Hop is able to bind Hsp70 and Hsp90 simultaneously and can inhibit the ATPase activity of Hsp90 (Schmid et al., 2012). It connects both chaperone cycles and promotes client transfer from Hsp70 to Hsp90. It has been proposed that Hop has additional interaction sites on the MD of Hsp90 (Schmid et al., 2012). Thereby, Hop prevents conformational changes and reduces ATPase activity (Schopf et al., 2017).

Peptidyl-prolyl isomerases (PPIases) are TPR-containing co-chaperones of Hsp90 and have been identified during studies of steroid hormone receptor (SHR) complexes (Peattie et al., 1992; Johnson and Toft, 1994). Large PPIases such as FK506-binding protein (FKBP) 51, FKBP52, and Cyclophilin 40 (Cyp40) are binding partners of Hsp90 (Johnson and Toft, 1994; Pirkl and Buchner, 2001). The PPIase domain catalyzes the isomerization of *cis-trans* peptide bonds at the N-terminal side of proline residues. The catalytic activities of PPIases can be assessed using a peptide assay with the peptide succinyl-Ala-Leu-Pro-Phe-pNA. FKBP12 and FKBP25 have catalytic activities of 2.2×10^6 and $0.8 \times 10^6\,\mathrm{M^{-1}\,s^{-1}}$, respectively (Albers et al., 1990; Galat et al., 1992). The PPIase activity of FKBP51 and FKBP52 is comparable with a $\frac{k_{cat}}{K_M}$ of $1.5 \times 10^6\,\mathrm{M^{-1}\,s^{-1}}$ (Pirkl and Buchner, 2001). The large PPIases possess chaperone activity and could be involved in client maturation. However, the role of PPIases in client complexes is poorly understood. FKBP51 and FKBP52 are a major topic of this thesis and are going to be discussed in more detail in section 1.3.

Cdc37 (cell division cycle 37 homolog) belongs to a group of Hsp90 co-chaperones without a TPR domain. The co-chaperone Cdc37 is specifically involved in the maturation of kinases. In addition, Cdc37 inhibits Hsp90 ATPase activity as well (Roe et al., 2004). The inhibitory mechanism was elucidated with cryogenic electron microscopy (cryo-EM) (Verba et al., 2016). Cdc37 is wrapped around the MD of Hsp90 and prevents lid closure and NTD dimerization (Fig. 4) (Roe et al., 2004; Verba et al., 2016).

While Hop keeps Hsp90 in an open conformation, the co-chaperone Aha1 (activator of Hsp90 ATPase) has the opposite role. Aha1 is a strong activator of the Hsp90 ATPase activity (Panaretou et al., 2002). Aha1 binds to both the NTD and MD in an asymmetric manner and promotes the formation of a closed state (Retzlaff et al., 2010; Li et al., 2013). Furthermore, Aha1 progresses the cycle by displacing Hop (Li et al., 2013). Aha1 and GR are competing for Hsp90 binding since they have overlapping binding sites and cannot bind simultaneously (Lorenz et al., 2014).

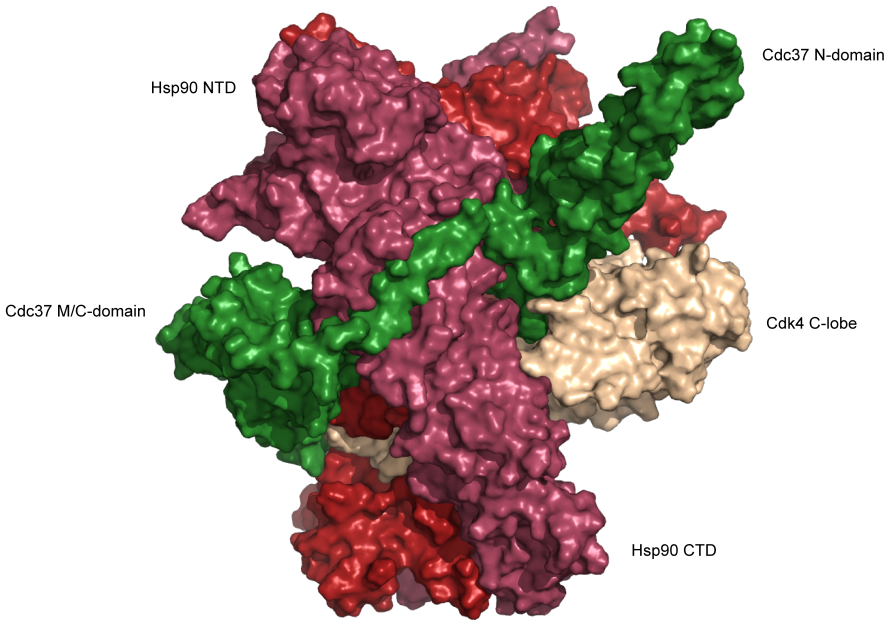

Figure 4: Atomic cryo-EM structure of the Hsp90:Cdc37:Cdk4 complex in surface representation (PDB ID 5FWM) (Verba et al., 2016). Cdc37 (green) is wrapped around the MD of Hsp90 (red and raspberry) and prevents lid closure and NTD dimerization. The Cdk4 C- and N-lobe (sand) are connected by the β5 sheet of Cdk4 that protrudes through the lumen of Hsp90.

At the late stage of client maturation, p23 enters the cycle and binds specifically to the closed conformation of Hsp90 (Grenert et al., 1999; Chadli et al., 2000; Richter et al., 2004). It stabilizes the closed conformation and inhibits Hsp90 ATPase activity, which could facilitate client maturation (Richter et al., 2004). The crystallographic structure reveals that p23 mainly binds to the NTD of Hsp90 but has some interaction sites on the MD as well (Ali et al., 2006). Upon ATP hydrolysis, p23 dissociates and Hsp90 switches into the open conformation again.

1.1.3 Role of Hsp90 in disease

The diverse roles and involvement of Hsp90 in cellular processes indicate that Hsp90 plays a major role in various diseases including cancer, neurodegenerative diseases, and infectious diseases (Schopf et al., 2017). Cancer cells are characterized by rapid proliferation and the presence of mutated proteins. Hsp90 plays a central role to control proteostasis as its clients, e.g. p53, viral Src kinase (v-Src), and telomerase, are driving forces in cancer growth (Schopf et al., 2017). Expression levels of Hsp90 are increased in breast cancer cells and are associated with a poor survival prognosis (Pick et al., 2007). An extensive study with tumor specimen coined the name epichaperome (Rodina et al., 2016). The epichaperome is formed under conditions of stress and can be described as a network of stable, survival-facilitating, high molecular weight complexes that have Hsp90 and heat shock cognate protein 70 (Hsc70) as starting points (Rodina et al., 2016). They identified two complexes based on their isoelectric point (pI), Hsp90 complexes with $pI < 4.9$ and Hsp90 complexes with $pI > 5$, and classified cancer cell lines into two classes. Type 2 cells contained mainly complexes with $pI < 4.9$ while type 1 cells

contained mainly complexes of the other species (pI > 5). Further characterization revealed that only type 1 cells functionally and physically integrate components of the Hsp90 and Hsp70 machinery. Rodina et al. (2016) call the integrated chaperome network of type 1 tumors the epichaperome. In type 2 cells, such an extensive network does not exist. Consequently, type 1 cells are much more sensitive to factors that target members of the epichaperome. The subsequent disruption of the epichaperome results in cell death. In contrast, type 2 cells survived when chaperome members were targeted as only a small, local part of the chaperome in the cells was affected. Interestingly, the epichaperome is a result of changes in the cellular environment and not in the chaperome. The transcription factor Myc, but not the oncogene v-Src, was able to transform type 2 cells into type 1 cells (Rodina et al., 2016).

Neurodegenerative diseases such as Alzheimer's and Parkinson's disease are also associated with Hsp90. Both diseases are characterized by protein aggregation and involve proteins that are Hsp90 client proteins. In the case of Alzheimer's disease, the plaque-forming protein amyloid-β (Aβ) and the phosphorylated tau protein are Hsp90 clients (Garnier et al., 1998; Campanella et al., 2018). Hsp90 can bind to Aβ and prevent its aggregation (Evans et al., 2006). The oligomerization and deposition of α-synuclein in Lewy bodies is a marker of Parkinson's disease. Hsp90 has been shown to prevent α-synuclein oligomerization and α-synuclein toxicity (Putcha et al., 2010).

High translation rates of viral proteins demand the help of chaperones to facilitate protein stability and protein folding. Virus-infected cells are more sensitive to Hsp90 inhibitors than non-infected cells (Geller et al., 2013; Schopf et al., 2017). In protozoan infections, Hsp90 has an important role in differentiation and development during the parasites life cycle (Banumathy et al., 2003).

1.2 The glucocorticoid receptor

One of the most studied client classes of Hsp90 are steroid hormone receptors (SHRs), especially the glucocorticoid receptor (GR). Other members of the family are the estrogen receptor (ER), the progesterone receptor (PR), the androgen receptor (AR), and the mineralocorticoid receptor (MR). The GR, a ligand-activated transcription factor, regulates numerous genes that are under the control of glucocorticoid response elements (GREs) (Heitzer et al., 2007). In its inactive form, the GR resides in the cytoplasm but translocates into the nucleus upon ligand binding. The native ligand glucocorticoid (GC), a steroid hormone, is released by the adrenal gland under the regulation of the hypothalamic-pituitary-adrenal (HPA) axis (Smith and Vale, 2006). GCs have a pivotal role as they are involved in several physiological processes ranging from metabolism, immune response, cardiovascular function, and mood and cognitive functions (Hawkins et al., 2012; Cruz-Topete and Cidlowski, 2015; Udi et al., 2010; Farrell and O'Keane, 2016; Joëls, 2011).

1.2.1 Structure and function

The GR shares common structural features with other SHRs. A conserved zinc-finger DNA binding domain (DBD) in the middle is flanked by an N-terminal domain (ND) and a C-terminal ligand binding domain (LBD) (Fig. 5) (Kumar and Thompson, 1999). The ND is unstructured unless it binds DNA and the GR forms dimers (Kumar and Thompson, 2012). The ND contains a major transactivation domain known as activation function-1 (AF-1) that is rich in negatively charged acidic amino acids (Heitzer et al., 2007). The AF-1 interacts with the transcription machinery and binds cofactors that are involved in transcription regulation (McEwan et al., 1993; Khan et al., 2012). The DBD is important for DNA binding and GR dimerization. The two zinc-finger motifs in the DBD each tetrahedrally coordinate one zinc ion. The second zinc-finger motif harbors the distal (D) box that is required for dimerization at the GRE (Vandevyver et al., 2014). The LBD is separated from the DBD by a 40 amino acid hinge region that provides flexibility. It contains a ligand-dependent transcriptional AF-2 domain (Bledsoe et al., 2002). Furthermore, the LBD has an important role in the interaction with chaperones, coregulators, other transcription factors, and in GR dimerization (Bledsoe et al., 2002; Vandevyver et al., 2014).

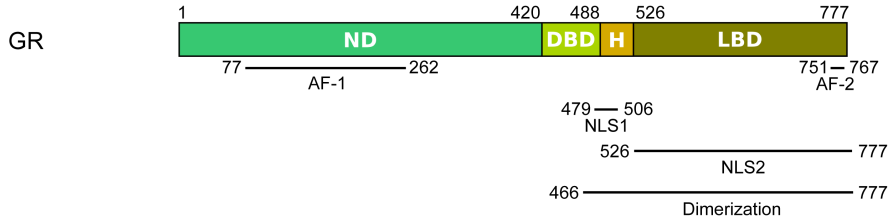

Figure 5: Schematic depiction of human GR. Domain boundaries are indicated by numbers. The N-terminal domain (ND), the DNA binding domain (DBD), the hinge region (H), and ligand binding domain (LBD) are colored in mint green, pale green, sand, and brown green, respectively. Functional motifs are indicated by bars and numbers of amino acid positions (Weikum et al., 2017; Liu et al., 2019; Timmermans et al., 2019).

Structurally, the ligand binding pocket is formed by 12 α-helices and four short β-strands that fold into a three layer helical domain (Fig. 6). A single-molecule study showed that the LBD can refold without bound hormone using several intermediate states (Suren et al., 2018). They were further able to identify helix 1 as a key structural element that needs to be positioned after hormone binding (Suren et al., 2018). Crystallographic studies highlighted the role of helix 12 in regulation of coregulator binding. The binding of agonists or antagonists altered the conformation and position of helix 12 (Schoch et al., 2010). Consequently, the conformational variety allows different transcriptional coregulators to bind and could interfere with translocation in the nucleus (Schoch et al., 2010).

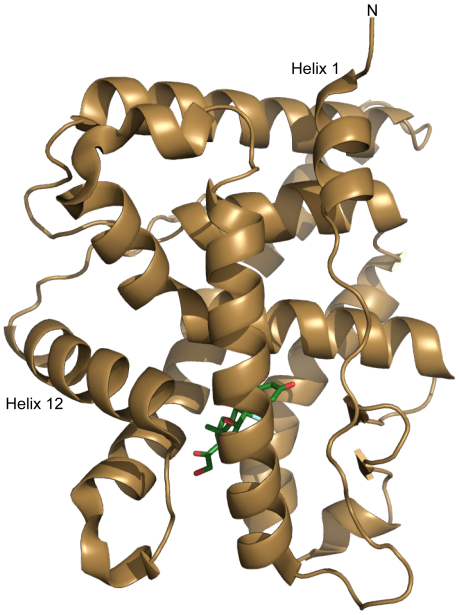

Figure 6: Overall arrangement of the GR-LBD in complex with dexamethasone (DEX) (PDB ID 4UDC) (Edman et al., 2015). DEX is shown as sticks in green.

In general, the transport of the activated GR could be facilitated by nuclear localization signals (NLS1 and NLS2), a nuclear export signal (NES), and a nuclear retention signal (NRS). NLS1, NES, and NRS are located in the DBD while NLS2 is located in the LBD (Tang et al., 1998; Black et al., 2001; Carrigan et al., 2007).

1.2.2 GR maturation

The manifold roles of the GR are controlled by Hsp90-dependent processes (Picard et al., 1990). Only the GR-LBD is necessary for the interaction with Hsp90 (Howard et al., 1990). The maturation of GR is maintained by a set of co-chaperones, which at least includes Hsp40, Hsp70, Hop, and p23 (Johnson and Toft, 1994; Dittmar et al., 1998). The current model of GR maturation is shown in Fig. 7.

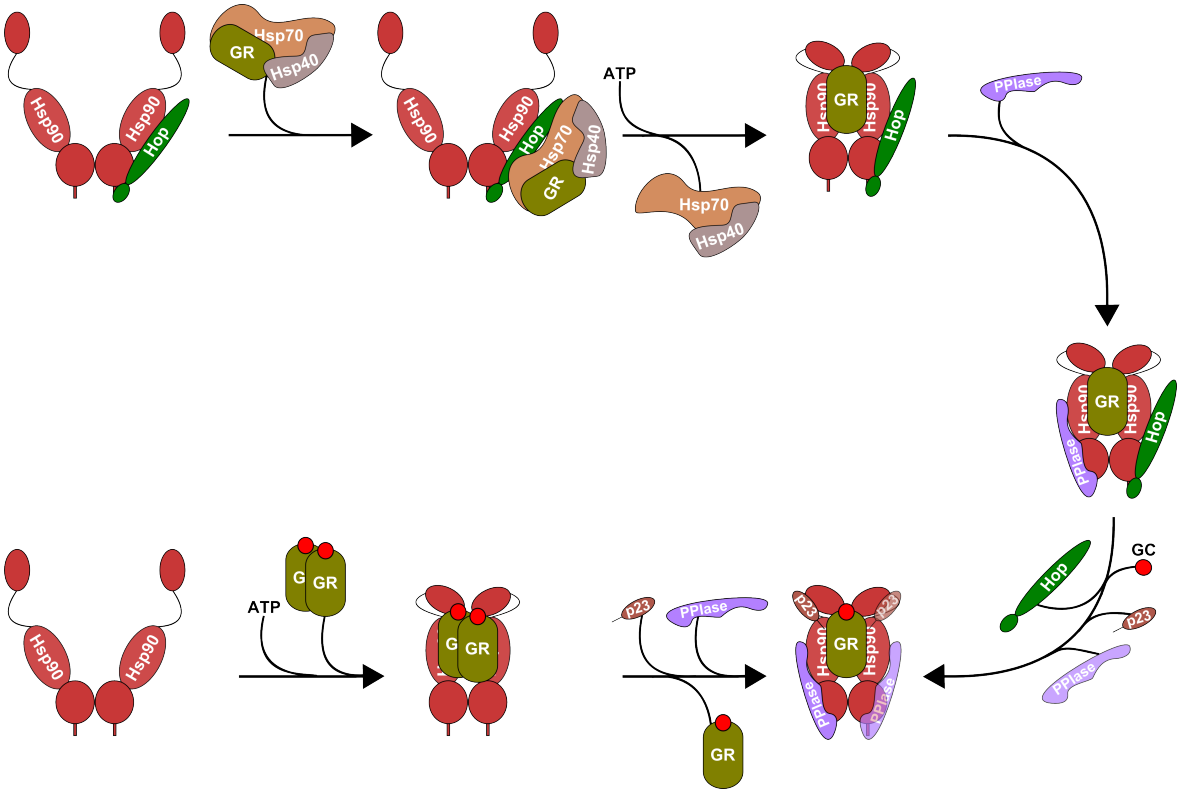

Figure 7: GR activation is regulated by co-chaperones. A schematic illustration of the Hsp90-driven activation of the GR-LBD is depicted. Upper pathway: The Hsp70:Hsp40 complex associates with partially folded GR-LBD. The adaptor co-chaperone Hop mediates the transfer of GR-LBD to Hsp90. The subsequent binding of ATP, which induces an intermediate Hsp90 state, and a large PPIase enable glucocorticoid (GC) binding to GR-LBD. The displacement of Hop and the binding of p23 produces the fully closed Hsp90 state. In the fully closed Hsp90 state, at least one p23 and one PPIase molecule are bound, but up to two molecules of each can be bound to this complex at the same time. Lower pathway: A second pathway that leads to activated GR is shown as well. Dimeric, hormone bound GR-LBD can also bind to Hsp90 on its own, independently of Hsp70:Hsp40. The binding of p23 and PPIase leads to the displacement of one GR-LBD molecule.

Similar to the PR, it is thought that Hsp40 acts on *de novo* synthesized GR (Hernández et al., 2002). Hsp40 mediates the transfer to Hsp70. The GR:Hsp70 complex can be modulated by Hsp70 co-chaperones such as Bag-1, Hip (Hsc70-interacting protein) or CHIP (carboxyl terminus of Hsc70-interacting protein) and leads to either GR activation or its degradation (Höfeld et al., 1995; Kullmann et al., 1998; Lüders et al., 2000; McDonough and Patterson, 2003). It has been proposed that Hsp70:Hsp40 unfold GR as ligand binding was prevented in such complexes (Kirschke et al., 2014). Hop connects Hsp70 and Hsp90 and brings GR in close

proximity (see section 1.1.2). ATP hydrolysis in Hsp90 is necessary to release GR from Hsp70 and transfer it onto Hsp90 (Kirschke et al., 2014). Subsequently, Hop is replaced by other TPR-containing co-chaperones, e.g. PPIases, which promote cycle progression and entry of p23 to stabilize the Hsp90:GR complex (Dittmar and Pratt, 1997; Prodromou et al., 1999; Li et al., 2011). The transport of activated GR into the nucleus is controversial. Earlier studies thought that GR dissociates from Hsp90 upon hormone binding and the exposed NLS would mediate nuclear translocation by nuclear import receptors (Pratt and Toft, 1997; Freedman and Yamamoto, 2004). Recent studies of the hormone-bound GR with Hsp90 provided results that contradict this model. GR was in a stable complex with Hsp90, even in hormone-bound state (Lorenz et al., 2014). This complex showed significant Hsp90 ATPase inhibition and thus an inhibition of the chaperone cycle. The co-chaperone p23, which inhibits Hsp90 ATPase activity, can bind simultaneously to the Hsp90:GR complex. The reduced ATPase activity could lead to an extended association of the GR and could play a role in Hsp90-dependent GR trafficking. Experimental evidence pointing to Hsp90-dependent trafficking was provided by the co-immunoprecipitation of GR, Hsp90, FKBP52, and the motor protein dynein, which suggests that GR is transported on microtubules (Silverstein et al., 1999; Galigniana et al., 2001).

1.3 FK506-binding proteins 51 and 52

PPIases are a superfamily of proteins which are highly conserved and bind immunosuppressant molecules. They are involved in protein folding and possess PPIase activity (Fischer, 1994). The family can be divided into two subfamilies: cyclophilins (Cyps) and FK506-binding proteins (FKBPs). As their name suggests, cyclophilins bind Cyclosporin A, a cyclic undecapeptide, while FKBPs bind macrolides like FK506 and Rapamycin (Barik, 2006). The FKBP family includes a wide range of proteins that share a PPIase domain and contain additional protein interaction domains (Solassol et al., 2011). They are named according to their molecular mass, which ranges from 12 kDa (FKBP12) to 133 kDa (FKBP133). The enzymatic function of PPIases is the isomerization of peptide bonds at the N-terminal side of proline residues to accelerate protein folding (Fig. 8) (Lang et al., 1987). Peptide bonds in proteins are predominantly in *trans* conformation except when they involve prolines, which can occur in either *trans* or *cis* (Ramachandran and Sasisekharan, 1968; Morgan and Rubenstein, 2013). The isomers are almost isoenergetic and a high activation energy limits the rate of interconversion between both forms (Wedemeyer et al., 2002). Consequently, PPIases lower the activation energy and accelerate isomerization (Lang et al., 1987).

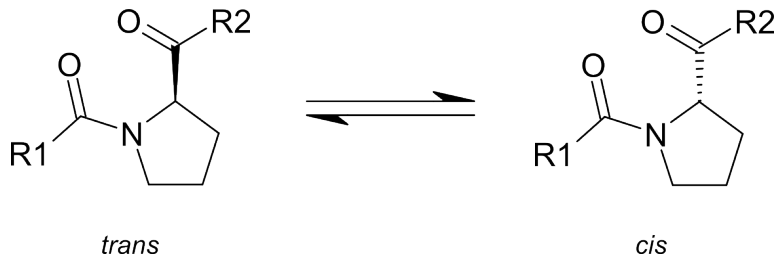

Figure 8: Isomerization reaction performed by PPIases. The peptide bond on the N-terminal side of proline is *cis-trans* isomerized by peptidyl-prolyl isomerases.

The co-chaperone FKBP51, which is encoded by the *FKBP5* gene, is a member of the PPIase subfamily of FK506-binding proteins. Its closest homolog is FKBP52, encoded by the *FKBP4* gene, with a sequence identity of 70 %. Both PPIases are composed of three domains (Fig. 9).

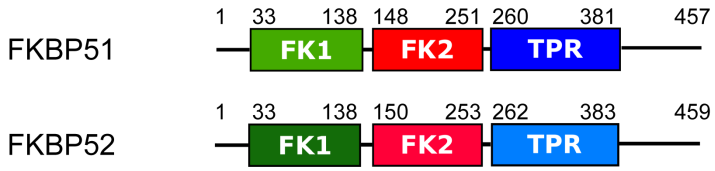

Figure 9: Schematic depiction of human FKBP51 and FKBP52. Domain boundaries are indicated by numbers. FK1, FK2, and TPR domain are colored in green, red, and blue, respectively.

The N-terminal FK506-binding domain (FK1 domain) contains the enzymatic peptidyl-prolyl *cis-trans* activity and binds immunosuppressant drugs like FK506 and Rapamycin. The FKBP-like domain (FK2) in the middle is structurally highly similar to the FK1 domain but has no PPIase activity and cannot bind FK1 inhibitors (Sinars et al., 2003). The third domain, a TPR domain, is located at the C-terminus. The TPR domain mediates the binding to Hsp90 (Young et al., 1998). Although FKBP51 and FKBP52 share high sequence identity, crystallographic structures suggest different domain orientations (Sinars et al., 2003; Wu et al., 2004). The three-dimensional structures of human FKBP51 and FKBP52 are shown in Fig. 10.

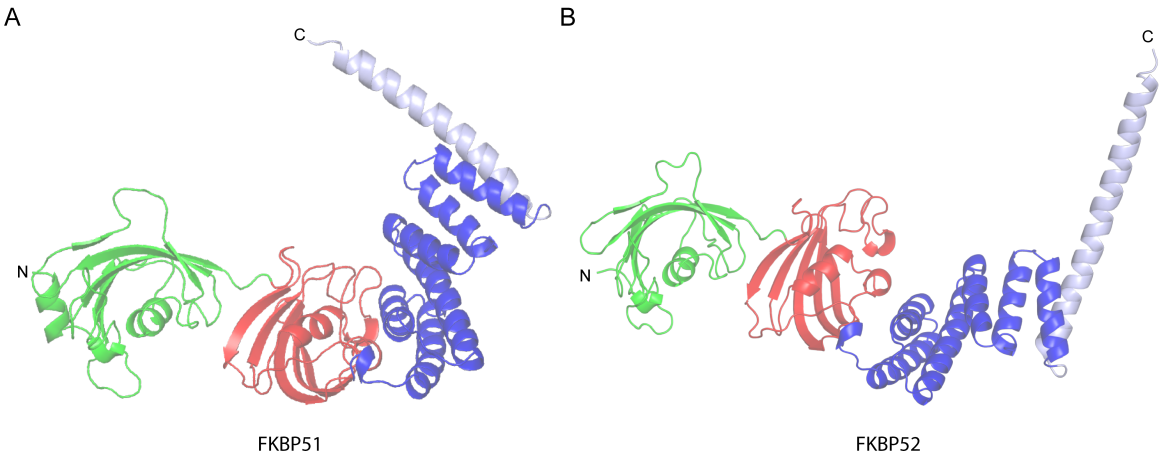

Figure 10: Three-dimensional structure of (A) human FKBP51 (PDB ID 5NJX) and (B) human FKBP52 (PDB ID 1Q1C and 1P5Q) (Draxler, 2016; Kumar et al., 2017; Wu et al., 2004). The FK1, FK2, and TPR domain are shown in green, red, and blue, respectively. The C-terminal α-helix is shown in light blue.

The FK1 domain is structurally made up of five antiparallel β-strands that wrap around a central α-helix. Furthermore, there is a short α-helix at the start of the FK1 domain. It is placed above the β-strands β1, β5, and β6 - creating a hydrophobic interface (Jacqueline et al., 2003; Galat, 2003; Bracher et al., 2011). The FK2 domain is structurally similar to the FK1 domain, but only shares 19% sequence identity (Schmidt et al., 2012). However, it lacks PPIase activity and does not bind FK506 or Rapamycin, since it is missing key residues in the binding pocket (Sinars et al., 2003). Additionally, an insertion event in the FK2 domain has occurred between β5 and the α-helix. Three additional amino acids - Asp195, His196, and Asp197 - are pushing into the binding pocket and block substrate binding (Sinars et al., 2003). While the deletion of the insertion does not affect binding of FKBP51 to Hsp90, the binding to steroid receptor complexes is reduced (Sinars et al., 2003).

The TPR motif consists of 34 amino acids (Sikorski et al., 1990). The consensus sequence is composed of a pattern of small and large hydrophobic amino acids. Only the residue positions 8 (Gly or Ala), 20 (Ala), and 27 (Ala) of the TPR motif are highly conservered. The other consensus positions have a preference for a class of amino acids rather than a specific amino acid (D'Andrea and Regan, 2003). Structurally, the TPR domain adopts a helix-turn-helix arrangement with antiparallel helices (D'Andrea and Regan, 2003). The turn positions between both helices of the TPR motif show conservation for helix-breaking residues (D'Andrea and Regan, 2003). The TPR domain of FKBP51/52 has three repeats of the TPR motif and there is an additional seventh helix after the third TPR motif. Cheung-Flynn et al. (2003) have shown that the seventh helix contributes to proper Hsp90 binding as truncation constructs show less Hsp90 binding. The binding is mediated by an interaction with the conserved C-terminal Hsp90 MEEVD sequence (Scheufler et al., 2000; Brinker et al., 2002). The structure of FKBP51 in complex with a C-terminal Hsp90 peptide reveals extensive hydrogen bonding between TPR domain and peptide (Fig. 11) (Draxler, 2016; Kumar et al., 2017). The binding features a di-carboxylate clamp that is prominent for other TPR containing

co-chaperones (Scheufler et al., 2000; Blundell et al., 2017). Recent NMR studies suggest that complex formation with Hsp90 involves the FK1 and FK2 domains of FKBP51 as well (Oroz et al., 2018).

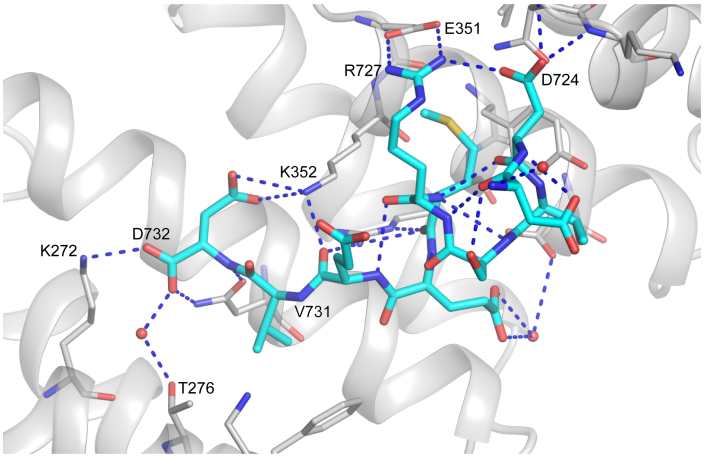

Figure 11: X-ray structure of the 12mer Hsp90α peptide (GDDDTSRMEEVD) (cyan) bound to the TPR domain of FKBP51 (light grey). Hydrogen bonds are shown as blue dashes. Important residues are highlighted (PDB ID 5NJX) (Draxler, 2016; Kumar et al., 2017).

1.3.1 FKBP51/52 and GR

FKBP51 is involved in pathways that modulate immune function, autophagy, and metabolism by interacting with a group of four proteins: Hsp90, SHRs, nuclear factor κ-light-chain-enhancer of activated B cells (NF-κB), and AKT/PH domain and leucine-rich repeat protein phosphatase (PHLPP) (Fries et al., 2017; Hahle et al., 2019).

The best understood function of FKBP51 centers around its role as a co-chaperone for Hsp90 complexes during hormone receptor maturation and intracellular trafficking in signal transduction of steroid hormones (Jääskeläinen et al., 2011; Heitzer et al., 2007; Echeverria and Picard, 2010). FKBP51 and FKBP52 alter GR signaling (Riggs et al., 2003; Denny et al., 2000). While FKBP51 lowers the GR response to hormone, FKBP52 increases GR response to hormone *in vivo* (Riggs et al., 2003; Denny et al., 2000; Baughman et al., 1991). As transcription of FKBP51 is upregulated by an activated GR, this constitutes a negative feedback regulation loop (Jääskeläinen et al., 2011).

Several studies investigated the role of the PPIase activity and the C-terminal TPR of FKBP51 in relation to the negative modulation of GR activity. The disruption of the interaction between FKBP51 and Hsp90 reverses the inhibitory effect of FKBP51 (Denny et al., 2005). In addition, the FK1 domain is relevant for the observed effects on GR signaling *in vivo* (Riggs et al., 2003, 2007). An approach applying random mutagenesis and chimera constructs identified two residues, A116 and L119, in a loop in the FK1 domain that mediate the inhibitory effect of FKBP51 on GR signaling (Riggs et al., 2007). In addition, chimera containing the FK1 domain of FKBP51 and FK2-TPR domains of FKBP52 and vice versa showed that neither the FK2 nor the TPR domain are involved in the observed GR signaling

potentiation (Riggs et al., 2003, 2007). In contrast to FKBP51, it has been described that FKBP52 binds to cytoplasmic dynein and could facilitate retrograde transport of the Hsp90:GR chaperone complex from the cytosol to the nucleus (Galigniana et al., 2001). Consequently, FKBP51 and FKBP52 have to be exchanged at some point in the cycle. The regulation of GR signaling and the roles of FKBP51 and FKBP52 are depicted in Fig. 12.

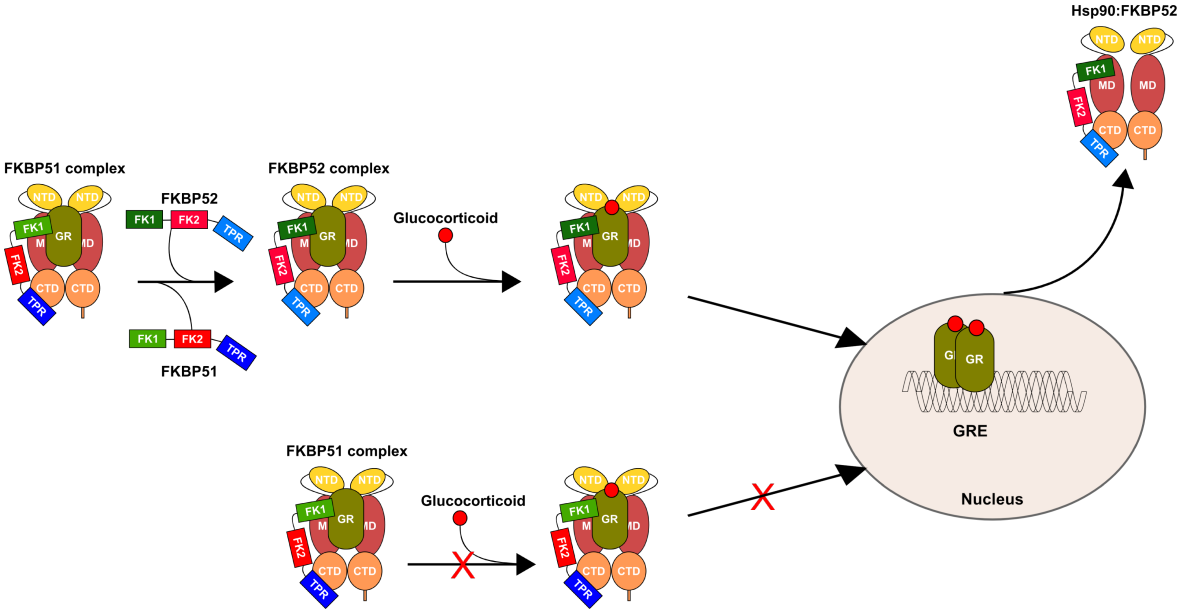

Figure 12: Regulation of GR signaling by FKBP51 and FKBP52. The exchange of FKBP51 and FKBP52 could facilitate GC binding. FKBP52 positively enhances GR transcription activity and it facilitates transport into the nucleus. In contrast, an Hsp90:GR:FKBP51 complex has reduced affinity for GCs and prevents nuclear translocation, which leads to inhibition of GR transcriptional activity.

1.3.2 Role of FKBP51 in disease

FKBP51 has been recognized as a potential drug target in oncologic diseases and psychological disorders (Schmidt et al., 2012). A low expression level of FKBP51 is linked with resistance to chemotherapeutic drugs (Li et al., 2008). Decreased expression levels of FKBP51 have also been detected in pancreatic cancer tissue samples (Pei et al., 2009; Hou and Wang, 2012). In pancreatic cancer, low levels of FKBP51 lead to hyperphosphorylation of the serine/threonine kinase AKT and thereby to the upregulation of the AKT signaling pathway (Pei et al., 2009). AKT is activated by phosphorylation at two residues, Thr308 and Ser473. Pyruvate dehydrogenase kinase isozyme 1 (PDK1) phosphorylates Thr308, while Ser473 is phosphorylated by mammalian target of rapamycin complex 2 (mTORC2) (Alessi et al., 1997; Sarbassov et al., 2005). Dephosphorylation of Thr308 by protein phosphatase 2 (PP2A) and Ser473 by PHLPP1 and PHLPP2 negatively regulate AKT (Padmanabhan et al., 2009; Gao et al., 2005). FKBP51 serves as a scaffolding protein that promotes the interaction between AKT and PHLPP (Fig. 13A) (Pei et al., 2009).

The role of FKBP51 in NF-κB signaling leads to cancer progression and drug resistance in acute lymphoblastic leukemia (ALL), glioma, and melanoma (Avellino et al., 2005; Jiang

et al., 2008; Romano et al., 2010). Bouwmeester et al. (2004) described an interaction between FKBP51 and inhibitor of NF-κB kinase subunit α (IKKα) that is necessary for its activation. The NF-κB signaling pathway is triggered by the activation of IKKα and leads to the expression of anti-apoptotic proteins, which in turn promote cell survival (Fig. 13B).

In prostate cancer, FKBP51 is associated with AR signaling (Makkonen et al., 2009). FKBP51 promotes the assembly of a chaperone complex composed of Hsp90, p23, AR, and ATP and shows increased binding of androgen hormone (Ni et al., 2010). As AR regulates gene expression of a variety of genes including FKBP51, a positive feedback loop is established (Fig. 13C). The upregulation of AR genes leads to cell growth and subsequently an androgen-independent state.

Psychological disorders such as depression and anxiety disorders are associated with GR signaling and changes in the expression level of FKBP51 (Binder, 2009). Single nucleotide polymorphisms (SNPs) in the *FKBP5* gene have been identified that lead to an increased intracellular level of FKBP51, which negatively affects GR signaling (Binder et al., 2008). Furthermore, it affects the regulation of the HPA axis, which is responsible for stress response and is implicated in the development of depression (Binder et al., 2004; Holsboer, 2000). Such SNPs have also been associated with diabetes and diabetes-related phenotypes (Pereira et al., 2014) and post-traumatic pain (Bortsov et al., 2013; Linnstaedt et al., 2018).

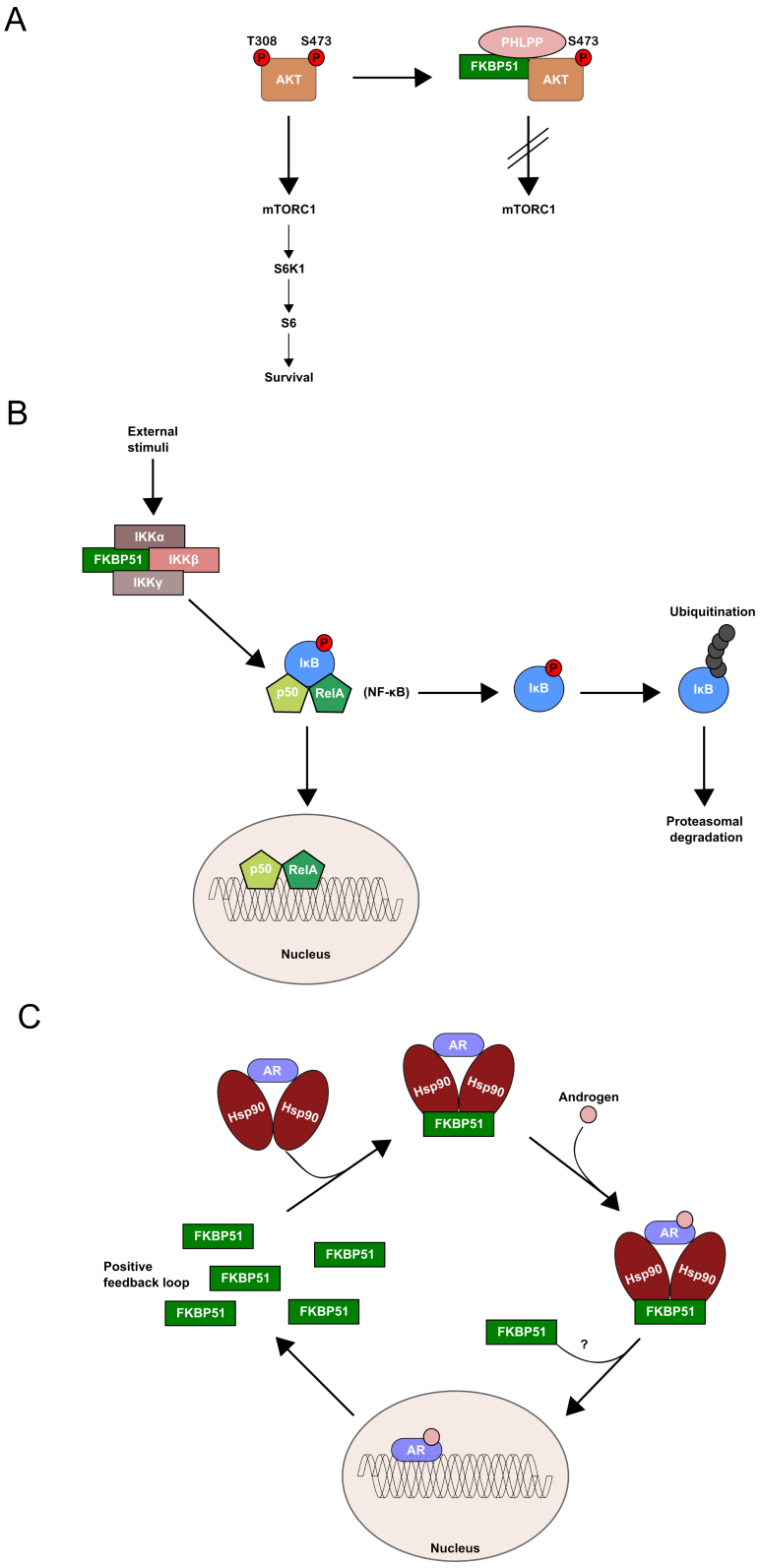

Figure 13: Proposed FKBP51 pathways and their involvement in diseases. (A) AKT signaling. FKBP51 mediates the interaction between PHLPP and AKT, which leads to dephosphorylation of AKT. AKT is inactive in this state and cannot activate mTORC1. The active AKT form starts a signaling cascade that leads to cell survival. (B) NF-κB signaling. It is hypothesized that FKBP51 activates IKKα, which leads to the activation of NF-κB and induces the expression of anti-apoptotic proteins. (C) AR signaling. FKBP51 promotes the formation of a complex that shows increased androgen hormone binding. The *FKBP5* gene encoding FKBP51 is under control of the AR and thus creates a positive feedback loop.

1.3.3 FKBP51/52 inhibitors

The first described ligands for FKBP proteins are the natural macrolides FK506 and Rapamycin (Sawada et al., 1987; Siekierka et al., 1989; Bierer et al., 1990). The chemical structures of both ligands are depicted in Fig. 14. Both ligands bind to the PPIase domain of FKBPs and inhibit the catalytic activity (Van Duyne et al., 1991). They act as immunosuppressants and dimerizing agents as they can bind two proteins simultaneously.

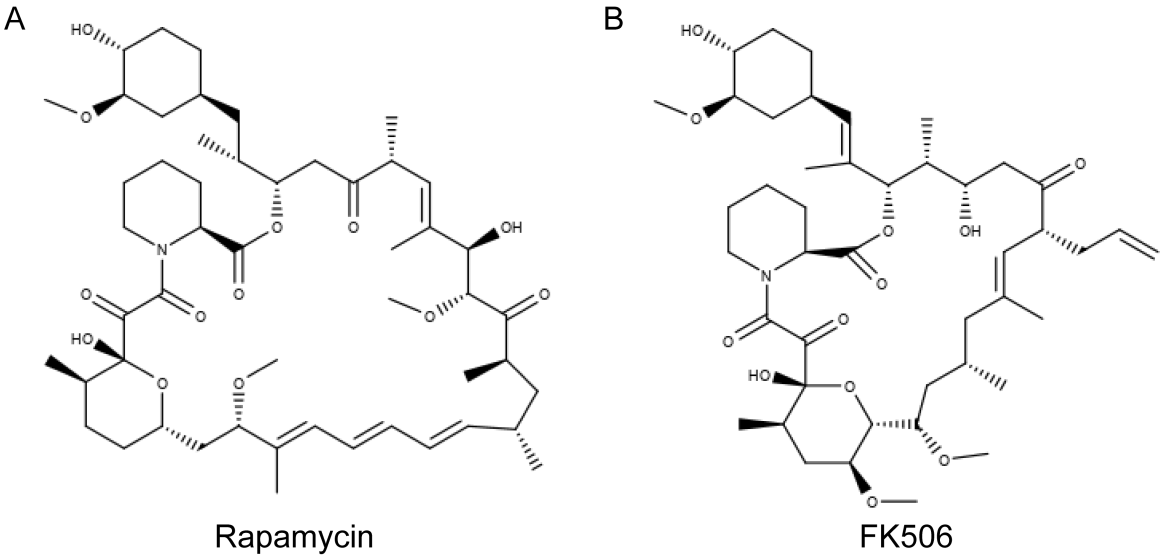

Figure 14: Chemical structures of natural FKBP inhibitors (A) Rapamycin and (B) FK506.

FK506 has been shown to bind FKBP proteins and calcineurin (Kissinger et al., 1995; Weiwad et al., 2006). The complex inhibits the phosphatase activity of calcineurin and prevents the dephosphorylation of its substrates (Liu et al., 1991; McCaffrey et al., 1993). The nuclear factor of activated T cells (NFAT) is activated through dephosphorylation by calcineurin and translocates into the nucleus (Shaw et al., 1995). FK506 prevents the activation of the immune response as NFAT is retained in the cytosol and the expression of interleukin-2 (IL-2) and the subsequent proliferation of T cells is inhibited (Shaw et al., 1988; Fujita et al., 1986).

Rapamycin acts in a similar way as FK506. It acts as a dimerizing agent for FKBP proteins and mTORC1. The latter regulates cell growth and proliferation through phosphorylation of S6 kinase 1 (S6K1) and eukaryotic initiation factor 4E binding protein (4E-BP1) (Fingar et al., 2002; Schalm et al., 2003). The inhibition of mTORC1 by Rapamycin blocks the activation of T cells and leads to a suppressed immune reaction.

FK506 and Rapamycin are unselective against the different FKBP proteins. However, their affinity varies depending on the FKBP protein (Kozany et al., 2009). An effort to achieve selectivity between FKBP51 and FKBP52 led to the discovery of ligands called selective antagonist of FKBP51 by induced fit (SAFit). SAFit1 and SAFit2 use an induced fit mechanism to selectively bind to FKBP51 with greater than 10,000-fold selectivity over FKBP52 (Gaali et al., 2015). The selectivity is achieved by a cyclized Cα-substituent that

induces conformational changes in the FK1 domain of FKBP51. To accomodate the Cα-substituent, the side chain of Phe67 is displaced and rotates between Lys58 and Lys60. Both lysines are stabilized by Phe129 (Gaali et al., 2015). In contrast, these conformational changes are energetically unfavorable in FKBP52 as the respective residues, Thr58, Trp60, and Val129, prevent Phe67 to adopt the same conformation. The SAFit inhibitors can be used to further study the biological function of FKBP51 and FKBP52 and investigate their role in GR maturation.

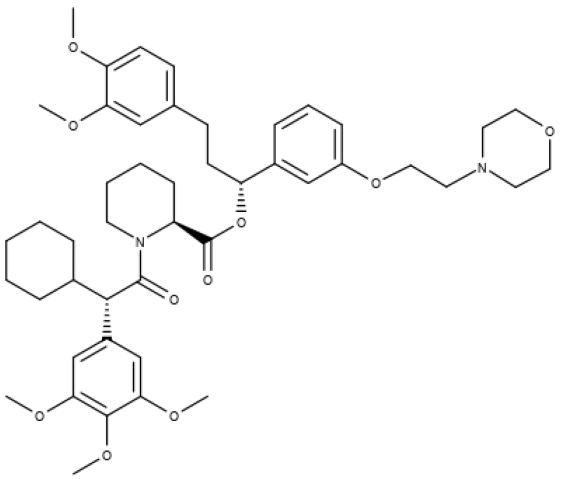

Figure 15: Chemical structure of the synthetic ligand SAFit2, which selectively binds to FKBP51.

2 Objective and significance

This PhD thesis focuses on the structural and biophysical characterization of the interaction of FKBP51/52 and their binding partners, mainly Hsp90 and GR, to identify and clarify their role in Hsp90:GR complexes and glucocorticoid signaling.

In the first part, different protein constructs of both Hsp90α/β and FKBP51/52 are designed to biophysically investigate the interaction between Hsp90 and FKBP51/52 by isothermal titration calorimetry (ITC). ITC is suitable to observe and quantify the interaction, not only providing an insight into binding affinities but also into thermodynamic parameters. This allows for the first time to examine FKBP51/52 binding to both Hsp90 isoforms to highlight differences in binding. Furthermore, these results help to choose minimal constructs for structural studies of the Hsp90:FKBP51/52 complex.

In the second part, Hsp90α:FKBP51/52 complexes are characterized. Analytic size-exclusion chromatography (SEC) and nanoDSF are deployed to determine complexes together with small-angle X-ray scattering (SAXS). Until now, no full-length crystal structure of FKBP52 has been solved. SAXS is able to provide insight into the solution structures of FKBP51, FKBP52, and human Hsp90α/β, including domain organization, flexibility, and structural differences of Hsp90:PPIase complexes.

The last part of the thesis focuses on the role of FKBP51 and FKBP52 in hormone binding to GR. A fluorescently-labeled DEX analog is used to observe hormone binding to GR in Hsp90:co-chaperone complexes. Full-length and truncated FKBP51/52 constructs are used to identify the domains that affect hormone binding to GR. The findings contribute to a better understanding of the *in vivo* function of FKBP51 and FKBP52 and clarify their role in the Hsp90 chaperone cycle. The assay results are correlated with those of the Hsp90 ATPase activity assay to link hormone binding to changes in Hsp90 function. The literature proposes an exchange of FKBP51 with FKBP52 during the Hsp90 chaperone cycle (Davies et al., 2002). ATP analogs and the late-stage co-chaperone p23 are used to investigate at which stage FKBP51 and FKBP52 enter the chaperone cycle. In addition, analytical ultracentrifugation (AUC) is used to determine if p23 and PPIases can bind simultaneously to Hsp90:GR complexes. To have a better understanding and evaluate the assays for future drug discovery projects, the published FKBP inhibitors Rapamycin, FK506, SAFit2, and Benztropine as well as the Hsp90 inhibitor Radicicol are tested in the hormone binding and ATPase activity assay.

In summary, the results of this thesis contribute to a better understanding of the roles of FKBP51 and FKBP52 in the Hsp90 chaperone machinery and their role in GR maturation. The insights into PPIase biochemistry help to clarify the effect of FKBP51 in neurodegenerative diseases and its potential as a drug target.

3 Material and Methods

3.1 Equipment

All experiments in this thesis were performed with the equipment listed in Table 1.

Table 1: Equipment used in this thesis.

Equipment	Manufacturer
ÄKTA Explorer	GE Healthcare
ÄKTA Micro	GE Healthcare
ÄKTA Purifier	GE Healthcare
Biacore T200	GE Healthcare
Centrifuge 5702R	Eppendorf
Centrifuge Avanti J20 XP	Beckman Coulter
Centrifuge Avanti J25	Beckman Coulter
DryEase^{TM} Mini-Gel Drying System	Invitrogen
Fraction collector Frac950	GE Healthcare
Hoefer Processor Plus (Western blotting)	Amersham Biosciences
iBlot Dry Blotting System	Invitrogen
MicroCal iTC$_{200}$	GE Healthcare
MicroCal Auto iTC$_{200}$	GE Healthcare
NanoDrop One	Thermo Scientific
Precision cuvettes (105.202-QS)	Hellma Analytics
Prometheus NT.48	NanoTemper
Rotor JA-25.50	Beckman Coulter
Rotor JLA-8.1000	Beckman Coulter
Sonopuls HD 2200	Bandelin
Spectrophotometer V-750	JASCO
Synergy H1 (plate reader)	BioTek

3.2 Chemicals

All experiments in this thesis were performed with the chemicals listed in Table 2.

Table 2: Chemicals used in this thesis.

Chemical	Supplier
Ampicillin sodium salt	Sigma-Aldrich
AMP-PNP	Roche
ATP	Sigma-Aldrich
ATPγS	Jena Bioscience
β-Mercaptoethanol	SERVA Electrophoresis GmbH
Benztropine	Boehringer Ingelheim Pharma GmbH & Co. KG
BSA	Sigma-Aldrich
DEX	ACROS Organics™
DMSO	Sigma-Aldrich
DTT	Carl Roth GmbH
Dexamethasone Fluorescein	Sigma-Aldrich
Factor Xa Protease	Promega GmbH
Glycerol	Merck KGaA
HEPES	Carl Roth GmbH
Imidazole	Merck KGaA
IPTG	Carl Roth GmbH
Kanamycin sulfate	SERVA Electrophoresis GmbH
KCl	Sigma-Aldrich
$MgCl_2$	Merck KGaA
NaCl	Carl Roth GmbH
NADH	Sigma-Aldrich
PEP	Sigma-Aldrich
PK/LDH from rabbit muscle	Sigma-Aldrich
Ponceau S solution 0.1 % (w/v)	Sigma-Aldrich
Radicicol	Sigma-Aldrich
Rapamycin	Boehringer Ingelheim Pharma GmbH & Co. KG
SAFit2	Boehringer Ingelheim Pharma GmbH & Co. KG
TCEP-HCl	Thermo Fisher
Thrombin	Sigma-Aldrich
TRIS	SERVA Electrophoresis GmbH
Tween 20	SERVA Electrophoresis GmbH

3.3 Consumables

All experiments in this thesis were performed with the consumables listed in Table 3.

Table 3: Consumables used in this thesis.

Consumable	Supplier
0.2 µm sterile filtration filters	Sartorius Stedim
1-Step™ NBT/BCIP substrate solution	Thermo Scientific
96 DeepWell PP Plate Natural	Thermo Scientific
384 Well Small Volume™ HiBase Polystyrene Microplates	Greiner Bio-One
α-mouse IgG coupled AP (rabbit)	Sigma-Aldrich
α-penta-His IgG (mouse)	Qiagen
Amicon® Ultra 0.5 mL Centrifugal Filters	Merck Millipore
Amicon® Ultra 4 mL Centrifugal Filters	Merck Millipore
Amicon® Ultra 15 mL Centrifugal Filters	Merck Millipore
cOmplete™ EDTA-free	Roche
DNase I	Roche
DryEase™ Mini Cellophan	Invitrogen
Harvesting bags	Beckman Coulter
Hsp90α 15mer peptide	BIOTREND Chemikalien GmbH
InstantBlue™	Expedeon Inc.
Microplate seals	4titude
NAP-5 columns	GE Healthcare
Ni^{2+}-NTA	Macherey & Nagel GmbH & Co.KG
NuPAGE® 4-12 % Bis Tris Gels	Invitrogen
NuPAGE® MES 20 × SDS-running buffer	Invitrogen
PD-10 columns	GE Healthcare
Protein Test Mixture 6	SERVA Electrophoresis GmbH
Standard capillaries	NanoTemper
Thermograde standard thin-walled 96-well plates	Thermo Scientific

3.4 Bacteria strains

The bacteria strains listed in Table 4 were used in this thesis. They were cultured in LB medium. The media and plates used in this thesis were prepared by Boehringer Ingelheim Pharma GmbH & Co. KG.

Table 4: The following strains were used in this thesis.

E. coli strain	Genotype	Supplier
E. coli BL21(DE3)	F^- *ompT hsdS*$_B$ (r_B^- m_B^-) *gal dcm*	Novagen
E. coli XL1-Blue	*rec*A1 *end*A1 *gyr*A96 *thi*-1 *hsd*R17 *sup*E44 *rel*A1 *lac* [F' *proAB lacI*^{q} ZΔ*M15* Tn*10* (Tet^r)]	Agilent
Library Efficiency^{TM} DH5α Competent Cells	F^- Φ80*lacZ*ΔM15 Δ(*lac*ZYA-*arg*F) U169 *rec*A1 *end*A1 *hsd*R17(r_k^-, m_k^+) *pho*A *sup*E44 *thi*-1 *gyr*A96 *rel*A1 λ^-	Invitrogen

3.5 Protein constructs

All genes were synthesized at GeneArt Gene Synthesis Service (Life Technologies) and cloned into the respective vector from Novagen. The inserted genes were codon optimized for expression in *E. coli*. All protein constructs (Table 5) were designed with an N-terminal His-tag for purification using immobilized metal ion affinity chromatography (IMAC). The GR-LBDm construct has an additional N-terminal GST-tag.

Table 5: Protein constructs used in this thesis.

Construct	Denotation	Vector	Resistance	Molecular weight [Da]
Hsp90α 1-732	FL	pET-16	Ampicillin	87180.37
Hsp90α 279-732	ΔN	pET-28	Kanamycin	55352.96
Hsp90α 473-732	ΔNM	pET-28	Kanamycin	32049.28
Hsp90α 549-732	ΔNM2	pET-28	Kanamycin	23134.04
Hsp90β 1-724	FL	pET-16	Ampicillin	86181.26
Hsp90β 271-724	ΔN	pET-17	Ampicillin	55238.77
Hsp90β 465-724	ΔNM	pET-17	Ampicillin	31987.17
Hsp90β 542-724	ΔNM2	pET-17	Ampicillin	23080.06
FKBP51 1-457	FL	pET-17	Ampicillin	53653.75
FKBP51 1-140	ΔMC	pET-17	Ampicillin	18653.02
FKBP51 16-260	ΔC	pET-17	Ampicillin	30490.48
FKBP51 139-457	ΔN	pET-17	Ampicillin	38503.49
FKBP51 139-414	ΔN2	pET-17	Ampicillin	33826.43
FKBP52 1-459	FL	pET-24	Kanamycin	54213.07
FKBP52 1-140	ΔMC	pET-17	Ampicillin	18617.11
FKBP52 16-260	ΔC	pET-17	Ampicillin	30901.96
FKBP52 139-459	ΔN	pET-17	Ampicillin	39988.78
FKBP52 139-416	ΔN2	pET-17	Ampicillin	35356.95
GR 521-777	LBDm	pGEX4T	Ampicillin	31458.48

3.6 Buffers

All buffers used for protein purification and biophysical measurements were filtered using a 0.2 µm filter (Sartorius Stedim).

Table 6: Composition of buffers used for purification of Hsp90α/β constructs. The binding and wash buffer were supplemented with ATP for full-length Hsp90α/β constructs.

Buffer	Composition	pH
Lysis buffer	20 mM TRIS, 150 mM NaCl, 10% Glycerol, 10 mM Imidazole, Protease Inhibitor, DNase I	8.0
Binding buffer	20 mM TRIS, 150 mM NaCl, 10% Glycerol, 10 mM Imidazole, (3 mM ATP)	8.0
Wash buffer	20 mM TRIS, 150 mM NaCl, 10% Glycerol, 20 mM Imidazole, (1 mM ATP)	8.0
Elution buffer	20 mM TRIS, 150 mM NaCl, 10% Glycerol, 250 mM Imidazole	8.0
SEC buffer 1	20 mM TRIS, 150 mM NaCl, 10% Glycerol, 2 mM β-Mercaptoethanol	8.0
SEC buffer 2	20 mM TRIS, 150 mM NaCl, 10% Glycerol, 2 mM TCEP	8.0

Table 7: Composition of buffers used for purification of FKBP51/52 constructs.

Buffer	Composition	pH
Lysis buffer	20 mM TRIS, 300 mM NaCl, 10 mM Imidazole, Protease Inhibitor, DNase I	8.0
Binding buffer	20 mM TRIS, 300 mM NaCl, 10 mM Imidazole	8.0
Wash buffer	20 mM TRIS, 300 mM NaCl, 20 mM Imidazole	8.0
Elution buffer	20 mM TRIS, 300 mM NaCl, 250 mM Imidazole	8.0
SEC buffer	20 mM HEPES, 50 mM NaCl, 2 mM TCEP	7.5

Table 8: Composition of buffers used for purification of the GR-LBDm.

Buffer	Composition	pH
Lysis buffer	50 mM TRIS, 100 mM NaCl, 2 M Urea, 5 mM $MgCl_2$, 50 µM DEX 10 mM Imidazole, Protease Inhibitor, DNase I	7.9
SEC-cleavage buffer	50 mM TRIS, 500 mM NaCl, 2 mM TCEP, 2 mM $CaCl_2$, 50 µM DEX 10 % Glycerol, 0.5 % CHAPS	7.9

Table 9: Composition of buffers used for biophysical measurements and protein complex studies.

Buffer	Composition	pH
ITC buffer	20 mM HEPES, 20 mM KCl, 5 mM $MgCl_2$, 2 mM TCEP	7.5
Complex buffer	20 mM HEPES, 20 mM KCl, 2 mM TCEP	7.5
FP buffer	30 mM HEPES, 150 mM KCl, 5 mM $MgCl_2$, 2 mM DTT	7.5
ATPase buffer	40 mM HEPES, 150 mM KCl, 5 mM $MgCl_2$, 1 mM TCEP	7.5

3.7 Transformation of *E. coli* BL21(DE3)

Transformation of *E. coli* BL21(DE3) (Novagen) was performed according to the manufacturer's protocol. Prior to heat shock transformation, 100 µL bacterial cell suspension was thawed on ice. 10 ng of plasmid containing the gene of interest were added to the bacterial cell suspension and the mixture was incubated on ice for 5 min. Subsequently, a heat shock was carried out for 45 s at 42°C and the *E. coli* cells were incubated for 2 min on ice. After incubation, 900 µL pre-warmed super optimal broth (SOC) medium were added and the suspension was incubated at 37°C and 300 rpm for up to 60 min in a shaker. The suspension was plated on LB-agar plates containing the respective antibiotic (Table 5). The plates were incubated at 37°C over night. Colonies were picked on the next day and used to inoculate 100 mL LB medium. Cultures were grown at 37°C over night. Glycerol stocks were prepared by supplementing *E. coli* cultures with 15 % glycerol and stored at -80°C.

3.8 Protein expression

Proteins were expressed using *E. coli* BL21(DE3) cells. Precultures were inoculated with glycerol stock cultures in 100 mL LB medium with 0.1 $\frac{\mu g}{mL}$ of the corresponding antibiotic (Table 5) and incubated at 37°C and 120 rpm over night. Large scale cultures were inoculated with precultures in LB medium with antibiotics to a starting OD_{600} of 0.1 and incubated

at 37°C and 120 rpm. Protein expression was induced by addition of IPTG when an OD_{600} of 0.6 – 0.8 was reached. Additionally, 500 µM DEX were added at the same time for the GR construct. Final IPTG concentration, expression temperature and duration for each construct are shown in Table 10. The cells were harvested at 4,000 × g and 4°C for 20 min. The supernatant was discarded and cell pellets were stored at -80°C.

Table 10: Conditions for protein expression of constructs used in this thesis.

Construct	Temperature [°C]	IPTG [mM]	Duration [h]
Hsp90α 1-732	22	0.1	20
Hsp90α 279-732	22	0.1	20
Hsp90α 473-732	22	0.1	20
Hsp90α 549-732	22	0.1	20
Hsp90β 1-724	20	0.1	6
Hsp90β 271-724	20	0.1	4
Hsp90β 465-724	20	0.1	4
Hsp90β 542-724	20	0.1	4
FKBP51 1-457	20	1	20
FKBP51 1-140	20	1	20
FKBP51 16-260	20	1	20
FKBP51 139-457	20	1	20
FKBP51 139-414	20	1	20
FKBP52 1-459	20	1	20
FKBP52 1-140	20	1	20
FKBP52 16-260	20	1	20
FKBP52 139-459	20	1	6
FKBP52 139-416	20	1	20
GR 521-777	20	1	20

3.9 Protein purification

3.9.1 Cell lysis

The purification of expressed proteins requires the lysis of cells. Cell pellets were thawed on ice and resuspended in 30 - 40 mL lysis buffer (Tables 6 or 7) with cOmplete^{TM} EDTA-free protease inhibitor. Cells were lysed by sonication using the Sonopuls HD 2200 with a Titanteller TT 13. Cycles of 1 min length, 80% power and 50% sonication time were repeated four times. Afterwards, the soluble fraction was separated by centrifugation at 40,000 × g and 4°C for at least 45 min. The supernatants were pooled and used in subsequent purification steps. The pellet after sonication of 1 L expression culture was resuspended in 5 mL 1 × lysis buffer to analyze the insoluble fraction. Samples of the resuspended pellet and the supernatant were diluted 1:10 with lysis buffer and mixed in a 1:1 ratio with 2 × Laemmli buffer for sodium dodecyl sulfate polyacrylamide gel electrophoresis (SDS-PAGE) analysis (Laemmli, 1970).

3.9.2 Affinity chromatography for His-tagged constructs

The purification of proteins by affinity chromatography is based on a reversible interaction between the target protein and a ligand. The most common method is IMAC, where histidine-tagged (His-tagged) proteins interact with metal ions. A His-tag is a poly-histidine sequence that binds with high affinity to Ni^{2+}. After the removal of proteins that interact unspecifically with the Ni^{2+} matrix by washing with wash buffer (Table 6 and 7), the bound protein can be eluted with 250 mM imidazole, which mimics and competes with the side chains of the His-tag. Ni-NTA slurry (column volume (CV) = 6 mL) was filled into a PD-10 column and equilibrated with 10 CV binding buffer (Tables 6 or 7). The resin was resuspended in 1 CV binding buffer and mixed with the supernatant of the cell lysis step. Afterwards, it was washed with 10 CV binding buffer. The flow-through was collected and a sample was diluted 1:10 for SDS-PAGE analysis. An additional wash step was carried out with 5 CV wash buffer (Tables 6 or 7) and an undiluted sample was prepared for SDS-PAGE analysis. Proteins were eluted by incubating the resin with 1 CV elution buffer (Tables 6 or 7) for 5 min and collecting the elution. The elution step was repeated five times and a sample from each elution, containing the target protein, was diluted 1:10 for SDS-PAGE analysis. An undiluted sample of the Ni-NTA beads was taken to analyze the uneluted fraction. After analysis by SDS-PAGE, fractions containing the target protein were pooled and concentrated using Amicon® Ultra-15 centrifugal filters with a suitable molecular weight cut-off (MWCO).

3.9.3 Affinity chromatography for GST-tagged constructs

Glutathione S-transferase (GST) can be used as a purification tag since it interacts with the tripeptide (Glu-Cys-Gly) glutathione (GT) that can be coupled to agarose resin. After the removal of proteins that interact unspecifically with the GT matrix, the bound protein can be eluted by cleavage of the GST-tag on the column. GT-slurry (CV = 5 mL) was filled into a PD-10 column and equilibrated with 10 CV lysis buffer (Table 8). The resin was

resuspended in 1 CV lysis buffer, combined with the supernatant and incubated for one hour at 4°C. The flow-through was collected and a sample was diluted 1:10 for SDS-PAGE analysis. Three wash steps were carried out with 10, 2, and 2 CV lysis buffer and undiluted samples were prepared for SDS-PAGE analysis. For GST-tag cleavage of the GR construct, 2.5 CV cleavage buffer (Table 8) and thrombin (5,000 U) were added to the resin. The GST-tag was cleaved at 4°C over night. The flow-through was collected and a sample was diluted 1:10 for SDS-PAGE analysis. The resin was washed four times with 1 CV cleavage buffer (Table 8). The wash fractions were collected and samples were diluted 1:10 for SDS-PAGE analysis. An undiluted sample of the GT beads was taken to analyze the uncleaved fraction. After analysis by SDS-PAGE, fractions containing the target protein were pooled and concentrated using Amicon® Ultra-15 centrifugal filters with a suitable MWCO.

3.9.4 Size-exclusion chromatography

Size-exclusion chromatography (SEC), also known as gel filtration, separates molecules according to their size. The column material is made up of beads with pores. Smaller molecules can enter the pores and are retained longer on the column leading to a delayed elution. Larger molecules cannot enter the pores. Hence, they are eluted earlier.
The pooled fractions after affinity chromatography were concentrated to 4-10 mL and loaded onto either a HiLoad 26/60 Superdex^{TM} 75 or Superdex^{TM} 200 column (CV = 318 mL) depending on the molecular weight of the target protein. The column was equilibrated with 1.2 CV superdex buffer before sample injection (Tables 6, 7 and 8). After sample injection, proteins were eluted with a flow rate of 1.5 $\frac{mL}{min}$ and collected in 2 mL fractions. The absorption at 280 nm was analyzed to identify fractions for SDS-PAGE analysis. Fractions containing the target protein were pooled and concentrated using Amicon® Ultra-15 centrifugal filters with a suitable MWCO. The protein sample was concentrated to 5 $\frac{mg}{mL}$ for further purification steps (His-tag cleavage) or to 10 $\frac{mg}{mL}$ for final storage. For the latter, the protein was aliquoted, flash frozen in liquid nitrogen and stored at -80°C.

3.9.5 Proteolytic cleavage of fusion proteins

PPIase and full-length Hsp90β contained a TEV cleavage site between the His-tag and the protein sequence. In this case, the N-terminal His-tag was removed by proteolytic cleavage with His-tagged TEV protease. After size-exclusion chromatography, TEV protease was added in a 1:50 ratio (w/w) to the pooled and concentrated fractions and incubated at 4°C over night. For full-length Hsp90α, the N-terminal His-tag was removed by proteolytic cleavage with Factor Xa (FXa) protease, which was added in 1:100 ratio (v/v), over night. The cleaved protein was separated from uncleaved protein, His-tag, and TEV protease by batch affinity chromatography with Ni-NTA. In this step, Ni-NTA slurry (CV = 2 mL) was equilibrated with 10 CV SEC buffer (Tables 6 or 7) and added to the protein solution. After 1 h incubation at 4°C, the flow-through was collected and the resin was washed five times with 5 mL SEC

buffer. The washed fractions were collected and subsequently analyzed via SDS-PAGE. The pooled fractions were subjected to a final SEC step (3.9.4).

3.10 Protein analysis

3.10.1 SDS-PAGE

The purity of protein samples was analyzed via SDS-PAGE. Proteins are denatured by heating and addition of an anionic detergent, SDS, which leads to a constant charge per unit mass. Hence, proteins can be separated by their size through a polyacrylamide gel. Equal volumes of protein sample and 2 ×Laemmli buffer were mixed and incubated at 95°C for five minutes (Laemmli, 1970). Fractionated samples after size-exclusion and TEV cleavage were mixed with 4 × Laemmli buffer (1:3). The samples and sample marker were loaded on NuPAGE® 4-12 % Bis-Tris gels. Electrophoresis was carried out at 200 V for 35 min. Afterwards, the gel was stained with InstantBlue™ solution for one hour and destained with water for at least 30 min. The gel was dried in two layers of DryEase™ Mini Cellophan.

3.10.2 Western blot

Target proteins and the successful cleavage of purification tags can be detected using an immunological approach. A primary antibody is used to detect the target protein and substrate conversion is detected by an enzyme-linked secondary antibody. Proteins were prepared and separated by SDS-PAGE as described in 3.10.1. Afterwards, the separated proteins were transferred onto a nitrocellulose membrane using the iBlot™ Western Detection Kit and the iBlot™ Dry Blotting System according to the manufacturer's protocol. Proteins on nitrocellulose membrane were stained with Ponceau S in order to verify a successful transfer. The antibody coupling was carried out with the Processor Plus system (Hoefer). Briefly, the membrane was incubated with 3 % BSA for one hour. Afterwards, the membrane was washed three times with T-TBS (Table 11) for five minutes and incubated with a primary antibody solution (0.1 $\frac{\mu g}{mL}$ α-penta-His mouse in TBS) for one hour. Unbound primary antibody was removed by washing the membrane three times with T-TBS for five minutes. The primary antibody was detected by incubating the membrane for one hour with a secondary antibody (α-mouse IgG alkaline phosphatase rabbit diluted in 1:30,000 in TBS. Unbound secondary antibody was removed by washing the membrane five times for five minutes with T-TBS. The secondary antibody was detected by incubation with 1-Step™ NBT/BCIP substrate solution.

Table 11: Composition of buffers used for Western blot.

Buffer	Composition	pH
TBS	50 mM TRIS, 150 mM NaCl	7.5
T-TBS	50 mM TRIS, 150 mM NaCl, 0.05% Tween 20	7.5

3.10.3 Mass spectrometry

Purified proteins were analyzed by mass spectrometry (MS) to validate the mass. MS analysis was performed by the Structural Analytics department at Boehringer Ingelheim Pharma GmbH & Co. KG. The protein was separated using an Waters ACQUITY UPLC M-class system and analyzed with a Waters Vion IMS QTof mass spectrometer by electrospray ionization time of flight mass spectrometry (ESI-TOF-MS).

3.11 Protein complex formation

Prior to structural studies involving both Hsp90 and FKBP, complexes were preformed and purified. To achieve this, Hsp90 and FKBP proteins were mixed in an 1:1.5 molar ratio with an excess of the smaller protein. Complex formation was facilitated by diluting the proteins in complex buffer (Table 9). Subsequently, the protein complex was purified by SEC on a Superdex^{TM} 200 Increase 10/300 GL column and eluted with a flow rate of 0.5 $\frac{mL}{min}$ into 0.5 mL fractions. Fractions containing proteins were analyzed by SDS-PAGE.

3.12 Biophysical methods

3.12.1 Nano differential scanning fluorimetry

Differential scanning fluorimetry (DSF) allows the determination of the protein melting temperature (T_m), thus providing information about its thermal stability. In general, the protein is subjected to a linear temperature gradient with or without a labeling molecule. The fluorescence of either the labeled molecule or the protein itself is recorded. For analysis, the first derivative of the fluorescence-temperature plot is calculated and the T_m is indicated by the maximum or minimum of that curve. In this thesis, the label-free nanoDSF method was used by measuring the intrinsic tryptophan and tyrosine fluorescence at wavelengths of 330 nm and 350 nm.
Usually, tryptophan residues are located and embedded in the hydrophobic core of a protein. Once these residues are exposed to the hydrophilic environment as the protein unfolds, the maximum of the fluorescence shifts from 330 nm to 350 nm. The T_m of the protein is determined at the inflection point of the fluorescence ratio (350 nm/330 nm) curve. Melting experiments were conducted using the Prometheus NT.48 instrument (NanoTemper). Standard capillaries (NanoTemper) were filled with 10 µL of 10 µM protein in SEC buffer (Tables 6 or 7) or complex buffer (Table 9). After determination of a suitable laser excitation power, melting curves were recorded with a rate of 1.5°C per minute from 20°C to 95°C. T_m values were calculated with the software PR.ThermControl (NanoTemper).

3.12.2 Isothermal titration calorimetry

ITC is used to determine the thermodynamic parameters of binding reactions in solution. This is possible by measuring the heat changes during the titration of one binding partner

to the other binding partner. The instrument, a calorimeter, consists of a reference cell, a sample cell, a syringe and an adiabatic case. The experiment is performed by titrating one binding partner from a syringe into a sample cell containing the other binding partner. The temperature is kept constant and the solution is stirred to allow even distribution. The calorimeter measures the energy, which is necessary to compensate for temperature differences between reference and sample cell during every injection. When binding events are observed, the necessary energy decreases with every injection as the binding partner in the sample cell is increasingly saturated. The molar binding enthalpy (ΔH), the dissociation constant (K_D) and the binding stoichiometry (N) can be determined with a sigmoidal fit of the binding energies and the known molar ratios of the two molecules. The molar free energy (ΔG) and molar binding entropy (ΔS) can be conceived with equation 1 (Pierce et al., 1999).

$$\Delta G = RT \cdot \ln K_D = \Delta H - T \cdot \Delta S \quad (1)$$

ITC experiments were performed with an automated setup using the MicroCal Auto iTC200 (GE Healthcare). All samples had their buffer exchanged into ITC buffer (Table 9) with NAP-5 columns according to the manufacturer's instructions. Proteins in ITC buffer were concentrated to 200 µM for syringe samples and 20 µM for cell samples using Amicon® Ultra 0.5 mL concentrators. The final protein samples and ITC buffer were loaded into a 96 DeepWell Plate (Thermo Scientific) with a volume of 380 µL for cell samples, 130 µL for syringe samples, and 400 µL buffer. ITC experiments were performed at 25°C with a stirring speed of 750 rpm and 4 $\frac{\mu cal}{sec}$ reference power. The injection scheme included 20 injections with 150 s spacing in between and an initial delay of 60 s. The first injection had a volume of 0.4 µL in 0.8 s and the following 19 injections had a volume of 2 µL in 4 s. ITC data were analyzed using the MicroCal Data Analysis iTC200 Software (GE Healthcare).

3.12.3 Small-angle X-ray scattering

SAXS exploits the elastic scattering of monochromatic X-rays at low angles and allows the structural characterization of proteins in solution under nearly native conditions (Kikhney and Svergun, 2015). It is necessary to collect the scattering pattern of the pure buffer and subtract it from the sample scattering. The resulting scattering pattern contains only the scattering of the protein. Information about the radius of gyration (R_g), molecular weight, the excluded particle volume and the maximal dimension (D_{max}) are directly determined from the scattering (Kikhney and Svergun, 2015).
Here, SAXS was used to analyze Hsp90 isoforms, PPIases, and Hsp90:PPIase complexes. SAXS experiments were carried out by Dr. Claire Pizzey (Diamond Light Source). Size-exclusion chromatography SAXS (SEC-SAXS) experiments were performed at beamline B21 at the Diamond Light Source. Protein samples with approximately 5 $\frac{mg}{ml}$ were loaded onto a Superdex™ 200 Increase 3.2/300 GL SEC column (GE Healthcare) in 20 mM HEPES pH 7.5, 20 mM KCl, 2 mM $MgCl_2$, 2 mM TCEP, and 200 µM ATP using an Agilent 1200 HPLC system.

The injection volume was 55 µl. The outlet from the column fed directly into the experimental capillary. SAXS data were recorded on an EIGER detector (Dectris) with an X-ray energy of 13.1 keV and sample to detector distance of 2.687 m in a series of 3 second frames. Data were automatically reduced according to standard protocols. Background corrections were applied by subtracting frames before the protein eluted from the column (frames were individually inspected and buffer only frames were identified from a flat region in the plot of the integral of the ratio of each frame) and data were averaged using ScÅtter (Rambo, 2019). The data were further processed and analyzed with ScÅtter and the ATSAS program package (Franke et al., 2017). ScÅtter was used to calculate the radius of gyration R_g and forward scattering I(0) via Guinier approximation and to derive the maximum particle dimension D_{max} and P(r) function. The *ab initio* model was derived using DAMMIN (Svergun, 1999). 13 individual models were created, then superimposed and averaged using DAMAVER and DAMFILT (Volkov and Svergun, 2003). Crystal structures of Hsp90β in a closed conformation (5FWK), FKBP51 (5NJX), FKBP52 (1P5Q and 1Q1C) or a solution SAXS model of Hsp90α were fitted to the averaged model using CHIMERA (Wu et al., 2004; Kumar et al., 2017; Verba et al., 2016; Pettersen et al., 2004; Krukenberg et al., 2009).

3.12.4 Fluorescence polarization

Fluorescence polarization (FP) or anisotropy are based on the observation of linearly polarized light, which can excite fluorophores, and the polarization of the emitted light. The degree of polarization is inversely related to the molecular rotation of the sample. Both, polarization and anisotropy, are described by two intensities. The light intensity parallel ($I_{\parallel}$) and perpendicular ($I_{\perp}$) to the excitation light plane. Polarization P and anisotropy r can then be calculated with the following equations.

$$P = \frac{I_{\parallel} - I_{\perp}}{I_{\parallel} + I_{\perp}} \tag{2}$$

$$r = \frac{I_{\parallel} - I_{\perp}}{I_{\parallel} + 2I_{\perp}} \tag{3}$$

The polarization of the emitted light is influenced by several aspects. Firstly, the rotational diffusion of the fluorophore while it is in the excited state. Secondly, the viscosity of the buffer and the size and shape of the molecule affecting the rotational diffusion. When the viscosity is low, the rotational diffusion of small molecules is faster than the emission. Thus, the emitted light is depolarized. The rotational behavior of a molecule can be used to study protein-ligand or protein-protein interactions as the rotational relaxation time of fluorophores is dependent on molar volume (Lea and Simeonov, 2011). Thus, binding and unbinding events will change the molecular size of the fluorescent molecule and influence the polarization or anisotropy of the emitted light.

In this work, FP was utilized in a hormone binding assay. FP experiments were performed to follow the binding of F-DEX to GR-LBDm, in the absence and presence of human Hsp90 and

various co-chaperone mixtures. Hormone-free GR-LBDm was acquired by dialysis against SEC-cleavage buffer without DEX (Table 8). The dialysis was performed over two days at 4°C and the dialysis buffer was changed twice. The dialyzed GR-LBDm was titrated into F-DEX to confirm that it adequately bound hormone and that the dialyzed GR-LBDm was hormone free. Measurements were performed in FP buffer (Table 9). Prior to the addition of F-DEX, the samples were incubated at RT for one hour. Experiments were conducted in 384 well plates in a BioTek Synergy H1 plate reader. The excitation wavelength was set to 490 nm and the emission wavelength to 520 nm. The observed association rate constant (k_{obs}) was determined by fitting a single exponential binding equation to the data in Origin 2017. Only the first three decimal places of the determined k_{obs} values are displayed in tables for readability. Statistical significance was calculated with five decimal places.

Table 12: Composition of FP assay sample.

Volume\concentration	Substance
50 nM	F-DEX (5 µM stock in DMSO)
1 µM	GR-LBDm
12 µM	Hsp90
12 µM	Co-chaperone
2 mM	ATP (20 mM stock in FP buffer)
2.5 µL	Compound (240 µM stock in 10 % DMSO) or 10 % DMSO
fill up to 25 µL	FP buffer

3.12.5 Regenerative ATPase assay

An enzymatic regenerative ATPase assay was carried out to determine the ATPase activities of Hsp90 in different complexes (Richter et al., 2008). The reaction is coupled to the enzyme pyruvate kinase (PK) which regenerates ATP and results in a constant ATP amount. ATPase activity is then indirectly measured by the conversion of NADH into its oxidized form by lactate dehydrogenase (LDH).

$$\mathrm{ATP} + \mathrm{H_2O} \xrightarrow{\text{Hsp90}} \mathrm{ADP} + \mathrm{P}_i \tag{4}$$

$$\mathrm{PEP} + \mathrm{ADP} \xrightarrow{\text{Pyruvate kinase}} \mathrm{Pyruvate} + \mathrm{ATP} \tag{5}$$

$$\mathrm{Pyruvate} + \mathrm{NADH} \xrightarrow{\text{Lactate dehydrogenase}} \mathrm{Lactate} + \mathrm{NAD^+} \tag{6}$$

NADH oxidation is directly proportional to the hydrolysis of ATP by Hsp90 as all three reactions react in 1:1 stoichiometry. The concentration of NADH can be spectrometrically followed by absorption at 340 nm using the spectrophotometer V-750 (Jasco). ATPase experiments were performed in ATPase buffer (Table 9). Prior to the addition of ATP, the

sample was incubated at 37°C for 5 min in the spectrophotometer in a quartz cuvette (Hellma Analytics) with a path length of 1 cm (d). Each experiment was carried out in parallel with a control containing the Hsp90 inhibitor Radicicol to determine the Hsp90-specific ATPase activity (Schulte et al., 1998). The reaction was started by the addition of ATP. The absorbance was measured at 340 nm at 37°C for 45 min. Afterwards, the control was subtracted from the sample without inhibitor. The slope ($\frac{dA}{dt}$) of the resulting curve was determined. Equation 7 was used to determined the catalytic rate constant (k_{cat}) of Hsp90. The extinction coefficient (ε) of NADH at 340 nm is 6200 $M^{-1}\,cm^{-1}$. Only the first two decimal places of the determined k_{cat} values are displayed in tables for readability. Statistical significance was calculated with five decimal places.

$$k_{cat} = -\frac{dA}{dt} \cdot \frac{1}{\varepsilon_{NADH} \cdot c_{Hsp90} \cdot d} \tag{7}$$

Table 13: Composition of 2 × ATPase premix.

Volume	Substance
19 µL	PEP (100 mM in ATPase buffer)
3.8 µL	NADH (50 mM in ATPase buffer)
25 µL	PK/LDH (600 U stock)
452.2 µL	ATPase buffer

Table 14: Composition of ATPase assay sample.

Volume\concentration	Substance
60 µL	2 × ATPase premix
10 µM	Hsp90
20 µM	Co-chaperone
20 µM	GR-LBDm
12 µL	ATP (20 mM stock in ATPase buffer)
1.2 µL	Radicicol (10 mM stock in DMSO)
fill up to 120 µL	ATPase buffer

3.12.6 Analytical ultracentrifugation

Analytical ultracentrifugation (AUC) provides information about size, shape and interactions of macromolecules. Two experimental types are available: sedimentation velocity and sedimentation equilibrium. The first provides first-principle hydrodynamic information about the size and shape of molecules (Laue and Stafford, 1999). The latter provides first-principle

thermodynamic information about molar masses, stoichiometries and association constants (Laue, 1995). The sedimentation coefficient s, the diffusion coefficient D and the molecular weight M can be determined for all species in the sample. Sedimentation boundaries are detected by either UV absorbance, interference or fluorescence. In the following, only sedimentation velocity experiments will be further covered as those experiments were performed in this thesis.
Centrifugal forces, which are exerted on a sample, will create sedimentation boundaries that depend on the molecular weight of protein species. Three forces need to be considered: the centrifugal, the buoyant and the frictional force. The Svedberg equation (8) can be derived by taking these forces into account (Gralen and Svedberg, 1940).

$$s = \frac{v}{\omega^2 r} = \frac{MD(1 - \bar{v}\rho)}{RT} \tag{8}$$

With s as the sedimentation coefficient [S], v the observed radial velocity of the macromolecule $[\frac{m}{s}]$, ω the angular velocity of the rotor $[\frac{m}{s^2}]$, r is the radial position, $\omega^2 r$ is the centrifugal field [N], M is the molecular weight $[\frac{g}{mol}]$, $\bar{v}$ is the partial specific volume $[\frac{cm^3}{g}]$, ρ is the density of the solvent $[\frac{g}{cm^3}]$, D is the diffusion coefficient $[\frac{m^2}{s}]$, R is the gas constant $[8.314\,\frac{J}{molK}]$ and T is the temperature in [K].

Information about the composition of Hsp90 and GR-LBDm containing complexes was generated by sedimentation velocity experiments in an Optima-XL-I Beckman centrifuge with absorbance optics. The experiments were carried out by Jannis Lawatscheck (Technical University of Munich). 1 µM of Atto488-labeled GR-LBDm was incubated with 3 µM of Hsp90α, 6 µM of FKBP51 or FKBP52, and 9 µM of p23 in 30 mM HEPES (pH 7.5), 150 mM KCl, 5 mM $MgCl_2$, 2 mM DTT, 2 mM ATP supplemented with 100 µM DEX. For experiments with fluorescently labeled hormone, 1 µM of a fluorescein-DEX derivate (F-DEX) and 1 µM of hormone free GR-LBDm were used with the same amounts of chaperone and co-chaperones. No additional DEX was added. The runs were conducted at 42,000 rpm, 20 °C and sedimentation was monitored using an Avis Fluorescence detection system. The raw data was converted into a dc/dt plot using SEDFIT v. 14.1 (Schuck, 2000). Data was further analyzed with Origin 2017.

4 Results

4.1 Biophysical characterization of FKBP51/52 and Hsp90α/β

4.1.1 The interaction between PPIases and Hsp90α is driven by polar interactions

Mammalians cells have two major cytoplasmic isoforms of Hsp90. Hsp90β, which is constitutively expressed, and Hsp90α, which is expressed during cellular stress (Zuehlke et al., 2015). Previous studies used ITC to investigate the interaction of full-length FKBP51 and FKBP52 with full-length Hsp90β and a combination of ITC and NMR to investigate the interaction of the three FKBP51 domains (FK1, FK2, and TPR) with the three Hsp90β domains (NTD, MD, and CTD) (Pirkl and Buchner, 2001; Oroz et al., 2018). The X-ray structure of FKBP51 in complex with a C-terminal Hsp90 peptide provided a first snapshot of the binding mechanism (Fig. 11) (Draxler, 2016; Kumar et al., 2017). The binding involves polar and charged residues of FKBP51 and Hsp90. This suggests that the affinity between chaperone and co-chaperone could be influenced by the buffer composition. To systematically investigate the interaction of FKBP51 and FKBP52 with Hsp90α and Hsp90β by ITC, the salt dependency of the interaction was addressed first. Binding affinities and thermodynamic binding parameters of FKBP51 and FKBP52 to Hsp90α in the presence of 20 mM and 140 mM KCl were determined by ITC.

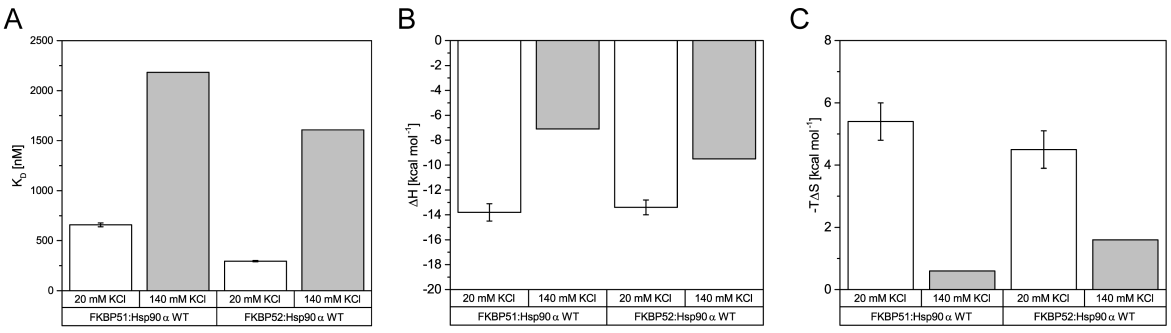

Figure 16: ITC studies with FKBP51/52 and Hsp90α to assess the impact of salt on binding affinities. Determined K_D (A), enthalpy (B), and entropy (C) values of FKBP51 and FKBP52 binding to Hsp90α in buffer containing 20 mM KCl or 140 mM KCl. Only experiments in buffer with a low salt concentration were carried out in triplicates. Error bars represent standard deviation (SD).

The titrations were fitted with an one-site binding model. In both salt concentrations, FKBP52 bound to Hsp90α with 2.2- and 1.4-fold higher affinity compared to FKBP51. When the KCl concentration of the buffer decreased from 140 mM to 20 mM, an increase of binding affinities by 3.3- and 5.4-fold was observed for FKBP51 and FKBP52, respectively (Fig. 16A). The same trend is observable in binding enthalpies and entropies (Fig. 16B and C). The enthalphic and entropic contributions increased for FKBP51 and FKBP52 as the salt concentration decreased from 140 mM to 20 mM (Fig. 16B and C). The derived binding data is shown in Table 15. The results show that FKBP51/52 and Hsp90α interact more strongly

under low salt conditions and indicate that polar interactions play a key role.

Table 15: Binding affinities (K_D) and thermodynamic parameters determined by ITC experiments between FKBP51/52 and Hsp90α to investigate the influence of salt (20 mM and 140 mM). Only experiments in buffer with a low salt concentration were carried out in triplicates. Data are shown as mean ± SD.

FKBP51	Salt [mM]	K_D [nM]	ΔG [$\frac{kcal}{mol}$]	ΔH [$\frac{kcal}{mol}$]	-TΔS [$\frac{kcal}{mol}$]	N
Hsp90α	20	658±19	-8.4±0.0	-13.8±0.7	5.4±0.6	0.9±0.1
Hsp90α	140	2183	-6.5	-7.1	0.6	0.8

FKBP52	Salt [mM]	K_D [nM]	ΔG [$\frac{kcal}{mol}$]	ΔH [$\frac{kcal}{mol}$]	-TΔS [$\frac{kcal}{mol}$]	N
Hsp90α	20	296±7	-8.9±0.0	-13.4±0.6	4.5±0.6	0.9±0.0
Hsp90α	140	1608	-7.9	-9.5	1.6	0.8

4.1.2 The main interaction between PPIases and Hsp90α is mediated by their C-terminal domains

The ITC experiments revealed that polar interactions are important between FKBP51/52 and Hsp90α. The change in salt concentration shifts the equilibrium towards complex formation. Therefore, further interaction studies were carried out with 20 mM KCl to identify potential binding sites. Cheung-Flynn et al. (2003) used radiolabeled C-terminally truncation mutants of FKBP51 and FKBP52 together with Hsp90 co-immunoprecipitation (Co-IP) to identify structural features that differentiate binding to Hsp90. The two full-length PPIases bind Hsp90β to a similar extent according to Co-IP. C-terminal truncations of FKBP51 and FKBP52, on the other hand, affected binding to Hsp90. In this setup, differences between FKBP51 and FKBP52 could be observed. Truncation constructs were used to systematically investigate the interaction between FKBP51/52 and Hsp90α and to identify the involved domains using ITC. For FKBPs, truncation constructs were designed that covered the FK1 domain (ΔMC) and the FK1 and FK2 domains (ΔC) to investigate potential weak secondary interaction sites (Fig. 17A). Additional constructs covering the FK2 and TPR domains with and without the last 40 C-terminal amino acids (ΔN and ΔN2) could highlight the influence of the C-terminal residues after the TPR domain on Hsp90 binding (Fig. 17A). For Hsp90, truncations were carried out from N- to C-terminus to identify secondary interaction sites next to the MEEVD motif. Hsp90 constructs covered the MD and CTD (ΔN), the last helix of the MD and the complete CTD (ΔNM), and only the CTD (ΔNM2). Experiments with truncation constructs of FKBP51/52 and Hsp90α were performed by Viktor Beke during his masters thesis under my supervision.

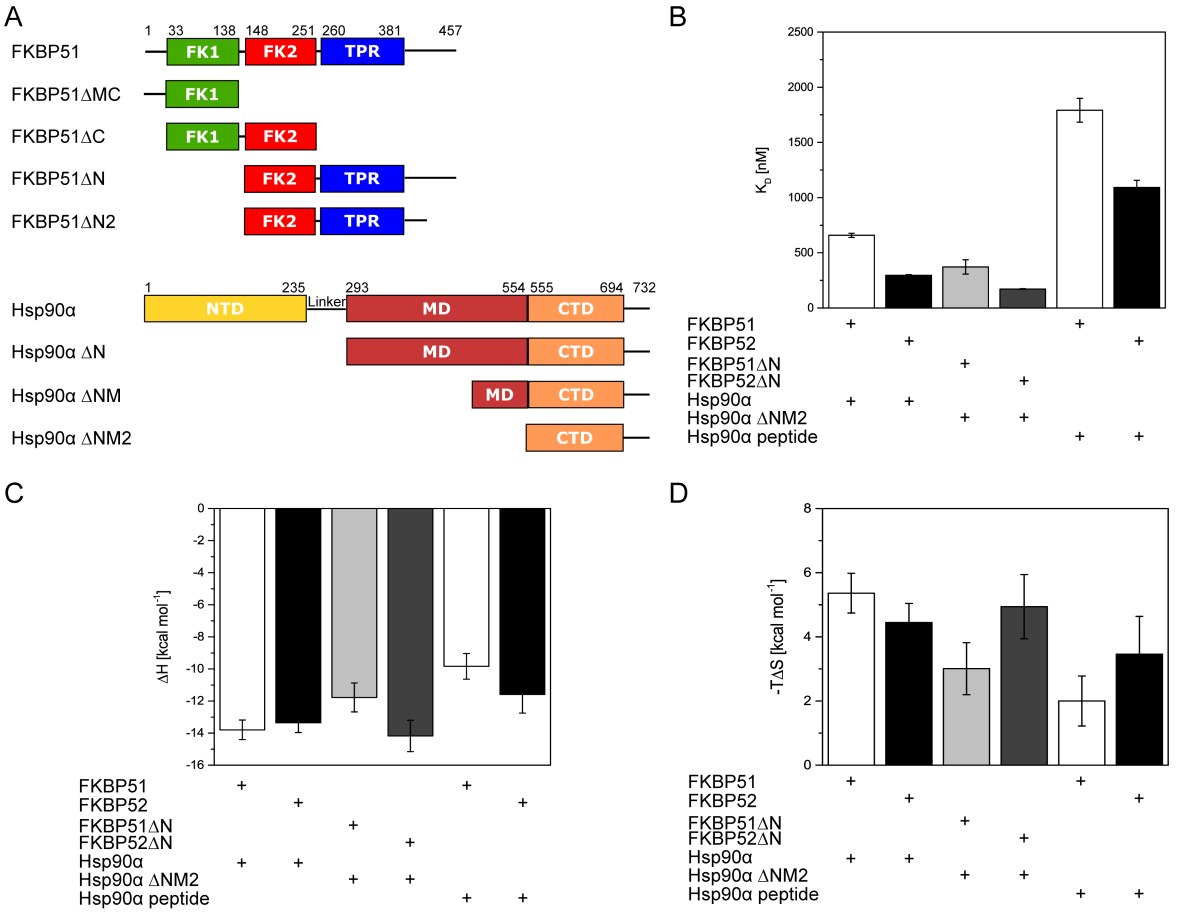

Figure 17: ITC studies of FKBP51 and FKBP52 with Hsp90α. (A) Schematic overview of domain architecture and truncation constructs of FKBP51 and Hsp90α. FKBP52 and Hsp90β constructs were designed accordingly. K_D (B), enthalpic (C), and entropic (D) analysis of FKBP51 and FKBP52 constructs binding to Hsp90α constructs. The Hsp90α peptide consists of the last 15 C-terminal amino acids (PLEGDDDTSRMEEVD). All experiments were carried out in triplicates. Data are shown as mean ± SD.

Again, the titrations were fitted with an one-site binding model. Overall, FKBP52 constructs have a higher affinity for Hsp90α compared to FKBP51 (Fig. 17B). Binding affinities of FKBP52 constructs were 1.5- to 2.5-fold higher compared to the corresponding FKBP51 constructs. For Hsp90α, the K_D values were around 660 nM when binding to FKBP51 and 300 nM when binding to FKBP52. The removal of the FK1 domain of FKBP51/52 (ΔN) and the NTD and MD of Hsp90α (ΔNM) led to a modest increase of the K_D with 370 nM and 170 nM, respectively (Fig. 17B). Titration of a C-terminal Hsp90α peptide containing the consensus binding sequence revealed a decrease in affinity with 1790 nM and 1090 nM for FKBP51 and FKBP52, respectively (Fig. 17B). No binding was observed for FK1 or FK1-FK2 constructs with Hsp90α (not shown). The thermodynamic profile indicates different binding modes for FKBP51 and FKBP52. The enthalpic contributions (ΔH) were tendentially decreasing for FKBP51, with values from -13.8 (FKBP51:Hsp90α) to -9.8 kcal mol^{-1} (FKBP51:Hsp90α 15mer peptide) (Fig. 17C). The enthalpic values showed no visible trend for FKBP52 with -13.4 (FKBP52:Hsp90α) and -11.6 kcal mol^{-1} (FKBP52:Hsp90α 15mer peptide) (Fig. 17C). The

entropic contribution (-TΔS) decreased for FKBP51 and Hsp90α from 5.4 to 2.0 kcal mol^{-1} (FKBP51:Hsp90α 15mer peptide), showing the same trend as the enthalpic contributions (Fig. 17D). In contrast, the entropic contributions did not change for FKBP52 with 4.5 (FKBP52:Hsp90α) and 3.5 kcal mol^{-1} (FKBP52:Hsp90α 15mer peptide) (Fig. 17D). Taken together, the results indicate interactions outside of the TPR domain of FKBP51 and the C-terminal domain of Hsp90α as well as different binding modes for FKBP51 and FKBP52. An overview of all measured combinations, their affinities and their thermodynamic properties are shown in Table 16.

Table 16: Results of ITC experiments with FKBP51/52 and Hsp90α. All experiments were carried out in triplicates. Data are shown as mean ± SD.

FKBP51	K_D [nM]	ΔG [$\frac{kcal}{mol}$]	ΔH [$\frac{kcal}{mol}$]	-TΔS [$\frac{kcal}{mol}$]	N
Hsp90α	658±19	-8.4±0.0	-13.8±0.7	5.4±0.6	0.9±0.1
Hsp90αΔN	863±38	-8.3±0.1	-15.9±2.4	7.6±2.3	0.9±0.2
Hsp90αΔNM	647±101	-8.4±0.1	-11.7±0.5	3.3±0.6	0.8±0.0
Hsp90αΔNM2	491±62	-8.6±0.1	-11.6±0.2	3.0±0.2	1.0±0.1
Hsp90α peptide	1791±107	-7.8±0.0	-9.8±0.8	2.0±0.8	1.0±0.1

FKBP51ΔN	K_D [nM]	ΔG [$\frac{kcal}{mol}$]	ΔH [$\frac{kcal}{mol}$]	-TΔS [$\frac{kcal}{mol}$]	N
Hsp90αΔN	508±39	-8.6±0.1	-12.9±0.5	4.4±0.6	1.0±0.0
Hsp90αΔNM	455±57	-8.7±0.1	-11.9±0.4	3.3±0.5	0.8±0.0
Hsp90αΔNM2	372±65	-8.8±0.0	-11.8±0.9	3.0±0.8	0.9±0.1

FKBP51ΔN2	K_D [nM]	ΔG [$\frac{kcal}{mol}$]	ΔH [$\frac{kcal}{mol}$]	-TΔS [$\frac{kcal}{mol}$]	N
Hsp90αΔN	254±109	-9.0±0.2	-12.4±0.5	3.3±0.6	0.9±0.0
Hsp90αΔNM	298±10	-8.9±0.1	-9.5±0.1	0.6±0.1	1.1±0.0
Hsp90αΔNM2	261±30	-9.0±0.1	-13.2±0.1	4.3±0.2	0.9±0.0

FKBP52	K_D [nM]	ΔG [$\frac{kcal}{mol}$]	ΔH [$\frac{kcal}{mol}$]	-TΔS [$\frac{kcal}{mol}$]	N
Hsp90α	296±7	-8.9±0.0	-13.4±0.6	4.5±0.6	0.87±0.0
Hsp90αΔN	176±24	-9.2±0.1	-14.1±0.2	4.9±0.3	0.9±0.0
Hsp90αΔNM	221±11	-9.1±0.0	-13.7±0.2	4.6±0.1	0.8±0.0
Hsp90αΔNM2	259±13	-9.0±0.0	-14.2±0.3	5.1±0.2	0.9±0.1
Hsp90α peptide	1092±65	-8.1±0.0	-11.6±1.2	3.5±1.2	1.1±0.1

FKBP52ΔN	K_D [nM]	ΔG [$\frac{kcal}{mol}$]	ΔH [$\frac{kcal}{mol}$]	-TΔS [$\frac{kcal}{mol}$]	N
Hsp90αΔN	152±23	-9.1±0.1	-14.3±1.0	5.0±1.0	0.9±0.0
Hsp90αΔNM	216±72	-9.2±0.2	-13.1±0.6	4.0±0.7	0.7±0.0
Hsp90αΔNM2	171±4	-9.3±0.0	-14.2±1.0	4.9±1.0	0.9±0.1

FKBP52ΔN2	K_D [nM]	ΔG [$\frac{kcal}{mol}$]	ΔH [$\frac{kcal}{mol}$]	-TΔS [$\frac{kcal}{mol}$]	N
Hsp90αΔN	159±10	-9.3±0.0	-13.3±0.6	4.0±0.6	0.9±0.1
Hsp90αΔNM	114±13	-9.5±0.1	-12.2±0.6	2.7±0.3	0.7±0.0
Hsp90αΔNM2	162±49	-9.3±0.2	-12.5±1.0	3.2±1.1	0.8±0.1

4.1.3 PPIases do not distinguish between human Hsp90 isoforms

As mentioned, mammalian cells have two cytoplasmic Hsp90 isoforms, Hsp90α and Hsp90β. The β isoform is constitutively expressed and the α isoform is expressed during stress (Zuehlke et al., 2015). They share 86% sequence identity at the amino acid level (Fig. 18A).

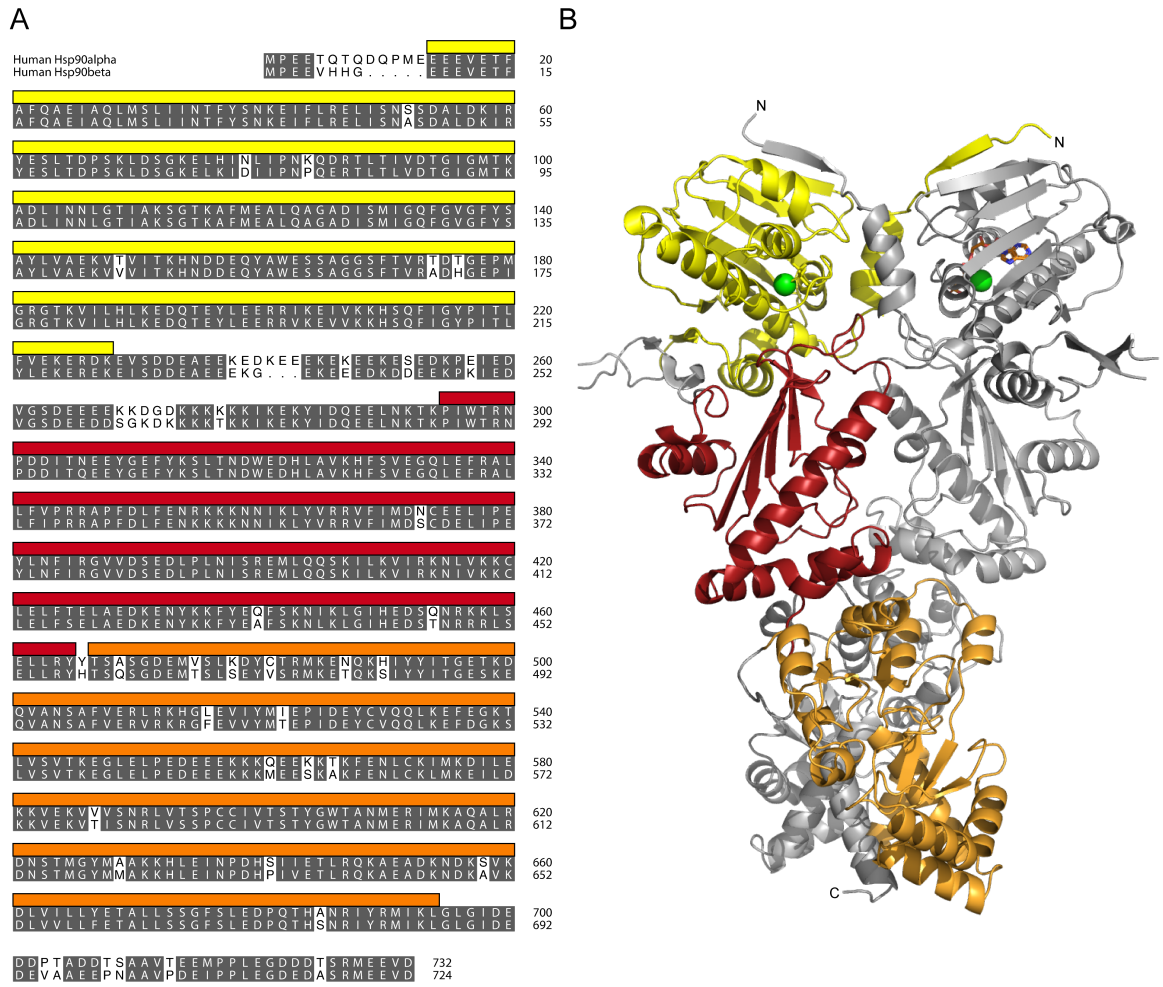

Figure 18: Sequence comparison of human Hsp90α/β. (A) Sequence alignment of Hsp90α and Hsp90β. Matching residues are shaded in grey and dots indicate gaps for optimal alignment. The NTD, MD, and CTD are depicted by a yellow, red, and orange bar, respectively. (B) Closed Hsp90β structure (PDB ID 5FWK) showing the domains depicted with the same color scheme as in (A) (Verba et al., 2016). Bound Mg^{2+} ions are shown as green spheres and bound ATP in sticks.

Hsp90α has eight additional residues in comparison to Hsp90β: Five at the N-terminus and three at the beginning of the charged linker. Furthermore, 16 amino acids are changed in the CTD and six downstream of the CTD. Considering the sequence differences in the C-terminal region, this led to the question if those differences could affect binding to FKBP51 or FKBP52. Hsp90β constructs were designed analogous to those for Hsp90α and affinities were determined by ITC.

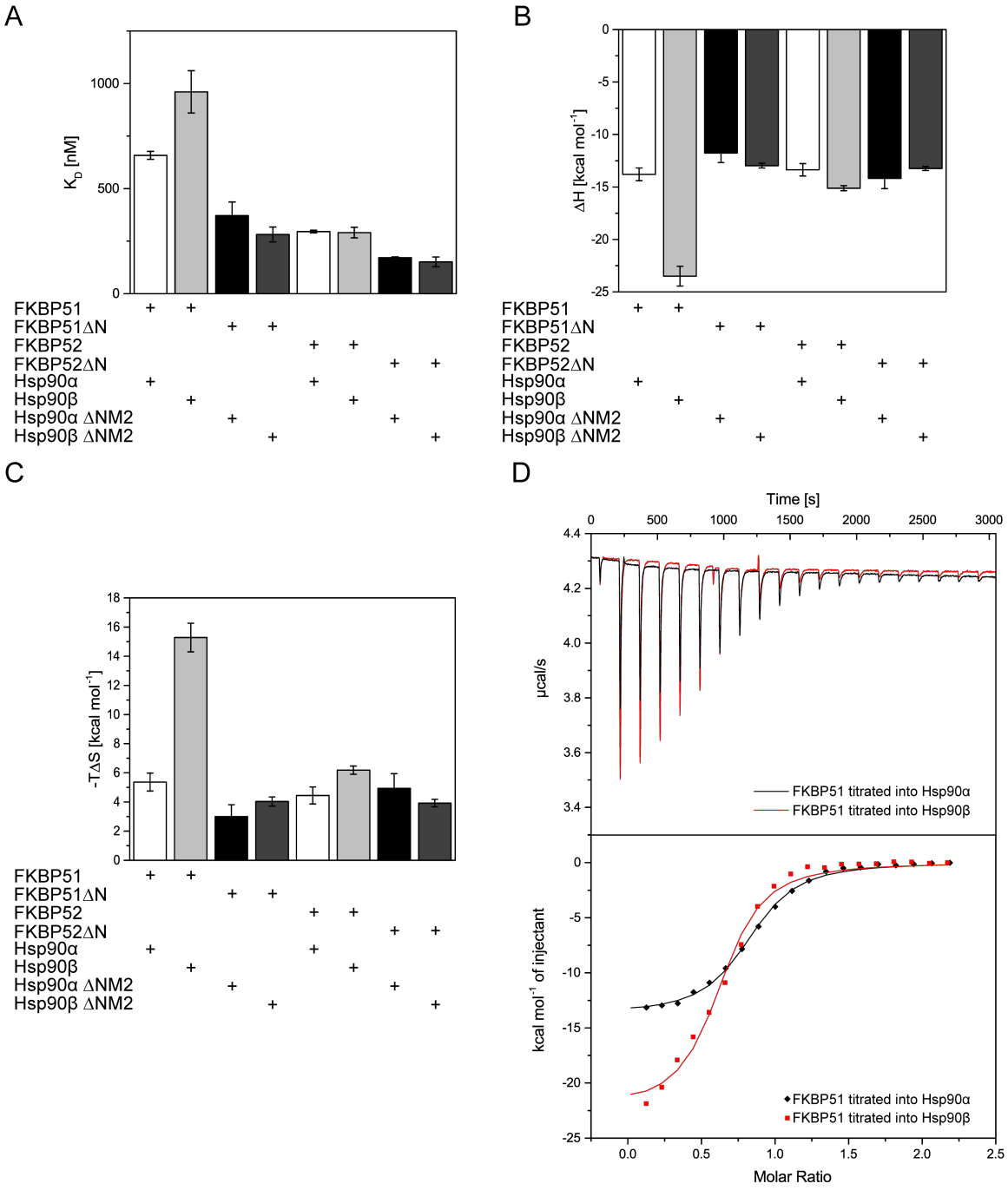

Figure 19: Comparison of ITC studies of FKBP51 and FKBP52 with Hsp90α and β. K_D (A), enthalpic (B), and entropic (C) analysis of FKBP51 and FKBP52 constructs binding to Hsp90α and Hsp90β constructs. All experiments were carried out in triplicates. Data are shown as mean ± SD. (D) ITC titrations of full-length FKBP51 with either full-length Hsp90α (black) or Hsp90β (red).

FKBP51 and FKBP52 bound with the same affinity to Hsp90α and Hsp90β (Fig. 19A). Neither binding enthalpies nor entropies showed a difference between binding of FKBP51 or FKBP52 to Hsp90α and Hsp90β (Fig. 19B and C). One outlier is the titration of full-length FKBP51 and Hsp90β, which yielded higher enthalpic and entropic contributions in comparison to FKBP51 and Hsp90α (Fig. 19B and C). In contrast to the titration of FKBP51 with Hsp90α,

the titration with Hsp90β showed a steep slope at the beginning which is not completely represented by a sigmoidal curve (Fig. 19D). Thus, the data has to be carefully interpreted as the quality of the fit is low. An overview of all measured Hsp90β combinations is shown in Table 17. In conclusion, FKBP51 and FKBP52 bind with the same affinity to Hsp90α and Hsp90β, indicating no effect of the minor sequence differences of the two isoforms on the interaction.

Table 17: Results of ITC experiments with FKBP51/52 and Hsp90β. All experiments were carried out in triplicates. Data are shown as mean ± SD.

FKBP51	K_D [nM]	ΔG [$\frac{kcal}{mol}$]	ΔH [$\frac{kcal}{mol}$]	-TΔS [$\frac{kcal}{mol}$]	N
Hsp90β	960±100	-8.2±0.1	-23.5±1.0	15.3±1.0	0.7±0.1
FKBP51ΔN	**K_D [nM]**	**ΔG [$\frac{kcal}{mol}$]**	**ΔH [$\frac{kcal}{mol}$]**	**-TΔS [$\frac{kcal}{mol}$]**	**N**
Hsp90βΔN	404±89	-8.7±0.1	-15.2±0.5	6.5±0.4	1.0±0.1
Hsp90βΔNM2	282±36	-8.9±0.1	-13.0±0.2	4.0±0.3	0.8±0.0
FKBP51ΔN2	**K_D [nM]**	**ΔG [$\frac{kcal}{mol}$]**	**ΔH [$\frac{kcal}{mol}$]**	**-TΔS [$\frac{kcal}{mol}$]**	**N**
Hsp90βΔN	167±22	-9.2±0.1	-12.5±0.6	3.3±0.7	0.9±0.0
Hsp90βΔNM2	179±23	-9.2±0.1	-10.8±0.2	1.6±0.3	1.0±0.0
FKBP52	**K_D [nM]**	**ΔG [$\frac{kcal}{mol}$]**	**ΔH [$\frac{kcal}{mol}$]**	**-TΔS [$\frac{kcal}{mol}$]**	**N**
Hsp90β	291±25	-8.9±0.1	-15.1±0.2	6.2±0.3	0.7±0.1
FKBP52ΔN	**K_D [nM]**	**ΔG [$\frac{kcal}{mol}$]**	**ΔH [$\frac{kcal}{mol}$]**	**-TΔS [$\frac{kcal}{mol}$]**	**N**
Hsp90βΔN	195±15	-9.2±0.0	-15.3±0.2	6.2±0.3	0.8±0.0
Hsp90βΔNM2	151±23	-9.3±0.1	-13.2±0.2	3.9±0.3	0.8±0.0
FKBP52ΔN2	**K_D [nM]**	**ΔG [$\frac{kcal}{mol}$]**	**ΔH [$\frac{kcal}{mol}$]**	**-TΔS [$\frac{kcal}{mol}$]**	**N**
Hsp90βΔN	145±71	-9.4±0.4	-14.6±1.4	5.2±1.7	0.9±0.0
Hsp90βΔNM2	144±26	-9.3±0.1	-11.1±1.1	1.8±1.1	0.8±0.1

4.2 Structural investigation of FKBP51/52 and Hsp90α/β

4.2.1 FKBP51 and Hsp90α form a stable complex

As shown in section 4.1.2, the interaction between FKBP51 and Hsp90α is in the nanomolar range under certain conditions. As the thesis aims at the structural and biophysical elucidation of FKBP51 and Hsp90 complexes, analytical SEC feasibility studies were carried out to determine if purification of a stable complex for structural studies is possible.

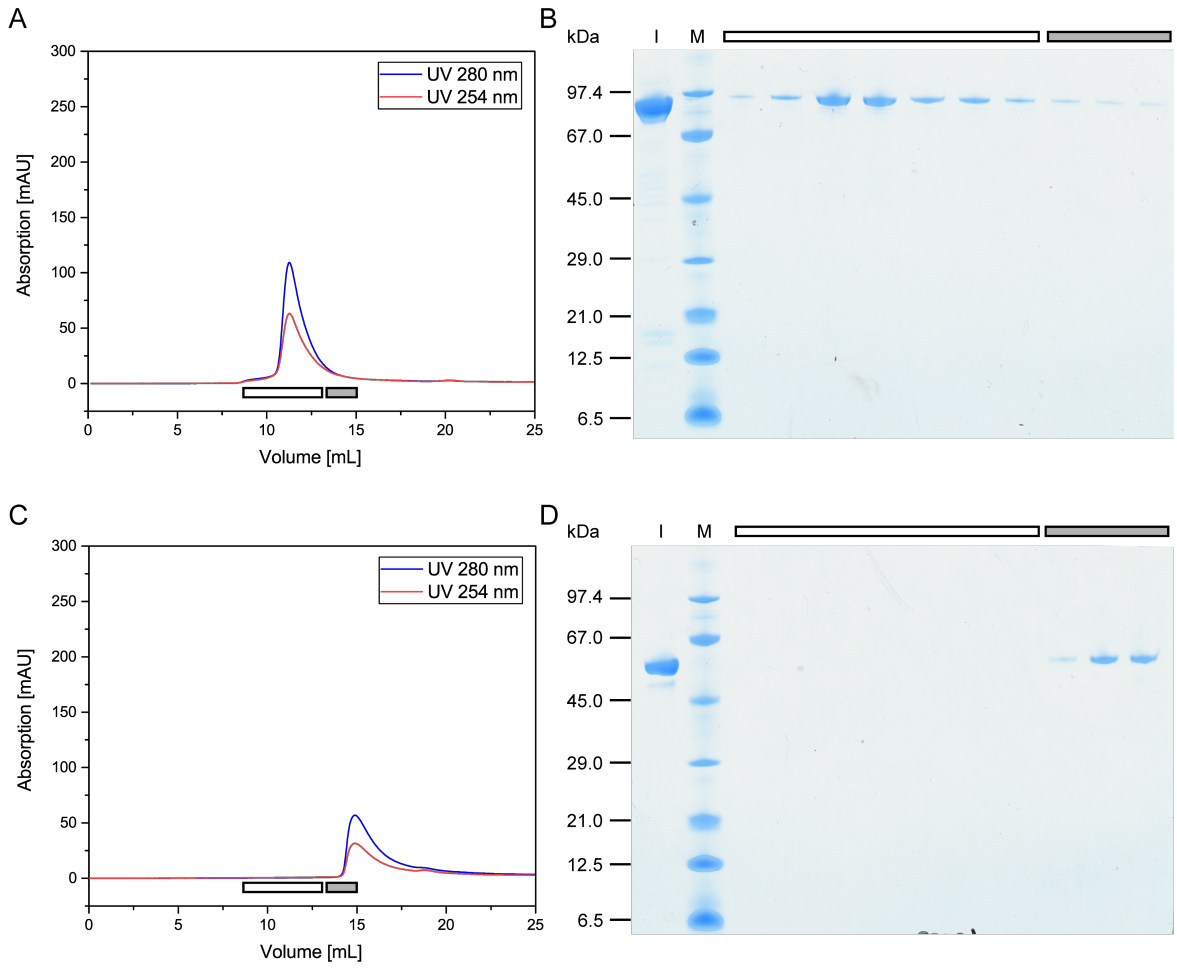

Figure 20: SEC chromatograms of Hsp90α and FKBP51 on a Superdex^{TM} 200 Increase 10/300 GL column. (A) SEC chromatogram of 75 µM Hsp90α. (B) Corresponding SDS-PAGE of Hsp90α SEC. (C) SEC chromatogram of 75 µM FKBP51. (D) Corresponding SDS-PAGE of FKBP51 SEC. Input fractions are marked with an I. The loaded marker lane is abbreviated with an M. The white bar covers fraction containing Hsp90α, whereas the grey bar highlights fractions containing FKBP51. UV absorption was detected at 254 nm and 280 nm.

Full-length Hsp90α eluted at 11.26 mL (Fig. 20A) and full-length FKBP51 at 14.88 mL (Fig. 20C). SDS-PAGE analysis revealed that Hsp90α and FKBP51 run below 97.4 kDa and between 45 and 67 kDa, respectively (Fig. 20B and 20D). The white bar covers fractions containing Hsp90α alone, whereas the grey bar highlights fractions only containing FKBP51 (Fig. 20B and 20D). Thus, both proteins could be separated during SEC. An Hsp90α:FKBP51

complex was preformed in a stoichiometry of 1:1.5. To shift the equilibrium towards complex formation, complex buffer (Table 9) was added to yield final protein concentrations of 75 µM and 112.5 µM for Hsp90α and FKBP51, respectively.

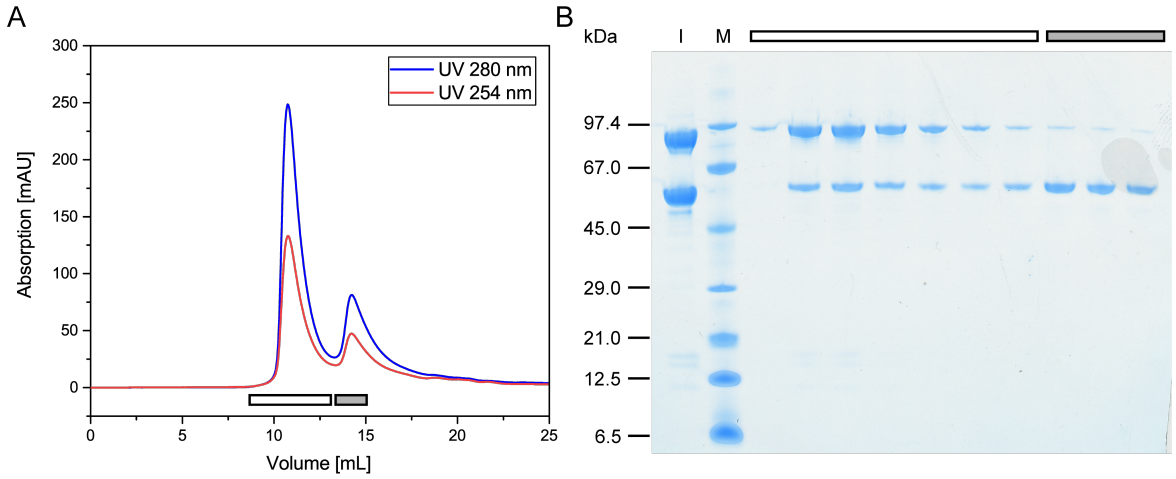

Figure 21: Complex formation of Hsp90α and FKBP51 on a Superdex^{TM} 200 Increase 10/300 GL column. (A) SEC chromatogram of a mixture containing Hsp90α and FKBP51 in 1:1.5 stoichiometry. (B) Corresponding SDS-PAGE of the SEC. The white bar covers fraction containing Hsp90α:FKBP51. The grey bar covers fractions with only FKBP51.

Two peaks were eluted with retention volumes of 10.75 mL (peak 1) and 14.23 mL (peak 2) (Fig. 21A). SDS-PAGE analysis confirmed complex formation by resolving two bands in the same fractions (white bar). To further characterize the complex, its thermal stability was determined using nanoDSF.

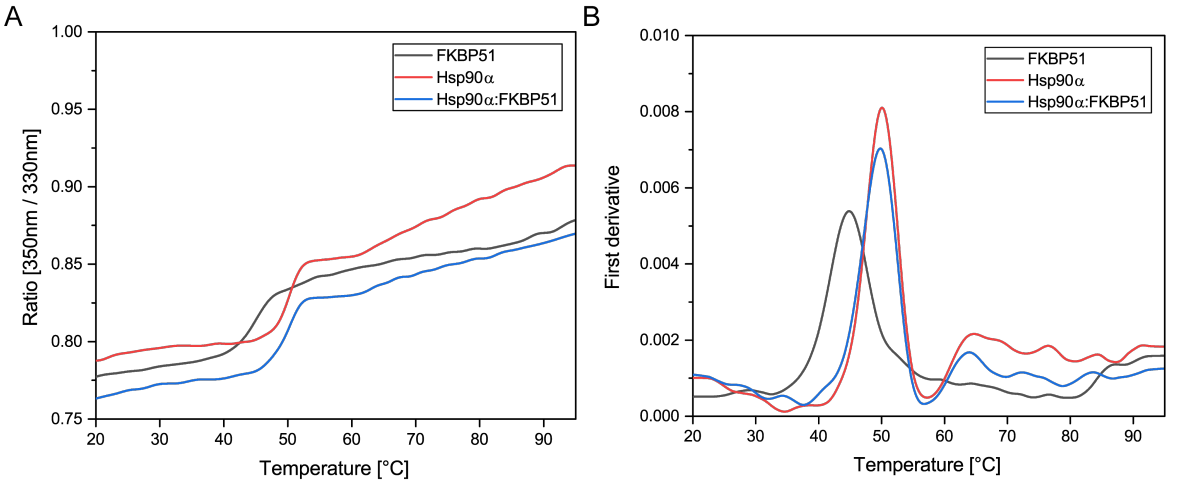

Figure 22: Melting curves of FKBP51, Hsp90α, and Hsp90α:FKBP51 measured by nanoDSF. (A) Ratio of fluorescence intensities at 350 nm and 330 nm depending on the temperature of the samples. (B) First derivative of the ratio curves. The three maxima show the T_m for FKBP51 (black), Hsp90α (red), and Hsp90α:FKBP51 (blue).

Melting curves are depicted in Fig. 22. The left part, Fig.22A, shows the ratio of fluorescence intensities at 350 nm and 330 nm for a temperature range from 20°C to 95°C. The melting

temperature (T_m) of the protein can be determined as the inflection point of the fluorescence curve. In general, the first derivative of the curve is calculated to transform the inflection point into a maximum (Fig. 22B). The determined T_m values were 44.8 °C (FKBP51), 50.0 °C (Hsp90α), and 49.7 °C (Hsp90α:FKBP51) (Table 18). The complex sample only showed one inflection point, thereby confirming complex formation of Hsp90α and FKBP51.

Table 18: T_m determined by nanoDSF for FKBP51, Hsp90α, and Hsp90α:FKBP51.

Sample	T_m [°C]
FKBP51	44.8
Hsp90α	50.0
Hsp90α:FKBP51	49.7

4.2.2 FKBP51 is more compact in solution than FKBP52

The Hsp90 system is highly dynamic and flexible, which has made crystallographic and cryo-EM studies difficult. Most structures of Hsp90 in complex with co-chaperones have been solved with yeast Hsp90 (Ali et al., 2006; Meyer et al., 2004; Roe et al., 2004). In recent years, Verba et al. (2016) were able to solve a high resolution structure of full-length human Hsp90β in complex with Cdk4 and Cdc37. To get a better understanding of the dynamics of Hsp90α:FKBP51/52 complexes, size-exclusion chromatography coupled to small-angle X-ray scattering (SEC-SAXS) in the presence and absence of ATP was performed to analyze the interaction of Hsp90α and FKBP51/52 in solution. Dr. Claire Pizzey carried out the experiments at beamline B21 at the Diamond Light Source. As a first step, the PPIases were analyzed alone.

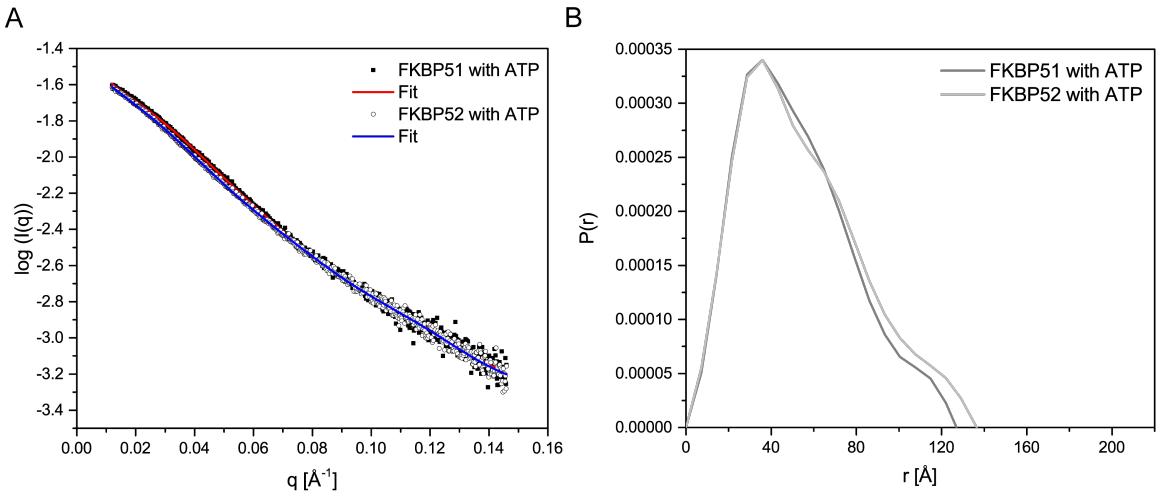

Figure 23: SAXS measurements of FKBP51 and FKBP52 in the presence of ATP. (A) Normalized scattering of FKBP51 (black square) and FKBP52 (circle) with ATP. (B) SAXS radial density distribution measurements of FKBP51 (dark grey) and FKBP52 (grey) with ATP.

For FKBP51 and FKBP52, one maximum could be observed in the SAXS radial density distribution P(r) in the presence of ATP (Fig. 23B). A D_{max} of 127 Å was determined for FKBP51 and 136 Å for FKBP52 (Fig. 23B). The radius of gyration (R_g) revealed differences for FKBP51 (46.53 Å) and FKBP52 (49.07 Å). The higher R_g of FKBP52 hints at a higher flexibility and/or a different domain orientation compared to FKBP51. The molecular mass was determined to be 72 kDa for both PPIases. The obtained solution properties of FKBP51 and FKBP52 are shown in Table 19.

Table 19: Results of SAXS experiments for FKBP51 and FKBP52.

	Nucleotide	R_g [Å]	D_{max} [Å]	M_w [kDa]
FKBP51	ATP	45.58	127	72
FKBP52	ATP	49.07	136	72

Ab initio models were calculated using the program DAMMIN (13 runs, cluster analysis) (Volkov and Svergun, 2003). The averaged models were converted into a density map using Chimera and X-ray structures of FKBP51 or FKBP52 were superimposed with the maps for size comparison (Fig. 24A and 24B) (Pettersen et al., 2004).

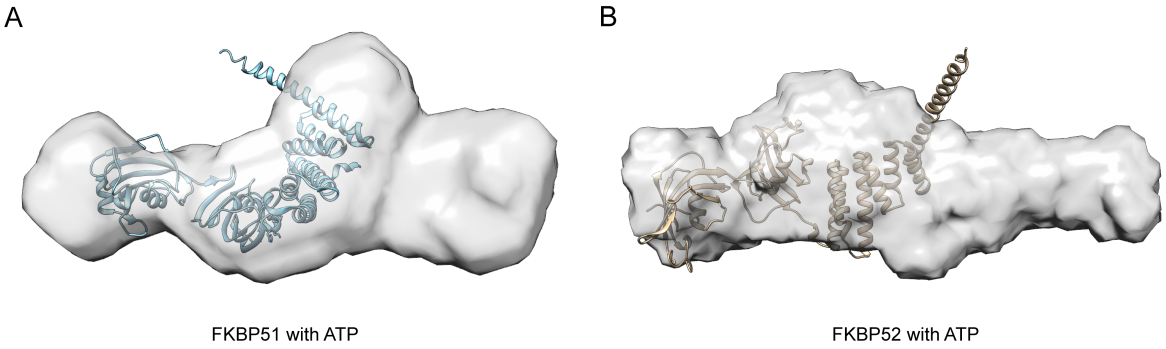

Figure 24: SAXS-derived *ab initio* models of FKBP51 and FKBP52 in the presence of ATP. (A) Derived SAXS envelope of FKBP51 in the presence of ATP with the crystal structure of FKBP51 superimposed (PDB ID 5NJX) (Kumar et al., 2017). (B) Derived SAXS envelope of FKBP52 in the presence of ATP with the crystal structures of FKBP52 superimposed (PDB ID 1P5Q and 1Q1C) (Wu et al., 2004).

The superimposed X-ray structures did not completely fill out the *ab initio* models (Fig. 24). The shapes of both models are elongated and best described as dumbbells. In contrast to FKBP52, the molecular shape of FKBP51 showed an extra extrusion (upwards), which could hint that the TPR domain can adopt different conformations (Fig. 24A). The results indicate that although FKBP51 and FKBP52 are composed of the same domains, the domains are differently orientated to each other in both proteins.

4.2.3 SAXS reveals differences between Hsp90α and Hsp90β in solution

The amino acid differences between Hsp90α and Hsp90β did not impact binding of FKBP51 and FKBP52. However, these differences between Hsp90α and Hsp90β could translate to structural changes in presence and absence of ATP. SAXS was used to compare Hsp90α and Hsp90β in solution.

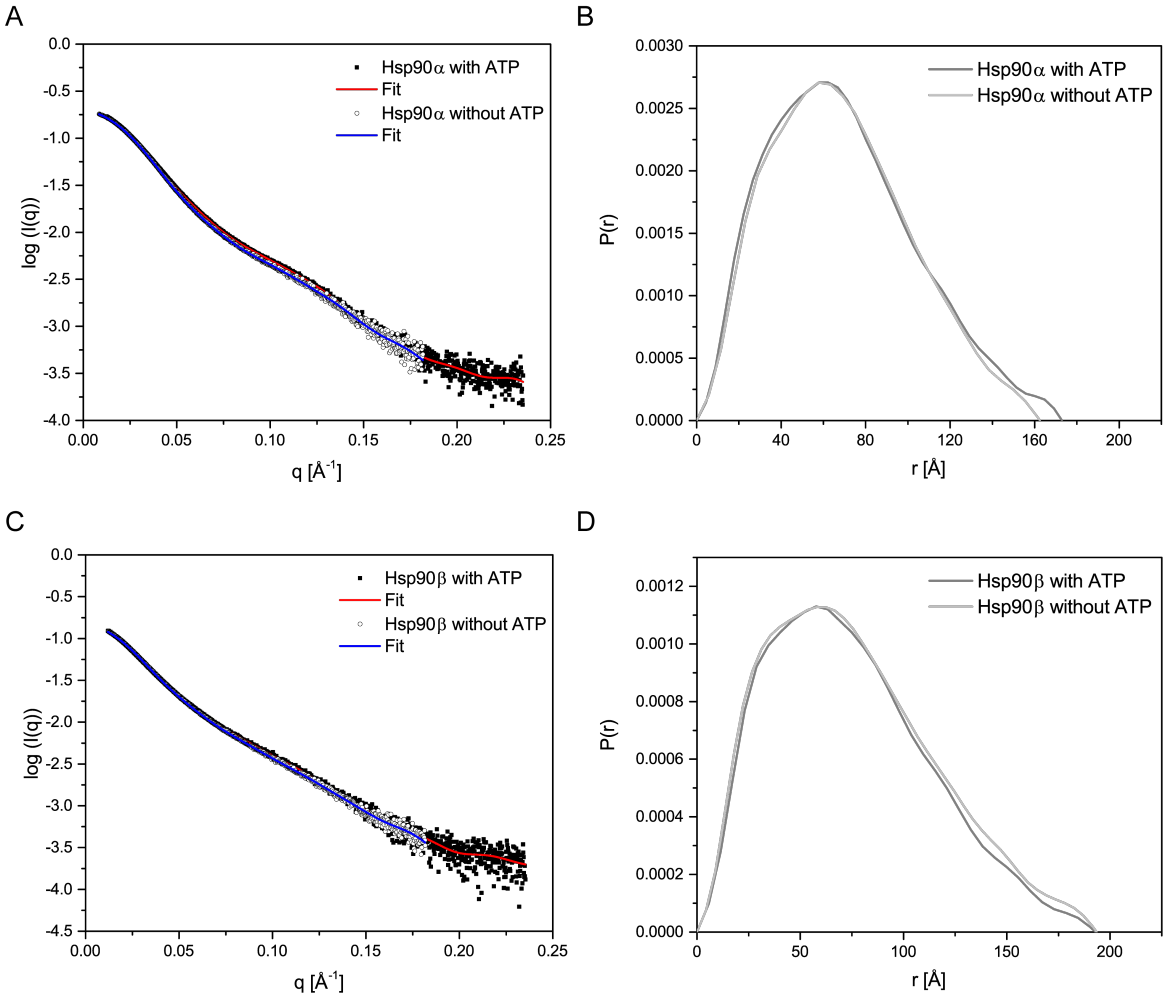

Figure 25: SAXS measurements of Hsp90α and Hsp90β in the presence and absence of ATP. (A) Normalized scattering of Hsp90α in the presence (black square) and absence (circle) of ATP. (B) SAXS radial density distribution measurements of Hsp90α in the presence (dark grey) and absence (grey) of ATP. (C) Normalized scattering of Hsp90β in the presence (black square) and absence (circle) of ATP. (D) SAXS radial density distribution measurements of Hsp90β in the presence (dark grey) and absence (grey) of ATP.

SAXS analysis showed one maximum for Hsp90α and Hsp90β in the P(r) distribution in the presence and absence of ATP (Fig. 25B and D). For Hsp90α, a D_{max} of 173 Å was determined in the presence of ATP and 162 Å in absence of ATP (Fig. 25B). The R_g was also similar in the presence of ATP (55.44 Å) and absence of ATP (53.99 Å). The molecular mass was 202 kDa (Hsp90α·ATP) and 215 kDa (without ATP), corresponding to a Hsp90α dimer. For Hsp90β, the D_{max} did not change in the presence or absence of ATP (193 Å). The R_g

was determined to be 61.55 Å (with ATP) and 59.70 Å (without ATP). The molecular mass of Hsp90β in solution was 199 kDa (without ATP) and 194 kDa (with ATP), indicating a Hsp90β dimer. The obtained solution properties of Hsp90α and Hsp90β are shown in Table 20.

Table 20: Results of SAXS experiments for Hsp90α and Hsp90β.

	Nucleotide	R_g [Å]	D_{max} [Å]	M_w [kDa]
Hsp90α	-	53.99	162	215
Hsp90α	ATP	55.44	173	202
Hsp90β	-	59.70	193	199
Hsp90β	ATP	61.55	193	194

Ab initio models were again calculated using the program DAMMIN (13 runs, cluster analysis). The averaged models were converted into a density map using Chimera and SAXS or cryo-EM structures of the open or closed Hsp90 conformation were superimposed onto the maps (Fig. 26).

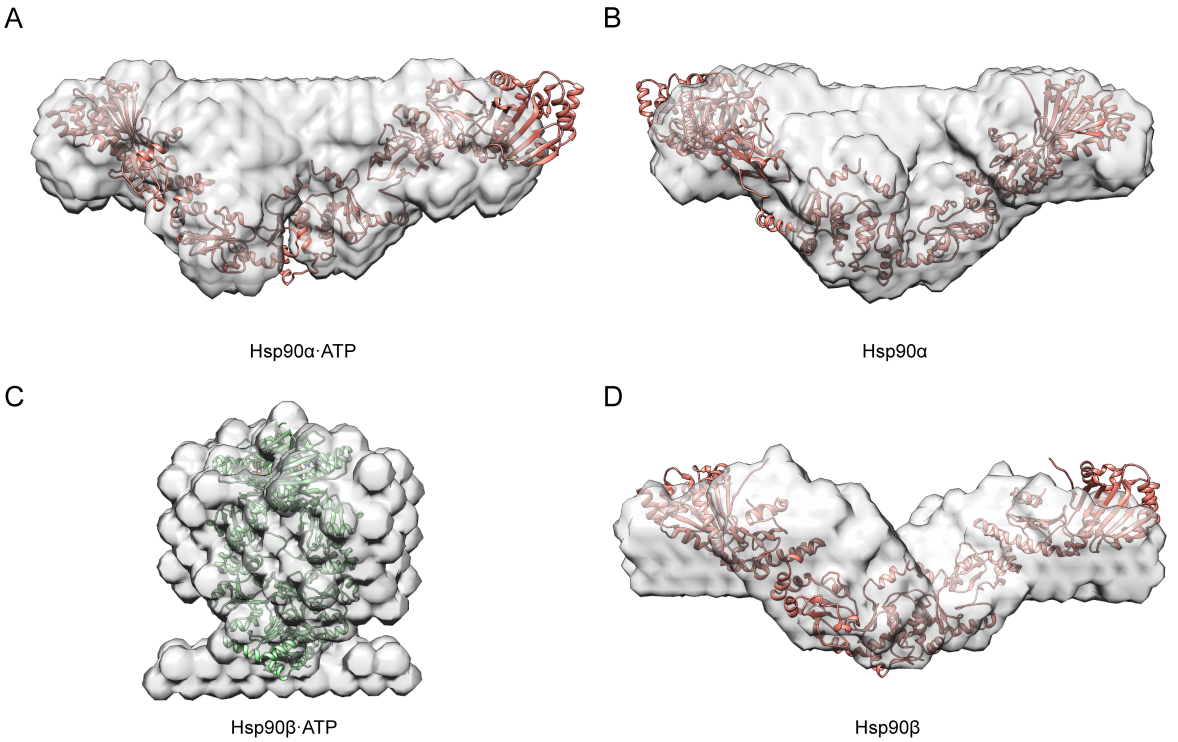

Figure 26: SAXS-derived *ab initio* models of Hsp90α and Hsp90β in the presence and absence of ATP. Hsp90α SAXS envelope in the presence of ATP (A) and absence of ATP (B) with a solution SAXS model of Hsp90α superimposed (Krukenberg et al., 2009). (C) Hsp90β SAXS envelope in the presence of ATP with a closed Hsp90β cryo-EM structure superimposed (Verba et al., 2016). (D) Hsp90β SAXS envelope in the absence of ATP with a solution structure of Hsp90α superimposed.

Hsp90α revealed similar models with and without ATP (Fig. 26A and B). The extended, open conformation can be superimposed with both *ab initio* models. In the presence of ATP, a

closed Hsp90β dimer was superimposed with the *ab initio* model, while the model represented the shape of an extended, open confirmation in the absence of ATP (Fig. 26C and 26D). In conclusion, the differences at the amino acid level between Hsp90α and Hsp90β seem to affect the structure in solution with Hsp90β being able to stay in the closed ATP formation longer.

4.2.4 FKBP51 and FKBP52 interact differently with Hsp90α

The determination of the SAXS profiles of Hsp90α, FKBP51, and FKBP52 was necessary to analyze Hsp90α:PPIase complexes. Binary complexes were formed under the same conditions as in section 4.2.1.

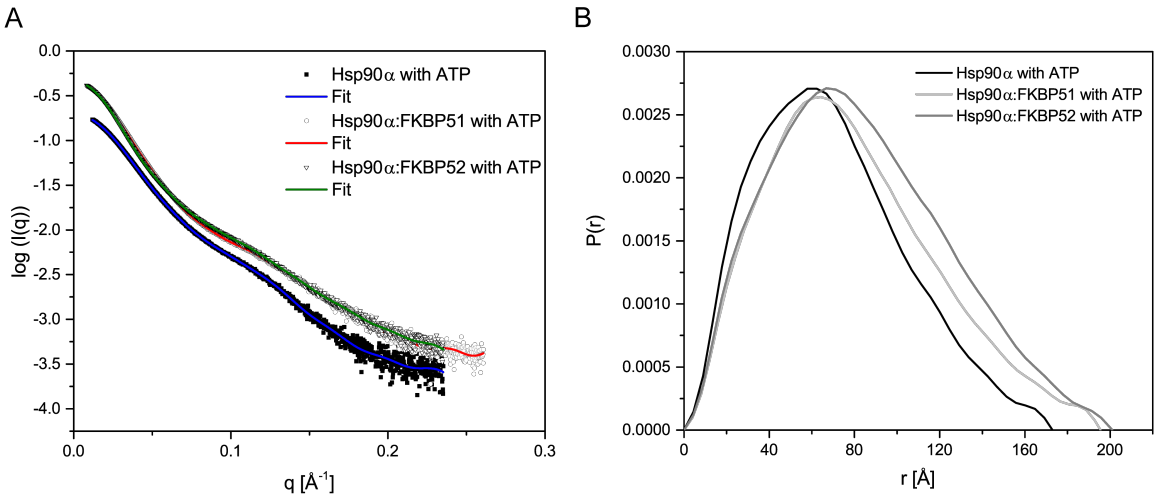

Figure 27: SAXS measurements of Hsp90α·ATP:FKBP51/52 complexes. (A) Normalized scattering of Hsp90α (black square), Hsp90α:FKBP51 (circle), and Hsp90α:FKBP52 (triangle) in the presence of ATP. (B) SAXS radial density distribution measurements of Hsp90α (black), Hsp90α:FKBP51 (light grey), and Hsp90α:FKBP52 (grey) in the presence of ATP.

Hsp90α·ATP:FBKP51 and Hsp90α·ATP:FKBP52 complexes revealed distinct features in comparison to apo Hsp90α (Fig. 27B). SAXS analysis showed one maximum for both complexes in the P(r) distribution (Fig. 27B). A D_{max} of 195 Å was determined for Hsp90α·ATP:FKBP51 and 201 Å for Hsp90α·ATP:FKBP52 (Fig. 27B). The latter complex had a higher R_g (64.64 Å) than Hsp90α:FKBP51 (61.78 Å). The molecular mass in solution was 289 kDa and 301 kDa, yielding stoichiometries of $(Hsp90\alpha)_2$:$(FKBP51)_1$ and $(Hsp90\alpha)_2$:$(FKBP52)_1$, respectively. The obtained solution properties of Hsp90α·ATP:FKBP51 and Hsp90α·ATP:FKBP52 are shown in Table 21.

Table 21: Results of SAXS experiments for Hsp90α:FKBP51 and Hsp90α:FKBP52 in comparison to only Hsp90α, FKBP51, and FKBP52.

	Nucleotide	R_g [Å]	D_{max} [Å]	M_w [kDa]
Hsp90α	-	53.99	162	215
Hsp90α	ATP	55.44	173	202
FKBP51	ATP	45.58	127	72
FKBP52	ATP	49.07	136	72
Hsp90α:FKBP51	ATP	61.78	195	289
Hsp90α:FKBP52	ATP	64.64	201	301

Ab initio models were again calculated using the program DAMMIN (13 runs, cluster analysis). The averaged models were converted into density maps using Chimera and structures were superimposed onto the maps taking into account the obtained stoichiometries (Fig. 28).

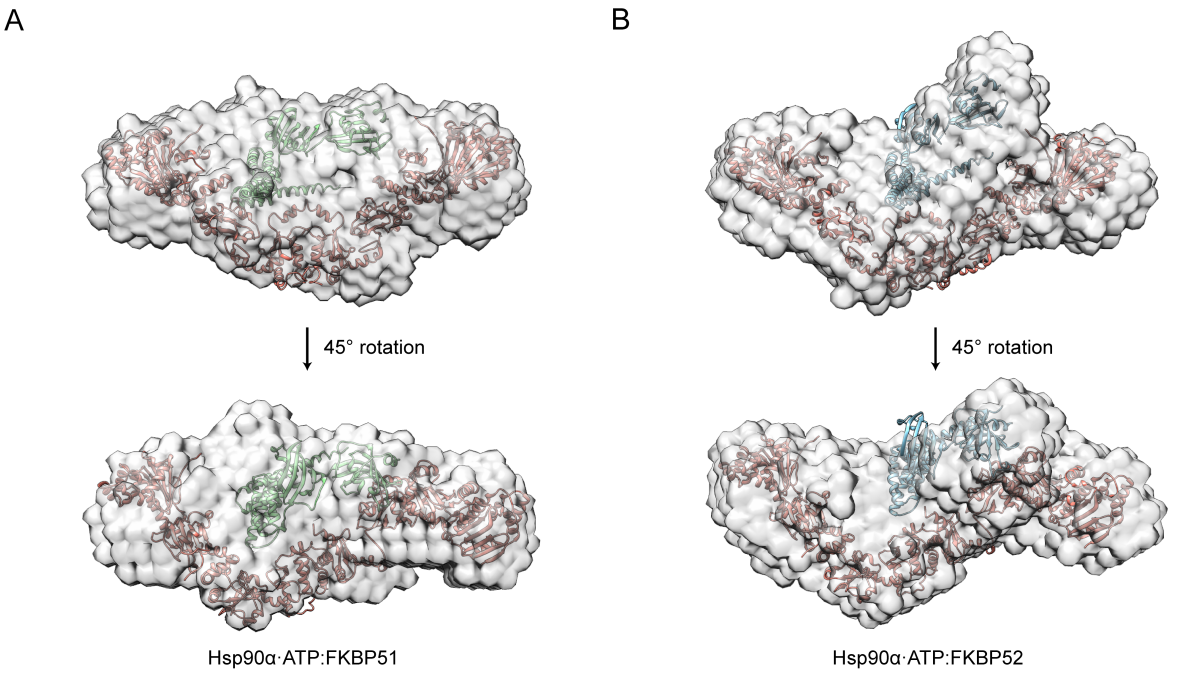

Figure 28: SAXS-derived *ab initio* models of Hsp90α·ATP:FKBP51/52 complexes. (A) SAXS model of Hsp90α·ATP:FKBP51 superimposed with the crystal structure of FKBP51 (PDB ID 5NJX) and the SAXS structure of Hsp90α in an extended conformation (Kumar et al., 2017). (B) SAXS model of Hsp90α·ATP:FKBP52 superimposed with the crystal structures of FKBP52 (PDB ID 1P5Q and 1Q1C) and a SAXS structure of Hsp90α in an extended conformation (Wu et al., 2004; Krukenberg et al., 2009).

The molecular shape of Hsp90α·ATP:FKBP51 showed a more compact structure in comparison to Hsp90α·ATP:FKBP52 (Fig. 28A and 28B). In contrast, the shape of Hsp90α·ATP:FKBP52 displayed a protrusion on one side (Fig. 28B). Overall, the SAXS experiments provide evidence that FKBP51 interacts differently with Hsp90α compared to FKBP52.

4.3 Co-chaperones influence hormone association to GR

4.3.1 GR-LBDm associates with Hsp90α

GR, a ligand-activated transcription factor, regulates numerous genes (Heitzer et al., 2007). The LBD of GR is necessary to interact with Hsp90 (Howard et al., 1990). The maturation of GR is maintained by a set of Hsp90 co-chaperones, which at least includes Hsp40, Hsp70, Hop and p23 (Kirschke et al., 2014; Lorenz et al., 2014). GR translocates into the nucleus upon ligand binding and regulates the expression of glucocorticoid-responsive genes (Zhou and Cidlowski, 2005). There is evidence that some co-chaperones modulate the response to hormones and thereby regulate GR function. The influence of co-chaperones on GR *in vitro* has been studied by monitoring the binding of fluorescein-labeled dexamethasone (F-DEX) by FP (Kirschke et al., 2014; Lorenz et al., 2014; Rutz et al., 2018). In this thesis, a GR-LBD construct harboring five stabilizing point mutations (F602S/A605V/V702A/E705G/M752T, abbreviated as GR-LBDm) was used to increase purification yields and protein stability (Seitz et al., 2010). To confirm that GR-LBDm still adequately bound hormone, GR-LBDm was titrated into F-DEX.

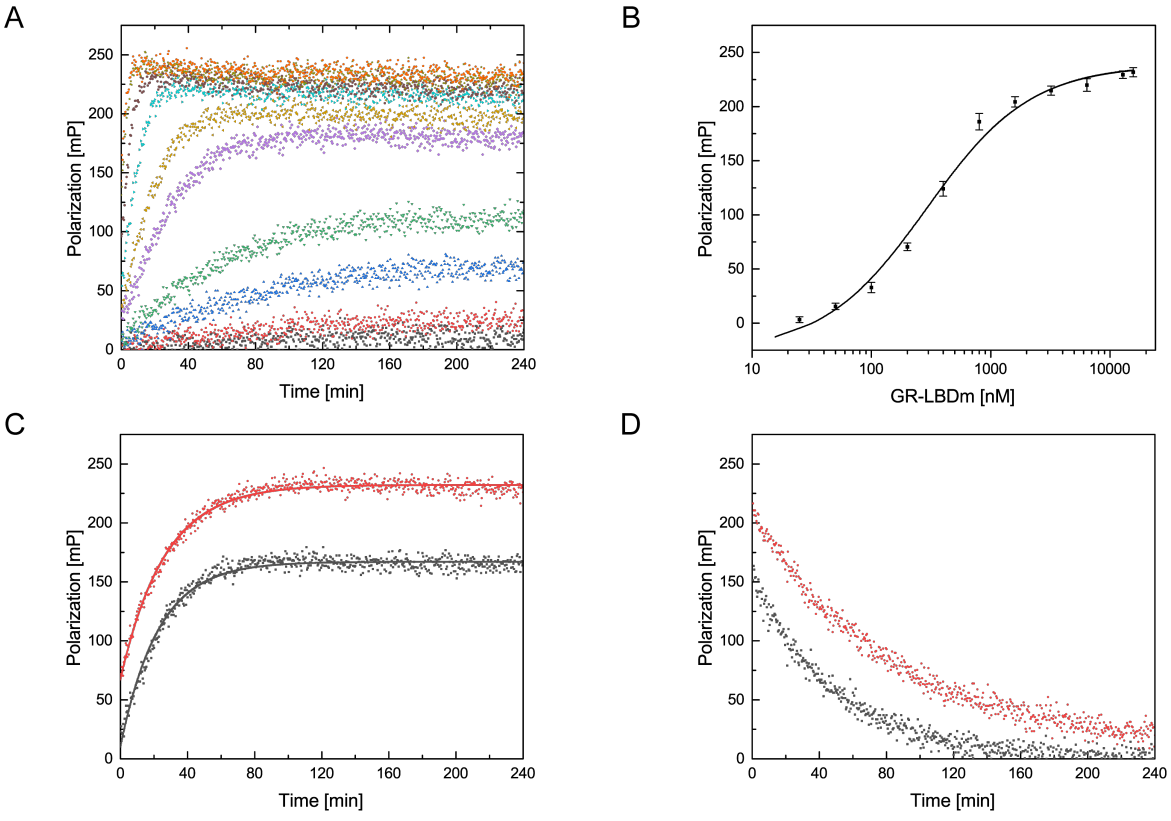

Figure 29: Hormone association to apo GR-LBDm alone and in complex with Hsp90α. (A) Association kinetics of 0.050 to 15.6 µM GR-LBDm to 50 nM F-DEX. (B) Equilibrium binding of 50 nM F-DEX to GR-LBDm measured by FP. Data are shown as mean of four independent experiments (± SD). Fitting the titration data yielded a K_D of 293±41 nM (±SD). (C) Binding of 50 nM F-DEX to 1 µM apo GR-LBDm in black or to 1 µM apo GR-LBDm and 12 µM Hsp90α in red. (D) Hormone dissociation kinetics were induced by adding an excess of 100 µM DEX to 50 nM F-DEX and 1 µM GR-LBDm (black) or to 50 nM F-DEX, 1 µM GR-LBDm, and 12 µM Hsp90α (red).

The stabilized GR mutant GR-LBDm bound F-DEX (Fig. 29A) with a K_D of 293±41 nM (Fig. 29B). To determine if Hsp90α influences the K_D of GR-LBDm and F-DEX, one would theoretically add Hsp90α in a 12-fold excess during the GR-LBDm titration to ensure complete Hsp90:GR formation. Consequently, 187.2 µM Hsp90α would have been required to be added at the highest GR-LBDm concentration (15.6 µM). This was not feasible as the Hsp90α material was limited and it was above the Hsp90α stock concentration. Hsp90α and GR-LBDm were preincubated before association experiments were carried out to test if Hsp90α influences hormone binding. The presence of Hsp90α led to a higher overall polarization signal, corresponding to a larger complex and showing that Hsp90α binds to GR-LBDm (Fig. 29C). Hsp90α did not affect hormone binding to GR-LBDm (k_{obs} 0.038±0.004 and 0.034±0.005 min^{-1}). The addition of unlabeled DEX to GR-LBDm:F-DEX or Hsp90α:GR-LBDm:F-DEX in steady-state showed that F-DEX is displaced faster from GR-LBDm than from Hsp90α:GR-LBDm (k_{obs} 0.021±0.002 and 0.013±0.001 min^{-1}) (Fig. 29D). The interaction with Hsp90α could stabilize or induce a conformation that keeps GR in a hormone-bound active state.

4.3.2 PPIases prolong hormone association

The influence of FKBP51 and FKBP52 on hormone-dependent gene activation has been studied *in vivo* in *Saccharomyces cerevisiae* (*S.cerevisiae*) (Riggs et al., 2003). An *S.cerevisiae* reporter model with expression plasmids for GR, either FKBP51 or FKBP52, and a lacZ reporter plasmid was used to determine PPIase effects on hormone-dependent gene activation upon hormone treatment. It was shown that only FKBP52 potentiates glucocorticoid signaling, while FKBP51 did not have any effect on hormone signaling (Riggs et al., 2003). The opposing effects were primarily mapped to the FK1 domain (Riggs et al., 2003, 2007). In the previous section, it was shown that GR-LBDm binds hormone with and without Hsp90α. To get a better understanding of the opposing roles, the effects of FKBP51 and FKBP52 on hormone binding *in vitro* were investigated.

FKBP51 and FKBP52 affected hormone association to Hsp90α:GR-LBDm (Fig. 30A and 30B). The determined k_{obs} was 0.034±0.0015 min^{-1} for Hsp90α:GR-LBDm (Fig. 30C). A 2.4- and 8.5-fold reduction in hormone association was observed in comparison to Hsp90α:GR-LBDm in the presence of FKBP51 or FKBP52, respectively (Fig. 30C). Hsp90α was necessary to mediate the interaction and bring FKBP51/52 in close proximity to GR-LBDm (Fig. 30C). Deletion of the FK1 domain on either FKBP51 or FKBP52 accelerated hormone binding to almost Hsp90α:GR-LBDm levels (0.7- and 0.8-fold) (Fig. 30C). The assay was validated by the addition of 480 µM 15mer Hsp90α peptide, which should displace FKBP51 and FKBP52 from Hsp90α:GR-LBDm complexes and thus increase hormone association. In case of full-length PPIases, hormone association was accelerated 2.2- and 5.8-fold for FKBP51 and FKBP52, respectively, in the presence of 480 µM 15mer Hsp90α peptide (Fig. 30D). The determined k_{obs} and fold change values are shown in Table 22. In conclusion, the *in vitro* GR hormone association data shows differential effects of FKBP51 and FKBP52 and identified the FK1

domain as a key mediator of those effects. Intriguingly, FKBP52 strongly reduced hormone binding which is surprising as it was shown to have a potentiating effect *in vivo* (Riggs et al., 2003).

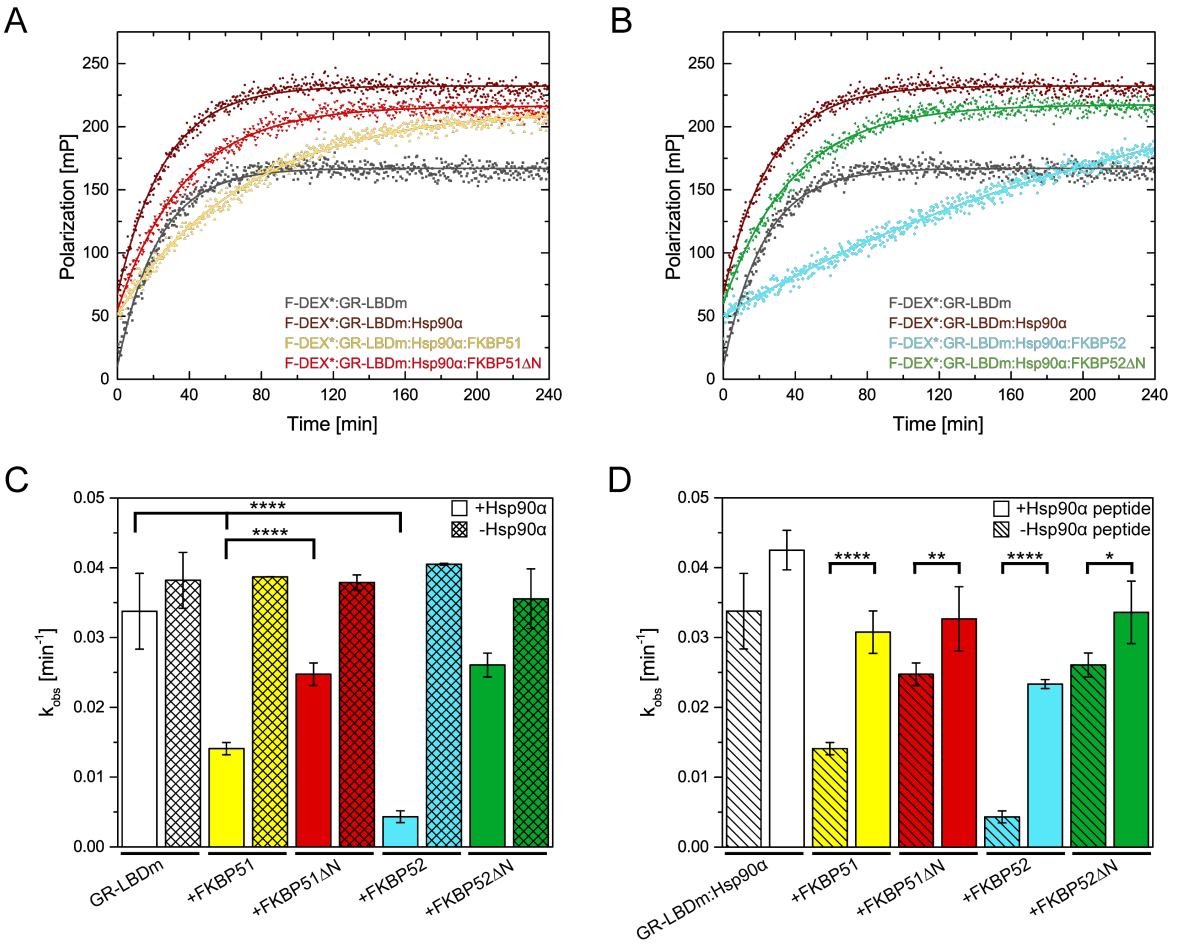

Figure 30: Hormone association experiments with apo GR-LBDm, Hsp90α, and PPIases. (A) Binding of 50 nM F-DEX to 1 µM apo GR-LBDm (dark grey), with 12 µM Hsp90α (brown), with 12 µM Hsp90α + 12 µM FKBP51 (yellow), and with 12 µM Hsp90α + 12 µM FKBP51ΔN (red). (B) Binding of 50 nM F-DEX to 1 µM apo GR-LBDm (dark grey), with 12 µM Hsp90α (brown), with 12 µM Hsp90α + 12 µM FKBP52 (light blue), and with 12 µM Hsp90α + 12 µM FKBP52ΔN (green). Fluorescently labeled component is marked with an asterisk. (C) Effect of PPIases on hormone binding to GR-LBDm in the presence (pattern-less) and absence (crossed pattern) of Hsp90α. (D) Effect of PPIases on hormone binding to Hsp90α:GR-LBDm in the presence (pattern-less) and absence (striped pattern) of a 15mer C-terminal Hsp90α peptide. Data are shown as mean values from four to six experiments (± SD). Experiments to investigate the effect of PPIases in the absence of Hsp90α were carried out as duplicates. Statistical significance was assessed using a two-sample *t*-test and a significance level of 0.05. Statistical significance is indicated with $p < 0.05$ (*), $p < 0.01$ (**), $p < 0.001$ (***), and $p < 0.0001$ (****).

Table 22: Effect of PPIases and 15mer Hsp90α peptide on hormone association in Hsp90α:GR-LBDm complexes. Average k_{obs} values are shown (±SD). Fold change is shown in relation to Hsp90α:GR-LBDm.

-Hsp90α			k_{obs} [min^{-1}]	Fold change
GR-LBDm			0.038±0.004	1.1
GR-LBDm		FKBP51	0.039±0.000	1.1
GR-LBDm		FKBP51ΔN	0.038±0.001	1.1
GR-LBDm		FKBP52	0.041±0.000	1.2
GR-LBDm		FKBP52ΔN	0.036±0.004	1.1

+Hsp90α				k_{obs} [min^{-1}]	Fold change
GR-LBDm				0.038±0.004	1.1
GR-LBDm	Hsp90α			0.034±0.005	1.0
GR-LBDm	Hsp90α	FKBP51		0.014±0.001	0.4
GR-LBDm	Hsp90α	FKBP51ΔN		0.025±0.002	0.7
GR-LBDm	Hsp90α	FKBP52		0.004±0.001	0.1
GR-LBDm	Hsp90α	FKBP52ΔN		0.026±0.002	0.8

+15mer Hsp90α peptide				k_{obs} [min^{-1}]	Fold change
GR-LBDm			peptide	0.040±0.003	1.2
GR-LBDm	Hsp90α		peptide	0.043±0.003	1.3
GR-LBDm	Hsp90α	FKBP51	peptide	0.031±0.003	0.9
GR-LBDm	Hsp90α	FKBP51ΔN	peptide	0.033±0.005	1.0
GR-LBDm	Hsp90α	FKBP52	peptide	0.023±0.001	0.7
GR-LBDm	Hsp90α	FKBP52ΔN	peptide	0.034±0.004	1.0

4.3.3 p23 accelerates hormone association in the presence of PPIases

The progression of the chaperone cycle requires a distinctive set of co-chaperones that bind to either the NTD or CTD of Hsp90 and thereby regulate client maturation (Sahasrabudhe et al., 2017). The co-chaperone p23 binds to the NTD of Hsp90, reduces Hsp90's ATPase activity and is thus beneficial for SHR maturation (Ali et al., 2006; Johnson and Toft, 1994). As p23 and FKBP51 or FKBP52 can bind simultaneously to the Hsp90:GR complex (Ebong et al., 2016; Johnson and Toft, 1994), the influence on hormone binding was investigated.

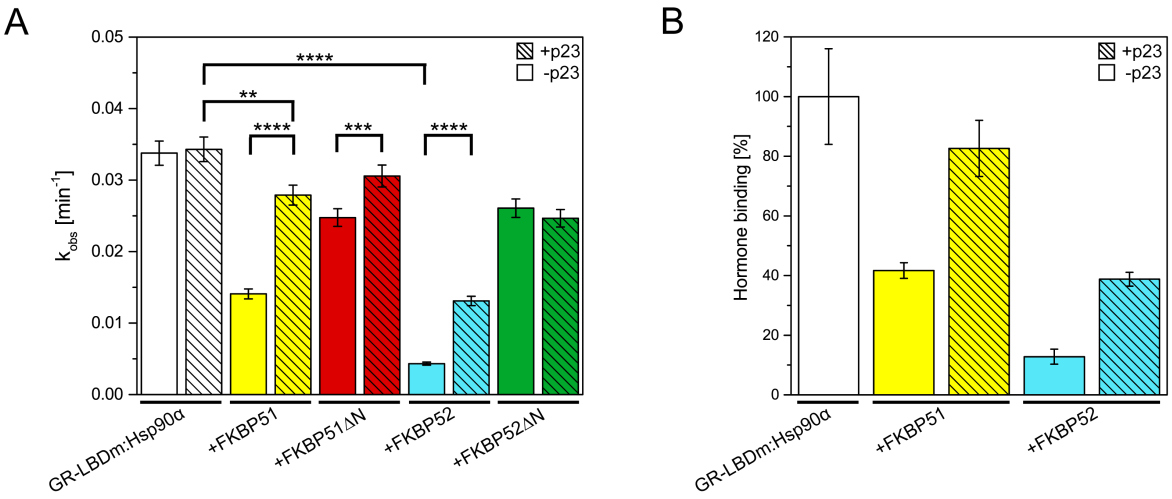

Figure 31: Influence of p23 on F-DEX association to GR-LBDm. (A) Hormone binding to GR-LBDm (1 µM) in complex with Hsp90α (12 µM) and different PPIase constructs (12 µM) in the presence (striped pattern) and absence (pattern-less) of p23 (12 µM). (B) Percentage of hormone binding in relation to Hsp90α:GR-LBDm. The k_{obs} of each sample were divided through the k_{obs} of Hsp90α:GR-LBDm to determine the percentage of hormone binding. Data are shown as mean values from four to six experiments (± SD). Statistical significance was assessed using a two-sample *t*-test and a significance level of 0.05. Statistical significance is indicated with $p < 0.05$ (*), $p < 0.01$ (**), $p < 0.001$ (***), and $p < 0.0001$ (****).

The presence of p23 had no effect on hormone association to Hsp90α:GR-LBDm (Fig. 31A). For complexes containing FKBP51 and FKBP52, hormone association was accelerated two- and three-fold by p23 (Fig. 31B). The determined k_{obs} values are shown in Table 23.

Table 23: Effect of p23 on hormone association in Hsp90α:GR-LBDm(:PPIase) complexes. Average k_{obs} values are shown (±SD). Fold change is shown in relation to Hsp90α:GR-LBDm.

	-p23		+p23	
	k_{obs} [min^{-1}]	Fold change	k_{obs} [min^{-1}]	Fold change
Hsp90α:GR-LBDm	0.034±0.005	1.0	0.034±0.003	1.0
+FKBP51	0.014±0.001	0.4	0.028±0.003	0.8
+FKBP51ΔN	0.025±0.002	0.7	0.031±0.002	0.9
+FKBP52	0.004±0.001	0.1	0.013±0.001	0.4
+FKBP52ΔN	0.026±0.002	0.8	0.025±0.002	0.7

Binding of p23 to Hsp90 is ATP-dependent (Johnson et al., 1996). Therefore, the effect of p23 and both PPIases, FKBP51/52, on hormone association in the presence and absence of nucleotides was investigated. The ATP analog ATPγS was used additionally as it induces a closed Hsp90 conformation (Hessling et al., 2009). Hormone association to Hsp90α:GR-LBDm was not affected by the nucleotide status (Fig. 32). In the presence of full-length (FL) and ΔN constructs of FKBP51, the observed hormone association rate was further prolonged by up to 50% in the absence of nucleotides or with ATPγS compared to the ATP state (Fig. 32). In contrast, hormone association in complexes with FKBP52 FL was completely prevented under those conditions. Binding rates were further diminished in FKBP52ΔN complexes with ATPγS and in the absence of nucleotides (Fig. 32). As expected, p23 was able to accelerate hormone association to the same extent in complexes containing PPIases and ATPγS or ATP, but it did not accelerate hormone association in such complexes without any nucleotide present (Fig. 32). Hence, the specific binding of p23 to Hsp90α likely accelerates hormone binding to Hsp90α:GR-LBDm:PPIase complexes either by competing with PPIases for binding to Hsp90 or by inducing conformational changes in Hsp90 or GR that prevent PPIase interaction. Hormone binding to GR-LBDm is influenced by FKBP51 and FKBP52. In addition, the Hsp90 nucleotide loading state played a role in PPIase-mediated hormone binding. Under conditions containing ATPγS or no nucleotide, hormone association was further slowed down in complexes containing either FKBP51 or FKBP52.

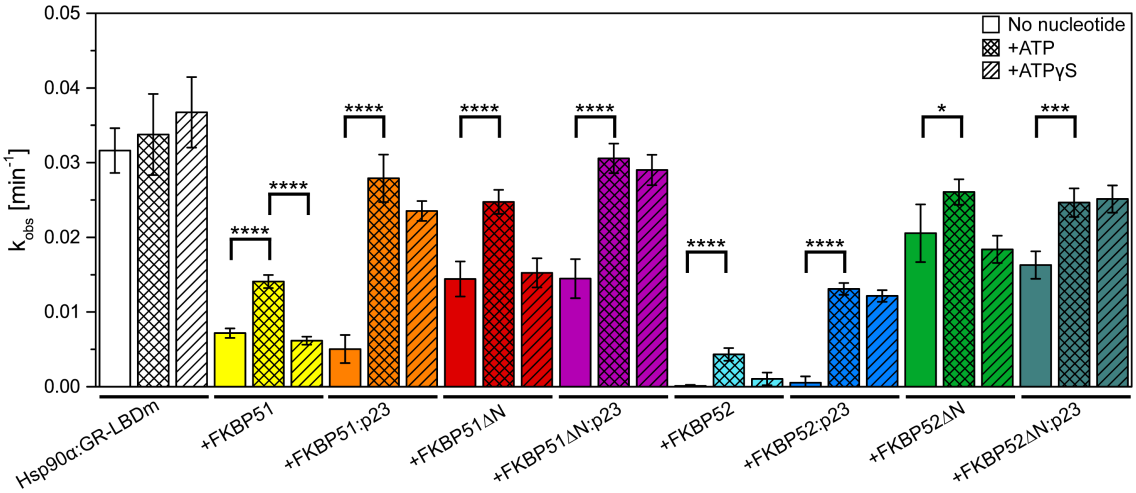

Figure 32: Influence of nucleotides on hormone association to GR. Average k_{obs} are shown for complexes with no nucleotide (pattern-less), with ATP (crossed pattern) and with ATPγS (striped pattern). Data are shown as mean from four to six experiments (± SD). Statistical significance was assessed using a two-sample *t*-test and a significance level of 0.05. Statistical significance is indicated with $p < 0.05$ (*), $p < 0.01$ (**), $p < 0.001$ (***), and $p < 0.0001$ (****).

Table 24: Influence of different nucleotides (ATP and ATPγS) and the absence of nucleotides on hormone association in GR-LBDm:Hsp90α(:co-chaperone) complexes. Average k_{obs} values are shown (±SD). Fold change is shown in relation to GR-LBDm:Hsp90α in the presence of ATP.

No nucleotide				k_{obs} [min^{-1}]	Fold change
GR-LBDm	Hsp90α			0.032±0.003	0.9
GR-LBDm	Hsp90α	FKBP51		0.007±0.001	0.2
GR-LBDm	Hsp90α	FKBP51	p23	0.005±0.002	0.1
GR-LBDm	Hsp90α	FKBP51ΔN		0.014±0.002	0.4
GR-LBDm	Hsp90α	FKBP51ΔN	p23	0.014±0.003	0.4
GR-LBDm	Hsp90α	FKBP52		0.0001±0.0001	0.0
GR-LBDm	Hsp90α	FKBP52	p23	0.001±0.001	0.0
GR-LBDm	Hsp90α	FKBP52ΔN		0.021±0.004	0.6
GR-LBDm	Hsp90α	FKBP52ΔN	p23	0.016±0.002	0.5

+ATP				k_{obs} [min^{-1}]	Fold change
GR-LBDm	Hsp90α			0.034±0.005	1.0
GR-LBDm	Hsp90α	FKBP51		0.014±0.001	0.4
GR-LBDm	Hsp90α	FKBP51	p23	0.028±0.003	0.8
GR-LBDm	Hsp90α	FKBP51ΔN		0.025±0.002	0.7
GR-LBDm	Hsp90α	FKBP51ΔN	p23	0.031±0.002	0.9
GR-LBDm	Hsp90α	FKBP52		0.004±0.001	0.1
GR-LBDm	Hsp90α	FKBP52	p23	0.013±0.001	0.4
GR-LBDm	Hsp90α	FKBP52ΔN		0.026±0.002	0.8
GR-LBDm	Hsp90α	FKBP52ΔN	p23	0.025±0.002	0.7

+ATPγS				k_{obs} [min^{-1}]	Fold change
GR-LBDm	Hsp90α			0.037±0.005	1.1
GR-LBDm	Hsp90α	FKBP51		0.006±0.001	0.2
GR-LBDm	Hsp90α	FKBP51	p23	0.024±0.001	0.7
GR-LBDm	Hsp90α	FKBP51ΔN		0.015±0.002	0.4
GR-LBDm	Hsp90α	FKBP51ΔN	p23	0.029±0.002	0.9
GR-LBDm	Hsp90α	FKBP52		0.001±0.001	0.0
GR-LBDm	Hsp90α	FKBP52	p23	0.012±0.001	0.4
GR-LBDm	Hsp90α	FKBP52ΔN		0.018±0.002	0.5
GR-LBDm	Hsp90α	FKBP52ΔN	p23	0.025±0.002	0.7

4.3.4 Deceleration of hormone association is independent of the Hsp90 isoform

The structural differences of the two human Hsp90 isoforms in solution could affect their interactions with client proteins and co-chaperones (section 4.2.3). FKBP51 and FKBP52 could mediate hormone association to GR-LBD differently depending on the Hsp90 isoform. Thus, hormone association was also determined in the presence of human Hsp90β.

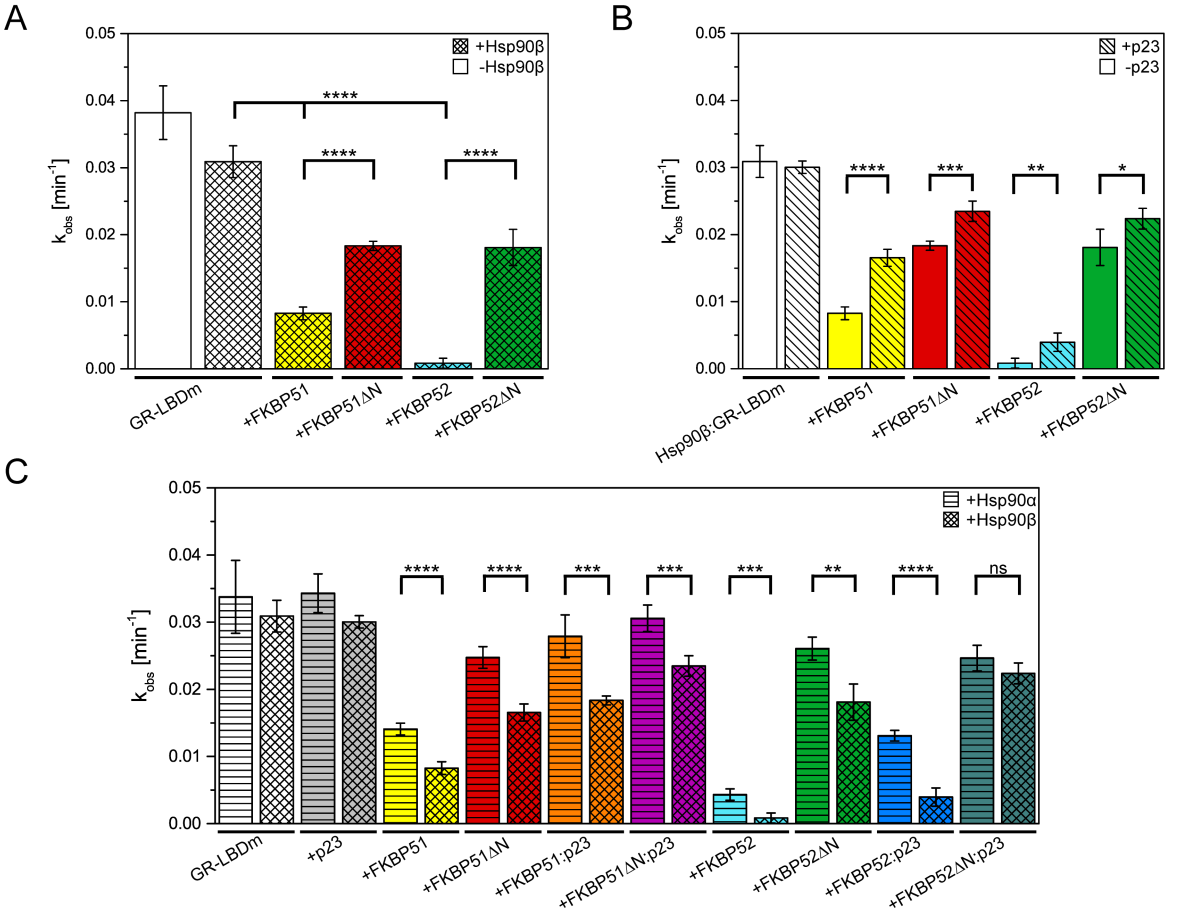

Figure 33: Hormone association experiments with apo GR-LBDm, Hsp90β, and PPIases. (A) Effect of PPIases on hormone association to GR-LBDm in the presence (crossed pattern) and absence (patternless) of Hsp90β. (B) Effect of p23 on hormone association to GR-LBDm in complex with Hsp90β and different PPIase constructs. (C) Comparison of k_{obs} between Hsp90α and Hsp90β complexes. Average k_{obs} determined from four experiments (± SD). Statistical significance was assessed using a two-sample *t*-test and a significance level of 0.05. Statistical significance is indicated with ns (not significant), $p < 0.05$ (*), $p < 0.01$ (**), $p < 0.001$ (***), and $p < 0.0001$ (****).

The GR-LBDm bound hormone with the same k_{obs} in the presence of Hsp90α and Hsp90β (Fig. 33C). FKBP51 and FKBP52 prolonged hormone association in Hsp90β:GR-LBDm complexes as well (Fig. 33A). The addition of p23 accelerated hormone association for FKBP51 (two-fold) and FKBP52 (four-fold) containing complexes (Fig. 33B). Complexes containing FKBP51 or FKBP52 showed 1.6- and 3.7-fold slower hormone association with Hsp90β compared to Hsp90α (Fig. 33C). Complexes containing FKBP52ΔN exhibited the

same hormone association behavior with Hsp90β and Hsp90α (Fig. 33C). The determined k_{obs} and fold change values are shown in Table 25. Hormone binding to Hsp90β complexes is overall slower in comparison to Hsp90α complexes, but retardation of hormone binding to GR-LBDm by FKBP51/52 shows the same trend for Hsp90α and Hsp90β.

Table 25: Comparison of hormone association rates to different Hsp90α and Hsp90β complexes. Average k_{obs} values are shown (±SD). Fold changes are shown in relation to either Hsp90α:GR-LBDm or Hsp90β:GR-LBDm.

	Hsp90α:GR-LBDm		Hsp90β:GR-LBDm	
	k_{obs} [min^{-1}]	Fold change	k_{obs} [min^{-1}]	Fold change
	0.034±0.005	1.0	0.031±0.002	1.0
+p23	0.034±0.003	1.0	0.030±0.001	1.0
+FKBP51	0.014±0.001	0.4	0.008±0.001	0.3
+FKBP51:p23	0.028±0.003	0.8	0.018±0.001	0.6
+FKBP51ΔN	0.025±0.002	0.7	0.018±0.001	0.6
+FKBP51ΔN:p23	0.031±0.002	0.9	0.023±0.002	0.7
+FKBP52	0.004±0.001	0.1	0.001±0.001	0.0
+FKBP52:p23	0.013±0.001	0.4	0.004±0.001	0.1
+FKBP52ΔN	0.026±0.002	0.8	0.018±0.003	0.6
+FKBP52ΔN:p23	0.025±0.002	0.7	0.022±0.002	0.7

4.3.5 Inhibitors can regulate hormone association

The influence of FKBP51/52 on hormone binding to GR has so far been studied by assessing the effects on expression levels of GR regulated genes or reporter constructs (Riggs et al., 2003). Here, it was shown that FKBP51 and FKBP52 modulate hormone association to GR via their FK1 domain. The deliberate use of inhibitors in the FP assay enables the possibility to explore whether FK1 inhibitors affect hormone association and if they distinguish between FKBP51 and FKBP52. Subsequently, inhibitors were used to determine their selectivity profile and to elucidate whether FKBP51 and FKBP52 use different mechanisms to exert their effects on GR. The FK1 binder Rapamycin and SAFit2 as well as a published complex disruptor, Benztropine (Sabbagh et al., 2018), were tested to investigate their impact on PPIase-mediated effects on hormone association. Radicicol, an N-terminal Hsp90 ATPase inhibitor, was used to gain additional information on the impact of Hsp90 on hormone association.

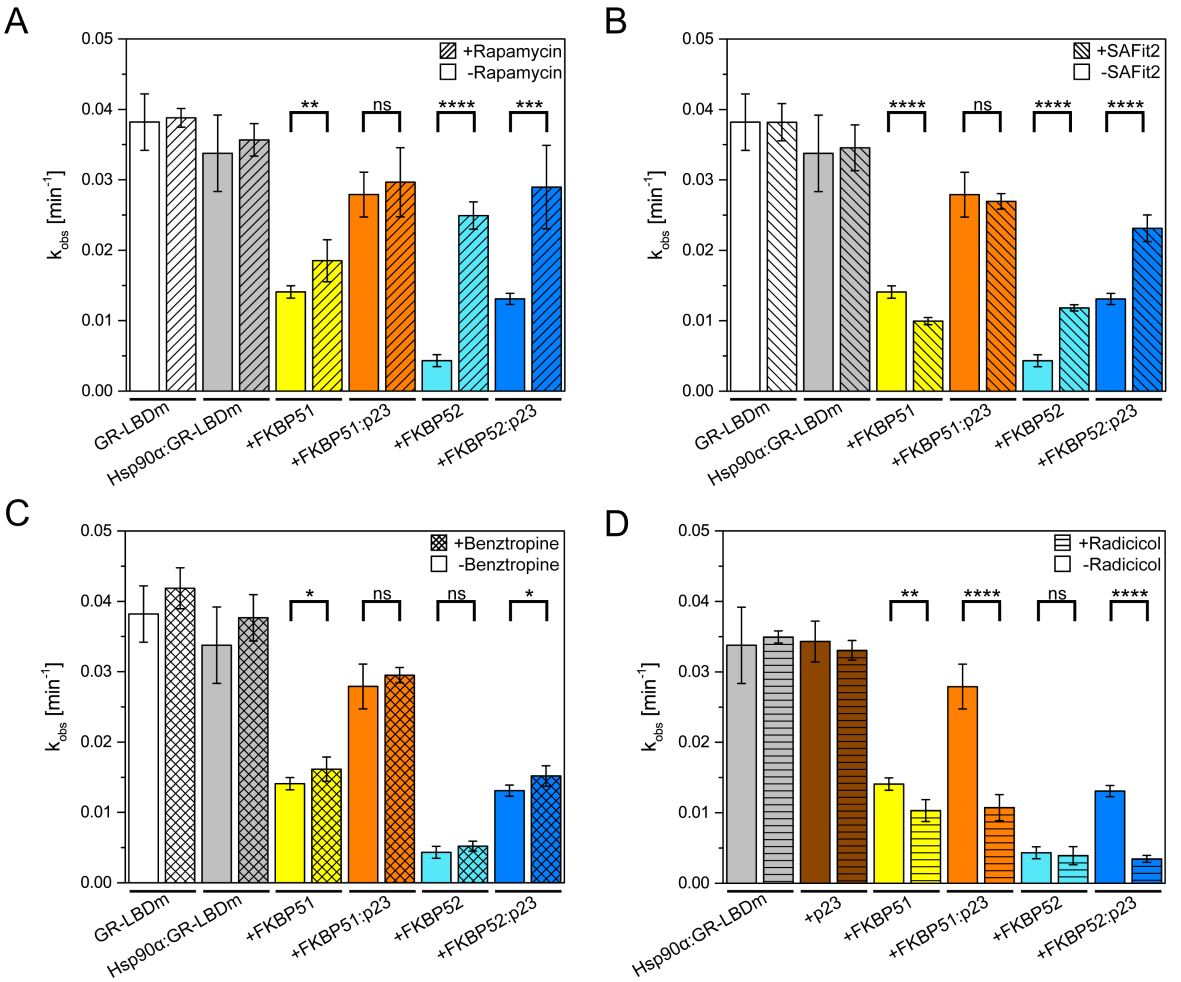

Figure 34: Influence of inhibitors on hormone association in co-chaperone complexes. Effect of 24 µM Rapamycin (A), 24 µM SAFit2 (B), 100 µM Benztropine (C) and 24 µM Radicicol (D) on hormone binding to GR-LBDm in complex with Hsp90α and different co-chaperones. Data are shown as mean k_{obs} values for complexes without (pattern-less) and with inhibitors (patterned) of four to six experiments (± SD). Statistical significance was assessed using a two-sample *t*-test and a significance level of 0.05. Statistical significance is indicated with ns (not significant), $p < 0.05$ (*), $p < 0.01$ (**), $p < 0.001$ (***), and $p < 0.0001$ (****).

Rapamycin had no effect on hormone association in the presence of GR-LBDm or Hsp90α:GR-LBDm (Fig. 34A). While the effect on FKBP51 was less pronounced, hormone association to FKBP52 complexes was significantly accelerated (6.3-fold increase) (Fig. 34A). Rapamycin did not accelerate hormone association in combination with FKBP51 and p23 but accelerated hormone association by 2.2-fold with FKBP52 and p23 (Fig. 34A). SAFit2 is supposed to be selective for FKBP51. In contrast to Rapamycin, it does not have the binding motif for mTOR and calcineurin and further lacks immunosuppressive activity (Gaali et al., 2015). The addition of SAFit2 had no effect on hormone association in the presence of GR-LBDm or Hsp90α:GR-LBDm (Fig. 34B). Surprisingly, hormone association was further decelerated for FKBP51 by an additional 0.7-fold and weakly accelerated for FKBP52 (3-fold acceleration). Hormone association was accelerated for FKBP52 and p23 (1.8-fold) but unchanged for FKBP51 and p23 with SAFit2 (Fig. 34B). The addition of Benztropine had no effect on hormone association (Fig. 34C). The *in vitro* hormone association data showed differential effects of FK1 binders on FKBP51 and FKBP52. Although Rapamycin binds to FKBP51 and FKBP52 with similar affinity (Kozany et al., 2009), an effect was only visible for FKBP52 complexes in this context. Based on this data, it can be suggested that both proteins interact differently with the Hsp90α:GR complex.

Radicicol had no effect on Hsp90α:GR-LBDm and Hsp90α:GR-LBDm:p23 complexes during hormone association (Fig. 34D). For Hsp90α:GR-LBDm:FKBP51 complexes, Radicicol slowed down hormone association by 29 % and had no effect in Hsp90α:GR-LBDm:FKBP52 complexes (Fig. 34D). As expected, p23 did not accelerate hormone association with Hsp90α:GR-LBDm:PPIase complexes in the presence of Radicicol (Fig. 34D). The Hsp90 inhibitor Radicicol prevents the binding of ATP and induces a conformation that cannot bind p23 (Schulte et al., 1998). Thereby, the findings from section 4.3.3 that p23-specific binding accelerates hormone association in Hsp90α:GR-LBDm:PPIase complexes were confirmed. The determined k_{obs} and fold change values are shown in Table 26.

Table 26: Influence of FKBP and Hsp90 inhibitors on hormone association in Hsp90α:GR-LBDm(:co-chaperone) complexes. Average k_{obs} values are shown (±SD). Fold change is shown in relation to Hsp90α:GR-LBDm without inhibitor.

No inhibitor				k_{obs} [min^{-1}]	Fold change
GR-LBDm	Hsp90α			0.034±0.005	1.0
GR-LBDm	Hsp90α	FKBP51		0.014±0.001	0.4
GR-LBDm	Hsp90α	FKBP51	p23	0.028±0.003	0.8
GR-LBDm	Hsp90α	FKBP52		0.004±0.001	0.1
GR-LBDm	Hsp90α	FKBP52	p23	0.013±0.001	0.4

+Rapamycin				k_{obs} [min^{-1}]	Fold change
GR-LBDm	Hsp90α			0.036±0.002	1.1
GR-LBDm	Hsp90α	FKBP51		0.019±0.003	0.6
GR-LBDm	Hsp90α	FKBP51	p23	0.030±0.005	0.9
GR-LBDm	Hsp90α	FKBP52		0.025±0.002	0.7
GR-LBDm	Hsp90α	FKBP52	p23	0.029±0.006	0.9

+SAFit2				k_{obs} [min^{-1}]	Fold change
GR-LBDm	Hsp90α			0.035±0.003	1.1
GR-LBDm	Hsp90α	FKBP51		0.010±0.001	0.3
GR-LBDm	Hsp90α	FKBP51	p23	0.027±0.001	0.8
GR-LBDm	Hsp90α	FKBP52		0.012±0.000	0.4
GR-LBDm	Hsp90α	FKBP52	p23	0.023±0.002	0.7

+Benztropine				k_{obs} [min^{-1}]	Fold change
GR-LBDm	Hsp90α			0.038±0.003	1.1
GR-LBDm	Hsp90α	FKBP51		0.016±0.002	0.5
GR-LBDm	Hsp90α	FKBP51	p23	0.030±0.001	0.9
GR-LBDm	Hsp90α	FKBP52		0.005±0.001	0.1
GR-LBDm	Hsp90α	FKBP52	p23	0.015±0.001	0.4

+Radicicol				k_{obs} [min^{-1}]	Fold change
GR-LBDm	Hsp90α			0.010±0.002	0.3
GR-LBDm	Hsp90α	FKBP51		0.010±0.002	0.3
GR-LBDm	Hsp90α	FKBP51	p23	0.011±0.002	0.3
GR-LBDm	Hsp90α	FKBP52		0.004±0.001	0.1
GR-LBDm	Hsp90α	FKBP52	p23	0.003±0.000	0.1

4.4 Co-chaperones modulate the ATPase activity in Hsp90:GR

4.4.1 PPIases alter the interaction of GR-LBDm with Hsp90α

The interaction of co-chaperones with Hsp90 depends on specific conformational states of Hsp90 and the loaded client protein (Schopf et al., 2017). Co-chaperones and clients can either inhibit (GR, p23), accelerate (Aha1) or have no effect on Hsp90 ATPase activity (Lorenz et al., 2014; Panaretou et al., 2002; Richter et al., 2004). Recently, FKBP51 has been shown to inhibit the Hsp90β ATPase activity (Oroz et al., 2018). So far it is unclear whether there is a connection between the influence of FKBP51 or FKBP52 on hormone binding to GR and on ATPase activity in Hsp90α:GR complexes. To address this question, the Hsp90α ATPase activity was investigated in complexes with GR and different co-chaperones.

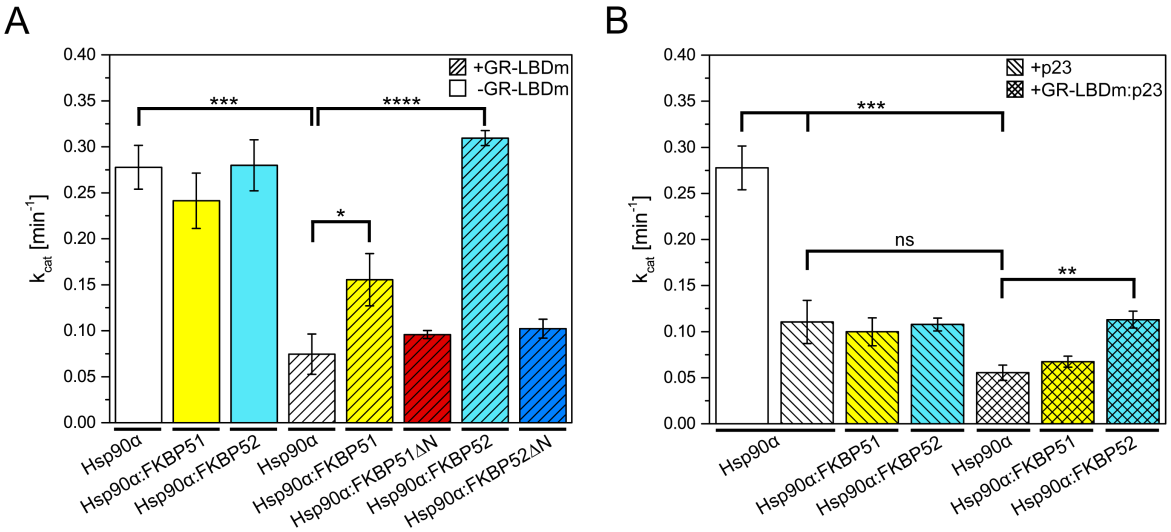

Figure 35: ATPase activity of Hsp90α in the presence of co-chaperones and GR-LBDm. (A) ATPase activity of Hsp90α in the presence of either FKBP51 or FKBP52 and GR-LBDm. (B) ATPase activity of Hsp90α in the presence of p23 in combination with FKBP51, FKBP52, and GR-LBDm. Average k_{cat} of three experiments is shown (±SD). Statistical significance was assessed using a two-sample *t*-test and a significance level of 0.05. Statistical significance is indicated with ns (not significant), $p < 0.05$ (*), $p < 0.01$ (**), $p < 0.001$ (***), and $p < 0.0001$ (****).

Hsp90α has an ATPase activity of 0.28±0.02 min^{-1} (Fig. 35). FKBP52 did not modulate the ATPase activity (100 % activity) (Fig. 35A). While the presence of FKBP51 led to a slightly reduced ATPase activity of 86 %, the difference to Hsp90α alone was not significant ($p = 0.1764$) (Fig. 35A). As expected, GR-LBDm inhibited ATPase activity by 75 % (Fig. 35A), which is in the same range as observed with yeast Hsp90 and GR (85 % inhibition) (Lorenz et al., 2014). The addition of FKBP51 to Hsp90α:GR-LBDm led to a small increase in ATPase activity (57 %) while FKBP52 could restore complete ATPase activity (111 %) (Fig. 35A). Stimulation of ATPase activity is dependent on the FK1 domain (Fig. 35A). Similar to observations made during hormone association, FKBP51 and FKBP52 apparently modulated the interaction between Hsp90α and GR-LBDm. In addition, the data suggests that there could be a link between Hsp90α ATPase activity and hormone binding to GR-LBDm. Next, the effects of

p23 on ATPase activity were investigated. It was confirmed that p23 significantly reduces Hsp90 ATPase activity by 61 % (Fig. 35B)(Richter et al., 2004). The concomitant binding of p23 and GR-LBDm had no synergistic effect on ATPase activity (Fig. 35B). PPIases could not recover complete ATPase activity in Hsp90α:GR-LBDm:p23 complexes. Instead, the ATPase activity was reduced to 25 % (FKBP51) and 39 % (FKBP52). The determined turnover rates and ATPase activities are shown in Table 27. These results support the hypothesis that p23 either leads to an at least partial displacement of the PPIases or stabilizes a conformation that reduces PPIase interaction with Hsp90α:GR-LBDm complexes.

Table 27: ATPase activity of Hsp90α and its modulation by GR-LBDm and co-chaperones. Average k_{cat} of three experiments is shown (±SD). Activity was calculated in relation to Hsp90α.

	k_{cat} [min^{-1}]	Activity [%]
Hsp90α	0.28±0.02	100
+GR-LBDm	0.07±0.02	25
+FKBP51	0.24±0.03	86
+FKBP52	0.28±0.03	100
+GR-LBDm:FKBP51	0.16±0.03	57
+GR-LBDm:FKBP51ΔN	0.10±0.00	36
+GR-LBDm:FKBP52	0.31±0.01	111
+GR-LBDm:FKBP52ΔN	0.10±0.01	36
+p23	0.11±0.02	39
+p23:FKBP51	0.10±0.02	36
+p23:FKBP52	0.11±0.01	39
+GR-LBDm:p23	0.06±0.01	21
+GR-LBDm:p23:FKBP51	0.07±0.01	25
+GR-LBDm:p23:FKBP52	0.11±0.01	39

Recently, it was published that FKBP51 inhibits the Hsp90β ATPase activity (Oroz et al., 2018). To exclude effects of different buffers which could explain the differences between the findings of Oroz et al. (2018) and the results within this thesis, the same experiment for FKBP51 was performed in the buffer used by this group (20 mM HEPES, 10 mM KCl, 1 mM DTT, 5 mM $MgCl_2$, pH 7.4) instead of our buffer system (40 mM HEPES, 150 mM KCl, 1 mM TCEP, 5 mM $MgCl_2$, pH 7.5).

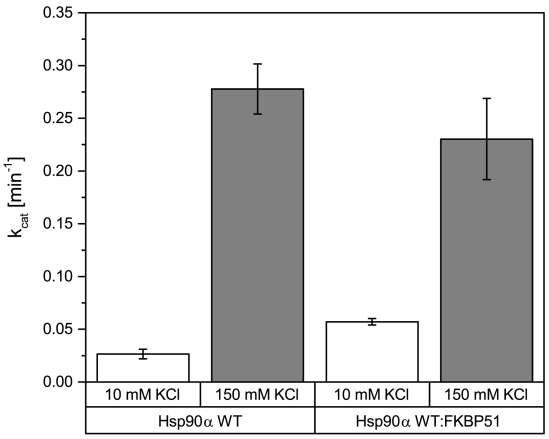

Figure 36: Influence of buffer composition on Hsp90α ATPase activity. The salt dependency of Hsp90α ATPase activity in the presence of FKBP51 in buffer containing either 10 or 150 mM KCl is shown for average k_{cat} values of three independent experiments (±SD).

Even under identical conditions to a previous publicaton (Oroz et al., 2018), no inhibitory effect of FKBP51 on the Hsp90α ATPase activity could be observed (Fig. 36). As expected, the Hsp90α ATPase activity was reduced in the presence of 10 mM KCl compared to 150 mM KCl (Richter et al., 2008).

Table 28: ATPase activity of Hsp90α and Hsp90α:FKBP51 in different buffers. Average k_{cat} of three experiments is shown (±SD). Activity was calculated in relation to Hsp90α in buffer containing 150 mM KCl.

	150 mM KCl		10 mM KCl	
	k_{cat} [min^{-1}]	Activity [%]	k_{cat} [min^{-1}]	Activity [%]
Hsp90α	0.28±0.02	100	0.03±0.00	11
+FKBP51	0.24±0.03	86	0.06±0.00	21

4.4.2 FK1 inhibitors prevent ATPase acceleration in the presence of GR-LBDm

FK1 inhibitors modulated hormone association in Hsp90α:GR-LBDm:PPIase complexes in earlier experiments. Next, the effects of Rapamycin and SAFit2 on the Hsp90α ATPase activity in complex with PPIases were studied.

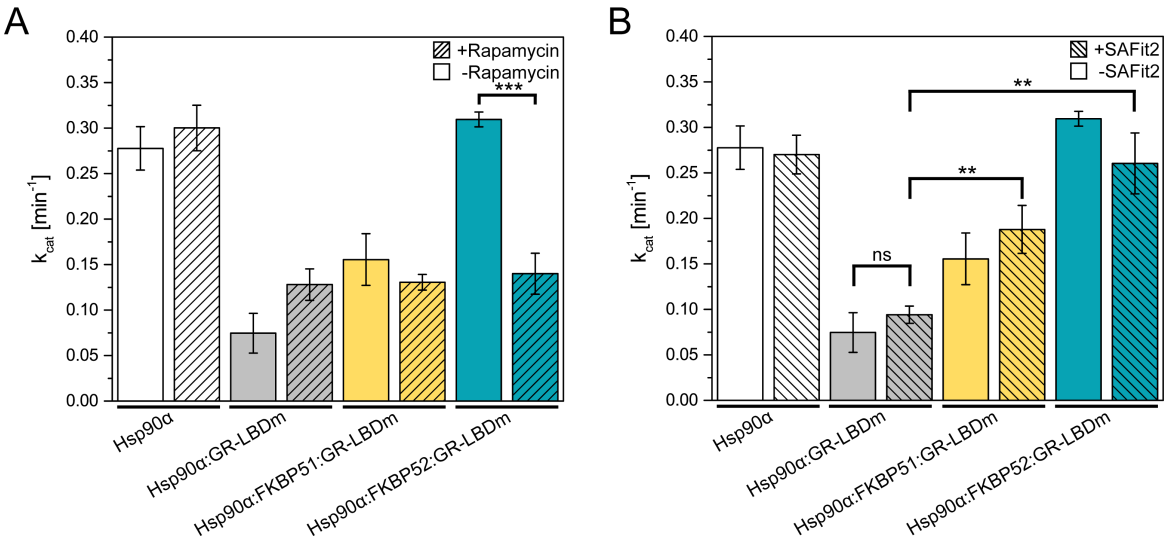

Figure 37: ATPase activity of Hsp90α in the presence of FK1 inhibitors. ATPase activity of Hsp90α in complex with co-chaperone and client protein in the absence (pattern-less) and presence (patterned) of FK1 inhibitor Rapamycin (A) and SAFit2 (B). Average k_{cat} values of three experiments are shown (±SD). Statistical significance was assessed using a two-sample *t*-test and a significance level of 0.05. Statistical significance is indicated with ns (not significant), $p < 0.05$ (*), $p < 0.01$ (**), $p < 0.001$ (***), and $p < 0.0001$ (****).

Similar to the hormone binding assay, Rapamycin had no effect on the ATPase activity in Hsp90α:GR-LBDm:FKBP51 complexes (Fig. 37A). However, inhibition of FKBP52 with Rapamycin led to an almost complete suppression of FKBP52-mediated ATPase acceleration and reduced ATPase activity from 111 % to 50 % (Fig. 37A). The selective inhibitor SAFit2 had no effect on ATPase activity in Hsp90α:GR-LBDm:FKBP51 (Fig. 37B). In contrast to Rapamycin, SAFit2 did not significantly inhibit FKBP52-mediated effects (93 % ATPase activity) (Fig. 37B). The determined k_{cat} values and ATPase activities in the presence of FK1 inhibitors are shown in Table 29. The influence on Hsp90α ATPase activity in the presence of GR-LBDm and FKBP51/52 supports the hypothesis that the two PPIases use distinct mechanisms to regulate hormone binding to GR-LBDm.

Table 29: ATPase activity of Hsp90α in the presence of FK1 inhibitors. Average k_{cat} of three experiments is shown (±SD). Activity is calculated in relation to Hsp90α in the absence of inhibitors.

	+Rapamycin		+SAFit2	
	k_{cat} [min^{-1}]	Activity [%]	k_{cat} [min^{-1}]	Activity [%]
Hsp90α	0.30±0.02	107	0.27±0.02	96
+GR-LBDm	0.13±0.02	46	0.09±0.01	32
+GR-LBDm:FKBP51	0.13±0.01	46	0.19±0.03	68
+GR-LBDm:FKBP52	0.14±0.02	50	0.26±0.03	93

4.5 Tetrameric Hsp90:GR complexes include PPIase and p23

The addition of p23 led to a strong acceleration of hormone association and a strong deceleration of the ATPase activity in Hsp90α:GR-LBDm:FKBP51/52 complexes. The binding of p23 to Hsp90α could either lead to an at least partial displacement of FKBP51 and FKBP52 or induce conformational changes that prevent FKBP51 and FKBP52 to interact with Hsp90α:GR-LBDm. Previous studies have used AUC to investigate the composition of Hsp90 complexes (Lorenz et al., 2014; Sahasrabudhe et al., 2017).
In collaboration with Jannis Lawatscheck at the Technical University of Munich, AUC with fluorescently labeled GR-LBDm was performed to determine the composition of GR-LBDm complexes after addition of p23.

Labeled	added components	AUC trace (signal vs. s-value)	s-value of complex	Fraction bound (labeled)
GR-LBDm*			2.4	0
GR-LBDm*	Hsp90α	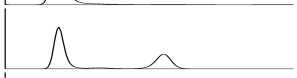	6.7	0.24
GR-LBDm*	Hsp90α, p23		8.8	0.06
GR-LBDm*	Hsp90α, FKBP51		7.4	0.29
GR-LBDm*	Hsp90α, FKBP51, p23		9.7	0.17
GR-LBDm*	Hsp90α, FKBP52		7.8	0.26
GR-LBDm*	Hsp90α, FKBP52, p23		9.8	0.12
F-DEX	GR-LBDm		2.5	0
F-DEX	GR-LBDm, Hsp90α		6.6	0.30
F-DEX	GR-LBDm, Hsp90α, p23		8.4	0.07
F-DEX	GR-LBDm, Hsp90α, FKBP51	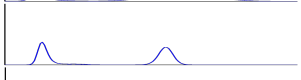	7.0	0.29
F-DEX	GR-LBDm, Hsp90α, FKBP51, p23		9.9	0.11
F-DEX	GR-LBDm, Hsp90α, FKBP52		7.7	0.44
F-DEX	GR-LBDm, Hsp90α, FKBP52, p23		9.5	0.11

Figure 38: Analysis of the composition of Hsp90α:GR-LBDm(:co-chaperone) complexes. AUC sedimentation velocity experiments were carried out using 1 µM Atto-488 labeled GR-LBDm (GR-LBDm*) to analyze complex formation with 3 µM Hsp90α, 6 µM FKBP51/52, and 9 µM p23 in the presence of 2 mM ATP and 100 µM DEX. To further investigate hormone binding to specific complexes, AUC sedimentation velocity experiments were carried out using 1 µM F-DEX to analyze GR-LBDm (1 µM) complex formation with 3 µM Hsp90α, 6 µM FKBP51/52, and 9 µM p23 in the presence of 2 mM ATP. Normalized dc/dt values were plotted against the apparent sedimentation coefficient (s).

GR-LBDm* sedimented with an s-value of 2.4 S, in line with its monomeric state and

published data (Lorenz et al., 2014). We observed complex formation between GR-LDBm* and Hsp90α (6.7 S) (Fig. 38). The addition of FKBP51, FKBP52 or p23 to the Hsp90α:GR-LBDm* complex led to the formation of Hsp90α:GR-LBDm*:co-chaperone complexes with distinct s-values of 7.4, 7.8 and 8.8 S, respectively (Fig. 38). FKBP52 containing complexes sedimented at higher s-values compared to FKBP51 complexes (7.8 S vs 7.4 S). This indicates that Hsp90α:GR-LBDm:FKBP51 complexes are more compact than Hsp90α:GR-LBDm:FKBP52 complexes and thereby support the derived SAXS models (Fig. 24). The addition of p23 to complexes containing either FKBP51 or FKBP52 resulted in even higher s-values of 9.7 and 9.9 S. To further investigate which complexes are able to bind hormone, AUC experiments with F-DEX were also carried out. Every tested complex was able to bind hormone (Fig. 38). These results imply that p23 and FKBP51/52 can bind simultaneously to Hsp90:GR-LBDm to form tetrameric complexes and do not directly compete for binding to Hsp90. The observed acceleration of hormone binding is thus likely due to the influence of p23 on the interaction between the FK1 domain of the PPIases with the Hsp90:GR complex.

5 Discussion

5.1 Biophysical characterization of FKBP51/52 and Hsp90α/β protein interaction

The disruption of the interaction between FKBP51 and Hsp90 or its function in the complex with Hsp90 could potentially be adressed in a therapeutic concept to normalize GC signaling. So far, it has been shown that the C-terminal MEEVD motif of Hsp90 is necessary for the interaction with the TPR domain of FKBP51/52 (Scheufler et al., 2000; Cheung-Flynn et al., 2003), but the roles of the FK1 and FK2 domains have not been clearly determined. Although, there is evidence that a weak interaction exists (Oroz et al., 2018). Furthermore, there have been no studies on whether FKBP51 and FKBP52 interact differently with Hsp90α/β.

Within this work, different domain constructs of human FKBP51 and FKBP52 were used to biophysically investigate the interaction with human Hsp90α and Hsp90β and to identify potential secondary interaction sites. Neither FKBP51 nor FKBP52 distinguished between Hsp90α and Hsp90β as they bound both isoforms with the same affinity. Therefore, FKBP51/52 would be equally present in pathways containing either Hsp90α or Hsp90β. According to prior data, it was confirmed that FKBP52 has a higher affinity to Hsp90α/β compared to FKBP51 (Pirkl and Buchner, 2001). However, the determined affinities in this thesis were four-fold lower than reported previously. Two major differences in the experimental setup could be identified that may explain the varying observations: the used expression host (*E.coli* versus insect cells) and the buffer composition. Post-translational modifications (PTMs) can influence interactions. In the case of Hsp90, the phosphomimetic Hsp90-Y313E has been shown to increase Aha1 binding by 3.5-fold (Xu et al., 2012). Thus, different PTM patterns of *E.coli* and insect cells could influence the interaction. In section 4.1.2, it was shown that the affinity of Hsp90α to FKBP51/52 increased as the salt concentration in the buffer was decreased. The FKBP51:Hsp90 peptide structure revealed that polar and ionic residues are important for the interaction (Fig. 11). The di-carboxylate clamp feature involves the C-terminal Hsp90-D732 residue which interacts with K272, K352, and N322 of FKBP51. Further salt bridges are formed between FKBP51-K352:Hsp90-E730 and FKBP51-E351:Hsp90-R727. The buffer used by Pirkl and Buchner (2001) included only 40 mM HEPES at pH 8.0 while the buffer in this thesis included 20 mM HEPES, 20 mM KCl, 5 mM $MgCl_2$, and 2 mM TCEP at pH7.5. Hence, the observed lower affinity to Hsp90α/β compared to Pirkl and Buchner (2001) could be caused by PTMs and the buffer composition.

Deletion of the NTD and MD of Hsp90 resulted in only a mild increase in affinity with full-length FKBPs, which highlights the role of the TPR domain and the C-terminal region of Hsp90. To further narrow down the interaction surface, constructs containing either the FK2 domain and the full C-terminal region (FKBPΔN) or the FK2 domain and a truncated C-terminus (FKBPΔN2) were used. Interestingly, the removal of the last 43 residues of FKBP51 led to a 2.5-fold higher affinity compared to the construct with the full C-terminal region (Table 16). These results imply that the last 43 residues, which are not part of a TPR

motif, are not involved in the interaction with Hsp90. On the contrary, they even had an adverse effect on the interaction and might sterically hinder binding. In contrast, Cheung-Flynn et al. (2003) found that binding of FKBP51/52 to Hsp90 was drastically reduced if FKBP51/52 was C-terminally truncated. They expressed radiolabeled constructs in rabbit reticulocyte lysate and performed Co-IP with Hsp90 to determine if the binding was affected. This indirect approach does not completely take protein quality and correct folding into account, which could influence the observed binding. In addition, their method description does not clearly state the used Hsp90 isoform. Species-specificity has been observed for the binding of co-chaperones to Hsp90 (Chadli et al., 2008). This could explain the variations to the published results. The C-terminal 15mer Hsp90α peptide, containing the consensus binding sequence MEEVD, alone bound with 2.7- and 3.7-fold lower affinity to FKBP51 and FKBP52 compared to full-length Hsp90, respectively. Additional residues in the CTD of Hsp90 are thus necessary to mediate high affinity binding. The thermodynamic profiles revealed differences in the binding of FKBP51 and FKBP52 to Hsp90α. Entropy contributions decreased for FKBP51:Hsp90 as domains were removed but not for FKBP52:Hsp90. Thus, both complexes seem to use distinct binding modes and FKBP51 has a larger interaction surface on Hsp90α than FKBP52. The observed findings are partially in contrast to the study of Oroz et al. (2018), who used NMR to identify regions on Hsp90β and FKBP51 that interact with each other. The group observed signal reduction for the FK1, FK2, and TPR domains upon addition of Hsp90β. However, even at very high concentrations of isolated subdomains (500 µM of FK1 or FK1-FK2 domains titrated into Hsp90α), no binding could be detected in this thesis using ITC. It is possible that either the interaction with the FK1 and FK2 domains of FKBP51 is of low affinity or unspecific since significant signal reduction in NMR was only observed at four- to five-fold excess of Hsp90. In addition, it is conceivable that signal changes in the FK2 domain are induced by the TPR:Hsp90 interaction and a change in the chemical environment. Lastly, binding of the TPR domain could modulate the affinity of the FK1 domain in an allosteric manner. Overall, the data suggest that binding sites outside of the C-terminal MEEVD sequence of Hsp90α are involved and at least two binding models are possible: either only the TPR domain of FKBP51 and FKBP52 interact with the CTD of Hsp90 or the FK2 and TPR domain interact with the MD and CTD of Hsp90, while the FK2 domain does not contribute to the overall affinity (Fig. 39).

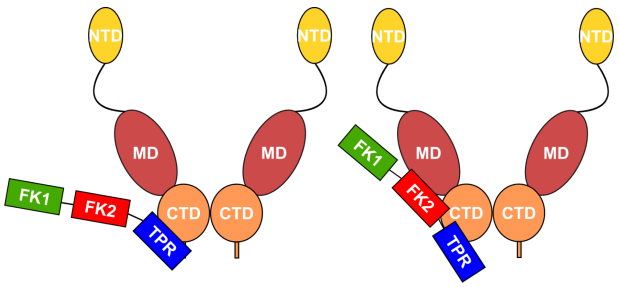

Figure 39: Interaction models between FKBP51/52 and Hsp90α based on ITC studies.

5.2 SAXS elucidates the structure of Hsp90:FKBP51/52

Most structures of Hsp90 in complex with co-chaperones have been solved with the yeast Hsp90 (Ali et al., 2006; Meyer et al., 2004; Roe et al., 2004). One exception is the cryo-EM structure of full-length human Hsp90β in complex with Cdk4 and Cdc37 (Verba et al., 2016). While full-length FKBP51, individual domains of FKBP52, and individual domains of human Hsp90α have been crystallized before, structural information on human Hsp90:PPIase complexes is lacking (Sinars et al., 2003; Kumar et al., 2017; Wu et al., 2004; Stebbins et al., 1997; Lee et al., 2011). Three-dimensional structures of Hsp90α:FKBP51 and Hsp90α:FKBP52 complexes could lead to a better understanding of their respective roles and elucidate part of their mechanistic differences with regards to client modulation.

To provide structural information on Hsp90:PPIase complexes, SAXS measurements were carried out. Experiments with PPIases alone suggested an elongated shape with a flexible domain arrangement for FKBP52 and a more compact and rigid domain arrangement for FKBP51, which was also reflected by a smaller R_g (Fig. 24). This serves as a first indication of their different function and interaction within the complex. The superimposed X-ray structures of FKBP51 and FKBP52 did not completely fill out the calculated SAXS models. The structure of both PPIases could be more fluid in solution and the captured crystallographic structure could represent just one of many possible conformational states. The TPR domain could adopt two conformations in FKBP51 that are evenly occupied. In contrast, the domains seem to be more spaced out on a straight line for FKBP52. Especially the interface between FK2 and TPR domain and the last helix after the TPR domain seem to adopt different orientations in FKBP51 and FKBP52, which could impact their functions.

Interestingly, the human Hsp90 isoforms behaved structurally different from each other. Hsp90α models were composed of a mixture of open and closed conformations even in the presence of ATP, which should lead to a closed conformation of the dimer (Fig. 26A and B). This is in line with the observations made by Southworth and Agard (2008) that human Hsp90α was predominately in the open conformation and that crosslinking was necessary to capture the closed conformation. Surprisingly, Hsp90β models were in an extended open conformation in the absence of ATP and in a closed, compact formation in the presence of ATP (Fig. 26C and D). Hsp90β had a six times lower ATPase activity compared to Hsp90α that could translate into a longer retention time in the closed conformation (Table 31). These conformational differences could also affect chaperone function and client maturation as the basal Hsp90β and stress-induced Hsp90α act under diverse circumstances. This has been shown for the constitutively expressed Hsc82 and the stress-inducible Hsp82 in *S. cerevisiae* (Girstmair et al., 2019).

Biophysical interaction studies suggest a minimalistic binding mode for Hsp90α and FKBP51/52. Only one domain of either FKBP51/52 and Hsp90α could be involved in the interaction (Fig. 39). Thus, the other domains would retain their flexibility and be able to interact with client proteins. SAXS experiments with Hsp90α and PPIases demonstrated that the highly dynamic complexes seem to interact differently. FKBP51 binds tighter to

Hsp90α in the presence of ATP and all three domains of FKBP51 could be involved, which would be consistent with the results of Oroz et al. (2018). In contrast, FKBP52 and Hsp90α seem to interact only via the TPR and CTD. In this case, the FK1 and FK2 domains of FKBP52 seem to point away from Hsp90. The larger R_g for Hsp90α:FKBP52 further provides evidence for such a model. The thermodynamic profiles determined by ITC support the model in which Hsp90α:FKBP51 complexes have a larger interaction surface compared to Hsp90α:FKBP52 complexes. The entropy contributions were reduced for truncation constructs of FKBP51 and Hsp90α compared to the full-length proteins. For FKBP52, however, the entropic contributions did not change. One Hsp90α dimer bound one molecule of FKBP51/52 as derived from the determined molecular weight (Table 21). This is in contrast to the observed equimolar stoichiometry of the ITC measurements and the literature (Pirkl and Buchner, 2001; Ebong et al., 2016; Oroz et al., 2018). As was shown earlier, the binding of Hsp90α and FKBP51/52 is highly susceptible to the salt concentration. Thus, differences in stoichiometry might be caused by the used buffers and the experimental setup. Hsp90 is one of the most abundant proteins in the cell, while co-chaperones are present in much lower numbers (Biebl and Buchner, 2019). To favor binding of two FKBP51/52 molecules to one Hsp90 dimer under such conditions, cooperative binding is necessary. The ITC results do not support such a binding mode. In addition, a proteomic study and analysis in HeLa cells showed that cytoplasmic Hsp90 co-chaperones are substoichiometric to the cytosolic pool of Hsp90α and Hsp90β (Geiger et al., 2012; Finka and Goloubinoff, 2013). They found substoichiometric molar ratios of 1:11 for FKBP51, 1:355 for FKBP52, and 1:7 for p23 (Finka and Goloubinoff, 2013). Therefore it is highly unlikely that two FKBP51/52 bind to one Hsp90 dimer at the same time.

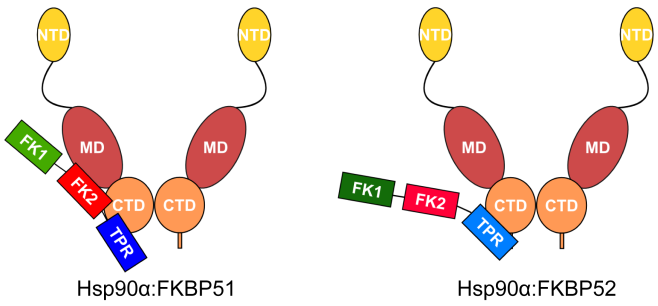

Figure 40: Improved models for Hsp90α:FKBP51 and Hsp90α:FKBP52 complexes based on SAXS and ITC studies.

Overall, the results provide an intriguing insight into the structural arrangement of Hsp90α:FKBP51 and Hsp90α:FKBP52 complexes. The interaction models can be revised based on the these findings (Fig. 40). FKBP51 and FKBP52 clearly interact differently with Hsp90α (Fig. 40). This may result in different interactions with the client protein as well.

5.3 Co-chaperones influence hormone association to GR

The Hsp90 chaperone cycle involves a plethora of different co-chaperones to regulate various cellular processes such as protein folding and DNA repair (Echeverria et al., 2011). Co-chaperone binding is highly dynamic and depends on specific conformational states of Hsp90 and the bound client protein (Schopf et al., 2017). The best-studied client protein is GR, which belongs to the class of SHRs. The two PPIases FKBP51 and FKBP52 are known to alter GR signaling (Denny et al., 2000; Riggs et al., 2003). In the current model, FKBP51-containing complexes are thought to keep GR in a low affinity state for hormone and retain the Hsp90:GR:FKBP51 complex in the cytoplasm (Wochnik et al., 2005). According to this model, once GR is in a hormone bound state, FKBP51 is displaced by FKBP52 which facilitates the transport of activated GR into the nucleus by binding to dynein (Silverstein et al., 1999; Davies et al., 2002). It has been shown that overexpression of FKBP51 leads to impaired GR signaling, deregulates the HPA axis and is thereby linked to several diseases such as depression (Binder et al., 2004). The elucidation of the detailed mechanism and differences between FKBP51- and FKBP52-mediated GR signaling could deliver ideas on therapeutic models. Various complexes were reconstituted to investigate the molecular mechanism of FKBP51- and FKBP52-mediated hormone binding *in vitro*.

In line with recent literature, GR was found to be able to bind hormone without chaperones (Kirschke et al., 2014; Lorenz et al., 2014). The determined K_D(F-DEX) of 293 nM is in the range of published values of 154 and 77 nM (Kirschke et al., 2014; Lorenz et al., 2014). The deviation could be caused by the used GR-LBD constructs as they differ in the number of mutations (five and one) and the presence of a purification tag (His, MBP and no tag). Hsp90 seems to have two roles in GR maturation: the reactivation of GR through its release from Hsp70, which unfolds GR, and the stabilization of GR to allow hormone binding and subsequent GR transcriptional activity (Kirschke et al., 2014).

Hsp90α did not affect hormone association but rather delayed hormone dissociation by 40 %, thereby keeping GR longer activated (Fig. 29). Surprisingly, both FKBP51 and FKBP52 significantly slowed down hormone association to GR by 2.4- and 8.5-fold, respectively. The addition of an Hsp90α C-terminal 15mer peptide, containing the consensus binding sequence, to PPIase-containing complexes led to normal hormone binding as the peptide competed with Hsp90α for FKBP51/52 binding. The absence of Hsp90α resulted in association rates on the same level as GR alone. Thus, FKBP mediates the observed effects on GR either indirectly by inducing changes in Hsp90α or directly and Hsp90α acts as a bridge to bring both proteins into close proximity. These findings are surprising as studies have observed divergent effects of FKBP51 and FKBP52 *in vivo* on GR-mediated gene expression. FKBP51 had an inhibitory effect on GR signaling in an *S.cerevisiae* model as well as in mammalian cells (Riggs et al., 2003; Wochnik et al., 2005; Schülke et al., 2010). In contrast, FKBP52 showed a potentiating effect in the *S.cerevisiae* model while it had no effect or reversed the FKBP51 effect in mammalian cells (Riggs et al., 2003; Davies et al., 2005; Schülke et al., 2010). Even though reporter systems that respond to hormones in yeast are established and widely

accepted, the findings have to be interpreted carefully as neither FKBP51/52 nor SHRs occur naturally in yeast. While yeast provides a null background to test the function of FKBP51/52 *in vivo*, the results could be misinterpreted as small FKBPs and other present co-chaperones could affect the reporter system as well. Thus, the findings by Riggs et al. (2003) may not be completely transferable to the *in vitro* model or mammalian cells. Intriguingly, the findings of this thesis lead to the hypothesis that FKBP51 reduces glucocorticoid binding in mammalian cells by slowing down hormone association.

The mechanism was further investigated by narrowing down which domains of FKBP51/52 might be responsible for GR regulation. Constructs lacking the FK1 domain showed an 1.8- and 6.5-fold faster hormone association rate compared to full-length FKBP51 and FKBP52, respectively. Thereby confirming that the FK1 domain is a major facilitator in FKBP51- and FKBP52-mediated glucocorticoid signaling (Riggs et al., 2003; Denny et al., 2005; Wochnik et al., 2005). Furthermore, the results suggest that FKBP51 and FKBP52 use distinct mechanisms to interact with and regulate the Hsp90:GR complex. FKBP52 has a stronger effect on GR via its FK1 domain. FKBP51 apparently addresses different interactions in the complex compared to FKBP52.

PPIases slowed down hormone association to a greater extent in Hsp90β complexes compared to Hsp90α complexes. Given that Hsp90β is constitutively expressed while Hsp90α is expressed under stress conditions, these results could suggest that FKBP51 and FKBP52 address different interactions within Hsp90β:GR and Hsp90α:GR. Faster hormone association to Hsp90α complexes under stress conditions could allow an immediate reaction of the cell to a changing environment. Thus, structural studies need to be carried out with Hsp90α:GR:FKBP51/52 and Hsp90β:GR:FKBP51/52 to gain a complete picture of GR regulation by FKBP51 and FKBP52.

Nevertheless, these results lead to the conclusion that both PPIases are different regulators of GR hormone association. Interaction models for hormone binding to GR can be proposed based on the obtained data (Fig. 41). As previously mentioned, the transfer of GR to Hsp90 from the inhibitory Hsp40:Hsp70 complex primes GR for hormone binding. Consequently, it was expected that Hsp90 would accelerate hormone binding to GR. Surprisingly, hormone association to GR was unaffected in Hsp90:GR complexes compared to only GR (Fig. 41A), but chase experiments with DEX revealed that hormone dissociation from GR is slower in the presence of Hsp90. In the context of GR activation, Hsp90 might affect the off-rate of hormone binding and keep GR longer in an activated state. The data suggests that FKBP51 regulates GC binding indirectly by using at least its FK1 domain and slows down association rates to 41.7 % (Fig. 41B). The FK1 domain could be positioned in the vicinity of the hormone binding pocket or above it and could thereby impair GC binding. In contrast, FKBP52 might regulate hormone binding to GR directly via its FK1 domain and induce conformational changes in GR that reduce hormone association to 12.8 % (Fig. 41C). The determined *in vitro* results suggest that FKBP51 causes reduced glucocorticoid binding *in vivo* by decelerating hormone binding to GR. The role of FKBP52 *in vivo* may need to be revisited because the *in*

vitro model revealed an almost complete suppression of hormone binding which is in contrast to Riggs et al. (2003) and Riggs et al. (2007). However, it is possible that the function of FKBP52 changes in the presence of other co-chaperones. Therefore, it would be interesting to evaluate the effects of FKBP51/52 on unfolded GR in studies with Hsp40 and Hsp70. It is conceivable that the PPIases perform opposing roles at this point with one accelerating the folding or transfer of GR while the other slows it down.

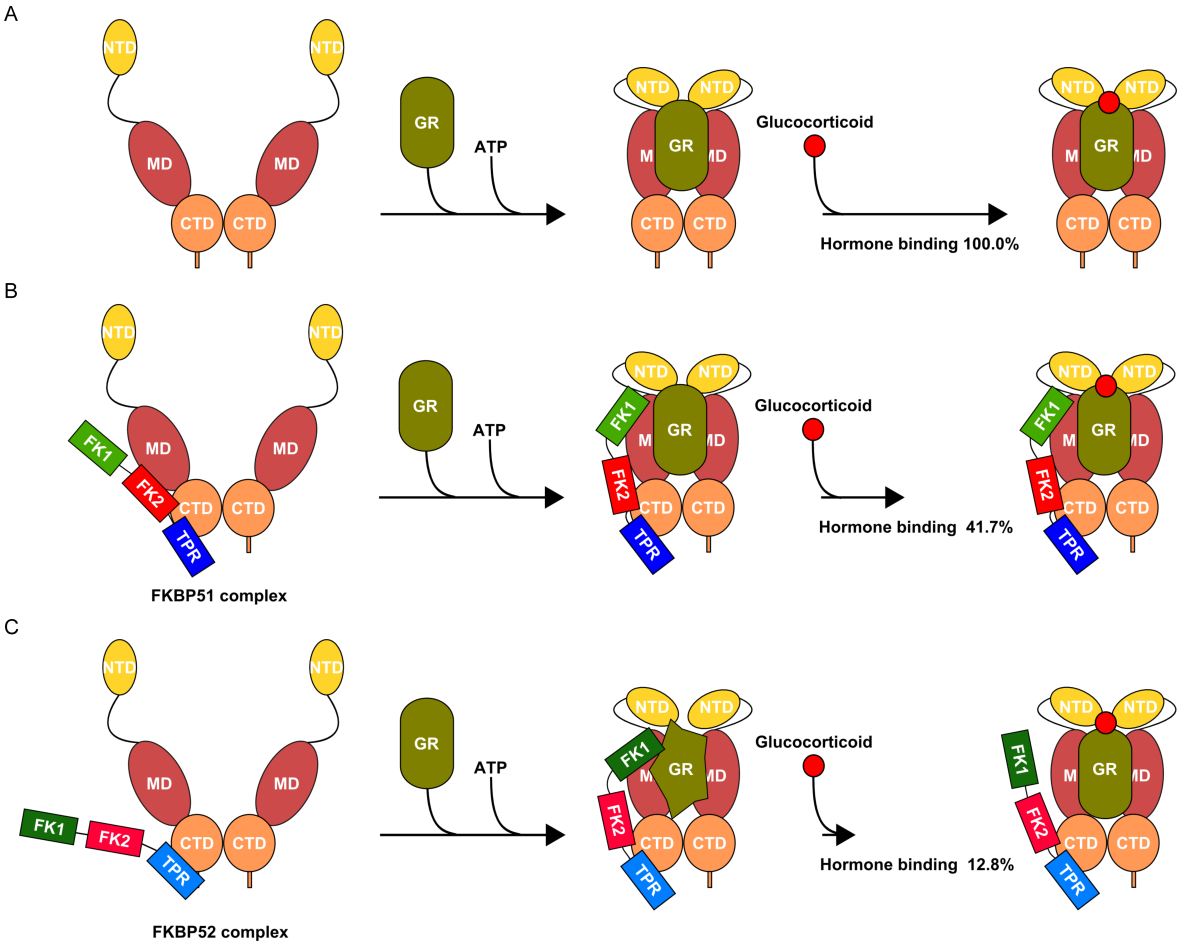

Figure 41: Models for hormone association to chaperone:GR(:PPIase) complexes based on *in vitro* experiments using the hormone binding assay. (A) Hormone association to Hsp90α:GR-LBDm complexes. Hsp90α is present in an open conformation. The binding of GR and ATP leads to a closed conformation. The hormone binding rate to the Hsp90α:GR-LBDm complex is not affected. (B) Hormone association to Hsp90α:GR-LBDm:FKBP51 complexes. FKBP51 is bound to the CTD of Hsp90α via its FK2 and TPR domain. The binding of GR and ATP to Hsp90α:FKBP51 rearranges interactions in the complex. FKBP51 indirectly regulates GR and slows down the hormone binding rate to 41.7 %. (C) Hormone association to Hsp90α:GR-LBDm:FKBP52 complexes. FKBP52 is bound to the CTD of Hsp90 via its TPR domain. The binding of GR and ATP to Hsp90α:FKBP52 rearranges interactions in the complex and GR. FKBP52 interacts directly with GR and thereby reduces the hormone binding rate to 12.8 %.

5.4 Binding of p23 accelerates hormone binding in the presence of PPIases

GR passes through the Hsp90 chaperone cycle before it is completely activated. Until now, it is thought that FKBP51 is bound to Hsp90:GR complexes in the mid stage and keeps GR in a low affinity state for GCs. FKBP51 will then dissociate upon hormone binding and be replaced by FKBP52 leading to a high affinity state (Davies et al., 2002). The hormone binding assay revealed significant inhibition of hormone binding in the presence of FKBP51 and FKBP52. This challenges the literature model that both PPIases act sequentially. Experiments with the co-chaperone p23, which acts at a late stage of the Hsp90 cycle and stabilizes a closed Hsp90 conformation, provided information about the time point of FKBP51 and FKBP52 being involved in the chaperone cycle.

The addition of p23 accelerated hormone association by 2- and 3.3-fold in Hsp90α:GR complexes containing FKBP51 or FKBP52, respectively. The acceleration is dependent on nucleotides (ATP or ATPγS), which is expected as p23 only binds when Hsp90 is in a nucleotide bound state (Johnson et al., 1996; Schulte et al., 1998). Consequently, p23 either competes with FKBP51/52 for binding to Hsp90 or p23 induces conformational changes that prevent interactions between FKBP51/52 and GR. To identify the composition of p23-containing complexes, AUC experiments were performed. AUC analysis revealed the presence of tetrameric complexes and verified that p23 can bind simultaneously with FKBP51 and FKBP52. These findings are partly in line with other *in vitro* experiments where Hsp90:GR:FKBP51:p23 complexes had been detected but FKBP52 did not bind together with p23 (Ebong et al., 2016). The binding of p23 might stabilize a conformation of Hsp90α that either induces conformational changes or sterically prevents the PPIases to fully interact with the Hsp90α:GR complex and modulate hormone binding. It is possible that p23 and FKBP51/52 have overlapping binding sites in the MD of Hsp90. The p23 binding site could have a higher affinity and lead to competitive displacement of the FK1 domain. In addition to tetrameric complexes, trimeric complexes (Hsp90α:GR:PPIase) were also detected in AUC experiments. Although, p23 was added in 1.5-fold excess in comparison to FKBP51 and FKBP52, the affinity of p23 to Hsp90α is too low to saturate all Hsp90α:GR:PPIase complexes under the given experimental conditions. This could also explain why hormone association in samples containing Hsp90α, GR, p23, and FKBP52 is still slowed down. Those samples could contain a mixture of three different complexes: Hsp90α:GR:FKBP52, Hsp90α:GR:FKBP52:p23, and potentially Hsp90α:GR:p23. Therefore, Hsp90α:GR:FKBP52 complexes would still contribute to the observed association rate and hormone association could not be accelerated to the initial level.

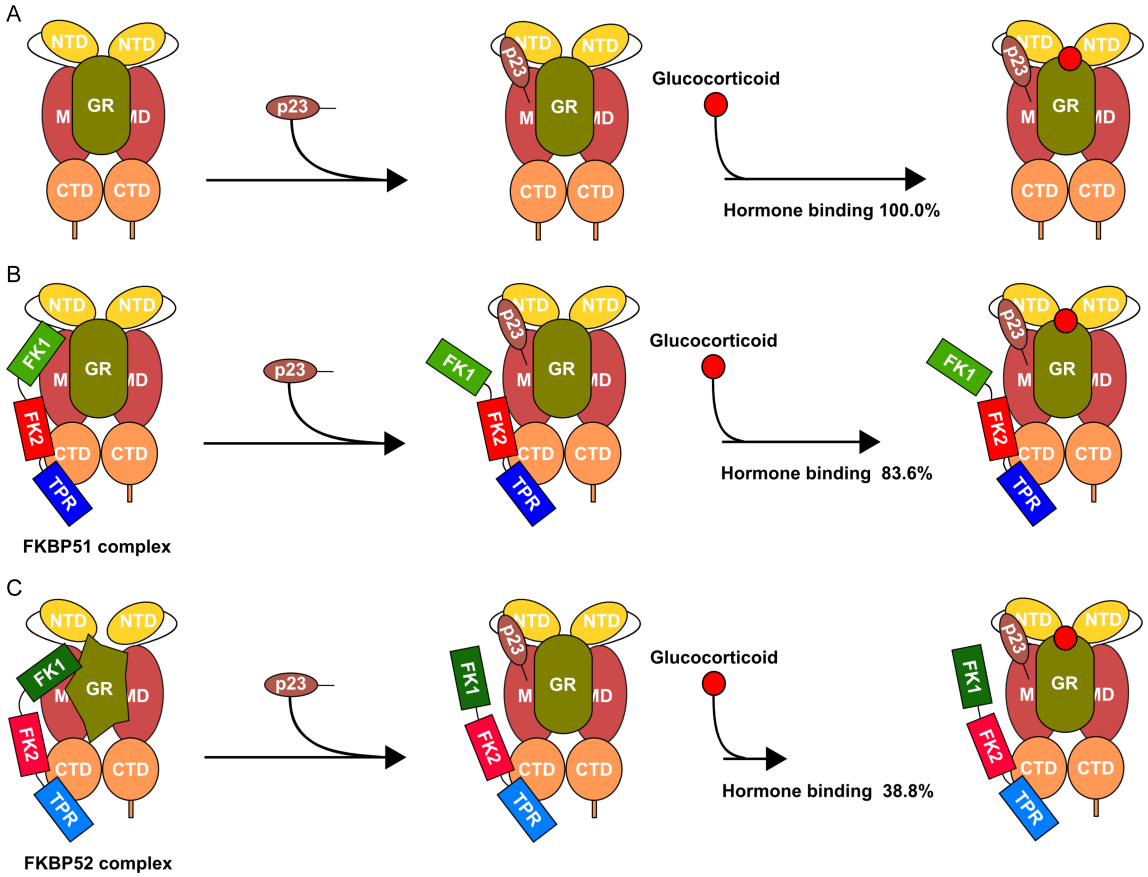

Figure 42: Models for hormone association to chaperone:GR:co-chaperone complexes upon p23 binding based on *in vitro* experiments using the hormone binding assay and AUC experiments. (A) Hormone association to Hsp90α:GR-LBDm complexes upon p23 binding. Hormone association is not affected. (B) Hormone association to Hsp90α:GR-LBDm:FKBP51 complexes upon p23 binding. The binding of p23 displaces the FK1 domain and thereby reverts the indirect effect of FKBP51 on GR. Hormone association is restored to 83.6 % in comparison to 41.7 % without p23. (C) Hormone association to Hsp90α:GR-LBDm:FKBP52 complexes upon p23 binding. The binding of p23 displaces the FK1 domain and thereby partially reverts the direct effect of FKBP52 on GR. Hormone association is elevated to 38.8 % in comparison to 12.8 % without p23.

The results generated by AUC contribute to the expansion of the first interaction model during hormone association (Fig. 41). While p23 enters the Hsp90 chaperone cycle at a late stage, it does not affect hormone association to GR (Fig. 42A). However, it accelerated hormone association in tetrameric complexes (Hsp90α:GR:PPIase:p23) presumably by either binding to the preferred interaction site of the FK1 domain or by inducing conformational changes that prevent FKBP51/52 from regulating GR (Fig. 42B and C). Theoretically, it is possible that p23 could completely reverse the effects of FKBP51/52 on hormone association. However, in this work, PPIase and p23 were added at the same concentration and even a 1.5-fold excess of p23 was not able to completely saturate all Hsp90:GR:PPIase complexes. Therefore, it is likey that the affinity of p23 is not high enough to completely overcome the PPIase effect in this setting. Subsequently, one of the roles of p23 could be to keep Hsp90 in a closed conformation, advance the chaperone cycle and allow hormone binding to GR. Thus, p23 indirectly regulates GR by restraining Hsp90 conformation and co-chaperone activity.

Experiments on the Hsp90 nucleotide loading state also suggest that the conformation of Hsp90α plays a role during the activation cycle. FKBP51 and FKBP52 exert an even stronger inhibitory effect on hormone association when Hsp90 remains in an open conformation or is forced into a closed conformation by ATPγS. In both cases Hsp90α is not able to undergo extensive conformational changes. This leads to the hypothesis that the interaction surface between PPIase and Hsp90:GR changes as Hsp90 cycles through different conformations. It seems that some conformations allow a stronger Hsp90:GR:PPIase interaction which translates to a stronger modulation of hormone binding to GR. In addition, even the FK2-TPR domains of FKBP51 could be involved in regulating hormone binding to GR as the ΔN construct prolonged hormone association by 1.7-fold under conditions where Hsp90α maintains an opened or closed conformation. This is also supported by experiments with Radicicol, which prolonged hormone association with FKBP51 FK2-TPR constructs.

The findings lead to the conclusion that FKBP51 and FKBP52 act at the beginning or middle of the chaperone cycle before p23 enters the complex to actively modulate GR. To further validate the sequential order of FKBP51 and FKBP52 in the Hsp90 chaperone cycle, one possiblity would be the establishment of a Förster resonance energy transfer (FRET) system between human Hsp90 and FKBP51/52 similar to the established yeast system (Li et al., 2013). Such a setup could provide insights into the modulation of FKBP51/52 by other co-chaperones.

5.5 PPIases alter the interaction of GR-LBD with Hsp90α

Co-chaperones and client proteins have been shown to modulate Hsp90 ATPase activity (Lorenz et al., 2014; Panaretou et al., 2002; Richter et al., 2004). For example, GR has been shown to inhibit its ATPase activity (Lorenz et al., 2014). Therefore, a possible link between hormone binding to GR and Hsp90 ATPase activity could exist. The ATPase activity of Hsp90α was determined in different client and co-chaperone complexes to evaluate if there is a link to FKBP51/52-mediated regulation of GC binding to GR.

Neither FKBP51 nor FKBP52 had an effect on ATPase activity of Hsp90α. This is in contrast to Oroz et al. (2018), who proposed that FKBP51 stabilizes Hsp90 in an extended state and thereby inhibits ATPase activity. The experimental setup differed in three aspects: 1.) readout of ATP turnover, 2.) composition of the applied buffer, and 3.) the used Hsp90 isoforms. In theory, both assays should yield the same results. Nevertheless, they were potentially missing an essential control. The addition of Radicicol leads to inhibition of the Hsp90 ATPase activity, which is necessary to ensure the specificity of the readout. Without this control, the presence of other ATPases, which may falsify the result, cannot be excluded. Consideration of background ATPases was not specifically addressed in the publication. To exclude buffer effects, the ATPase activity was determined in the buffer that was used in Oroz et al. (2018). Here, FKBP51 also did not inhibit the Hsp90α ATPase activity under those circumstances. However, it could be confirmed that the Hsp90α ATPase activity is in fact modulated by the salt concentration in the buffer. The activity increases with the

salt concentration, an observation that was also made by Richter et al. (2008). The ATPase activity of Hsp90β was significantly lower than Hsp90α (Table 31). Using Hsp90β in a low salt buffer could decrease the assay window, which could increase the impact of unspecific interactions and any detected changes would have to be analyzed carefully. In addition, it is noticeable that FKBP51- and FKBP52-mediated effects on hormone binding were differently pronounced depending on the Hsp90 isoform. Therefore, it is possible that the observed differences are due to the isoforms used.

As published in recent years, the binding of GR-LBDm to Hsp90α reduced ATPase activity four-fold in comparison to apo Hsp90α which is in line with the 85 % inhibition observed with yeast Hsp90 and GR-LBDm (Lorenz et al., 2014). Within this thesis, FKBP51 accelerated the ATPase activity of Hsp90α:GR by 1.8-fold while FKBP52 accelerated the ATPase activity by 3.4-fold. FKBP52 had a stronger effect on Hsp90α:GR complexes compared to FKBP51 similar to the hormone binding assay. This reinforces the assumption that FKBP51 and FKBP52 interact differently with Hsp90α:GR. The findings were mapped to the FK1 domain with deletion constructs and FK1 inhibitors. Rapamycin only prevented FKBP52 from accelerating the ATPase activity in Hsp90α:GR complexes but not FKBP51. SAFit2 had no effect on FKBP52-mediated acceleration of the ATPase. The applied concentration might not have been able to completely saturate FKBP52 since SAFit2 binds to FKBP52 with low affinity. The pronounced differences in the presence of FKBP51 and FKBP52 support a model in which both PPIases deploy different mechanism to regulate hormone association to GR. In line with the hormone binding results, p23 affected the ATPase activity and could reverse the effect of FKBP51 and FKBP52 in the presence of GR. Thus, further suggesting that FKBP51 and FKBP52 act during the early to mid phase of the chaperone cycle.

The ATPase activity of Hsp90α in different co-chaperone and client complexes and proposed interaction models are shown in Fig. 43. The results further support distinct roles for FKBP51 and FKBP52 in GR activation that not only affect hormone association but also the Hsp90 ATPase activity. By loading GR as a client, Hsp90α ATPase activity is significantly reduced (Fig. 43A and B). Hsp90α facilitates hormone binding to GR, but it is unclear what effects it has on GR folding. The binding of either FKBP51 or FKBP52 accelerates ATPase activity of Hsp90α:GR by 1.5- and 2-fold, respectively (Fig. 43C and D). Thus, a direct connection to the hormone binding results and models can be established. As the ATPase activity increases, hormone association decreases. A direct interaction of FKBP52 with GR could induce conformational changes that alter the interaction surface between GR and Hsp90α. Consequently, GR is not able to inhibit the ATPase activity of Hsp90 anymore. Another potential pathway includes the transfer of GR to Hsp90. ATP hydrolysis by Hsp90 is necessary to facilitate the transfer of GR and restore ligand binding activity (Kirschke et al., 2014). During this step, client-transfer complexes with FKBP52 (Hsp90:GR:Hsp70:Hop:FKBP52) have been detected (Ebong et al., 2016). Based on the data generated in this thesis, FKBP52 could facilitate GR activation by accelerating the hydrolysis of ATP by Hsp90 in the presence of GR. To investigate and validate this model, further *in*

vitro experiments are required.

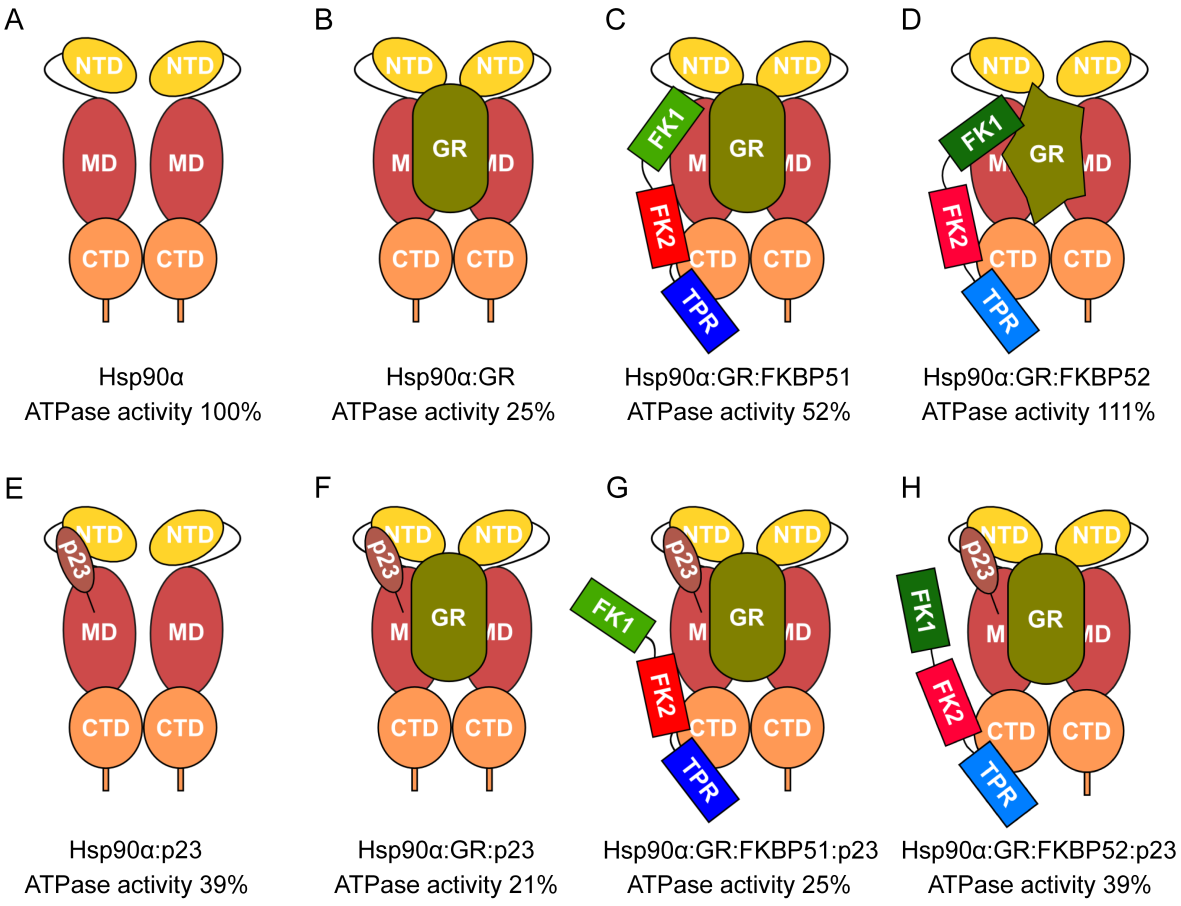

Figure 43: ATPase activity of Hsp90α in different co-chaperone and client complexes based on *in vitro* experiments. ATPase activity of only Hsp90α (A), with GR (B), with GR and FKBP51 (C), with GR and FKBP52 (D), with p23 (E), with p23 and GR (F), with p23, GR, and FKBP51 (G), and with p23, GR, and FKBP52 (H).

The addition of p23 further modulates Hsp90α ATPase activity (Fig. 43E-H). The co-chaperone p23 keeps Hsp90α in a closed conformation, which reduces ATPase activity (Fig. 43E). In Hsp90α:GR:p23 complexes, reduced ATPase activity could be beneficial for GR activation by either enabling proper folding or supporting hormone binding to a folded GR (Fig. 43F). Neither FKBP51 nor FKBP52 is able to restore complete ATPase activity in Hsp90α:GR:PPIase:p23 complexes (Fig. 43G and H). This supports the hypothesis that p23 modulates the interaction between FKBP51/52, Hsp90α, and GR. Taken together, the results indicate that FKBP51 and FKBP52 act during the early to mid phase of the chaperone cycle and allow proper folding of GR before it is activated by GCs. p23 acts at a late stage of the Hsp90 chaperoning cycle and increases the amount of active receptors (Grenert et al., 1999). It stabilizes a closed, dimerized conformation of Hsp90, which is induced by ATP, by binding in an interface between the two NTDs of Hsp90 (Ali et al., 2006). Consequently, the lifetime of the closed Hsp90 conformation is extended and ATP hydrolysis inhibited. The release mechanism of GR has not been elucidated, but ATP hydrolysis and adaption of an

open Hsp90 conformation has been linked to Hsp90 client release (Lorenz et al., 2014). In this context, the presence of p23 could give GR more time to complete its folding or to facilitate its transport to the nucleus. Thus, p23 aids in the final step during client maturation and outweighs the effects FKBP51 and FKBP52 have on chaperone-client complexes. The cycle moves forward once p23 enters the complex.

5.6 FKBP51 as a drug target

FKBP51 has been recognized as a potential drug target in oncologic diseases and psychological disorders (Schmidt et al., 2012). In squirrel monkey for example, FKBP51 drastically reduces GC binding to the GR and is elevated in squirrel monkey lymphocytes, which show GC resistance (Denny et al., 2000). Recently, it was shown in human H4 neuroglioma cells that the overexpression of FKBP51 lowered GR response upon stimulation (Hofmann, 2018). The GR-mediated gene expression in H4 cells was strongly increased after treatment with Rapamycin and FK506 and moderately increased after SAFit2 treatment (Hofmann, 2018). The hormone binding assay provides a tool to address the question whether FK1 inhibitors influence hormone association and further, if selectivity between FKBP51 and FKBP52 is necessary. Thus, FK1 binders and complex disruptors were analyzed in the context of hormone binding to Hsp90:GR:co-chaperone complexes.

The FKBP51-specific inhibitor Benztropine has been shown to restore GR activity by disrupting Hsp90:GR:FKBP51 complexes (Sabbagh et al., 2018), but it did not accelerate hormone association in the presence of FKBP51 under the experimental conditions used in this work. Benztropine might address a low affinity interaction in the high micromolar range and thus an eight-fold excess might not be sufficient to disrupt FKBP51-containing complexes. The investigated FK1 inhibitors depicted an intriguing insight into the mechanism and selectivity between both FKBPs. Rapamycin, an unselective FKBP binder, accelerated hormone association only slightly by 1.4-fold for FKBP51 but induced a significant increase for FKBP52 where a 6.3-fold acceleration was observed. Surprisingly, the FKBP51 selective binder SAFit2 decelerated hormone association further with FKBP51 while it marginally accelerated hormone association with FKBP52. SAFit2 binds selectively to FKBP51 and thereby lifts the inhibitory effect of the co-chaperone on GR signaling (Gaali et al., 2015). However, surface plasmon resonance (SPR) revealed that the selectivity of SAFit2 was only >125-fold over FKBP52 (Table 32). This is in contrast to the proposed $>10{,}000$-fold selectivity of SAFit2 by Gaali et al. (2015). The discrepancies may be due to the different assays that were used. In contrast to SPR, where binding is directly measured, Gaali et al. (2015) employed a competitive FP assay. Hence, they had to use two different tracer probes for FKBP51 and FKBP52 to defer binding affinities. The use of two separate tracers and the indirect detection method via competitive binding might explain the discrepancy in the determined selectivity.

Surface residues in the FK1 domain were identified to be responsible for the opposing effects on hormone regulation by FKBP51 and FKBP52 (Denny et al., 2005; Riggs et al., 2007). Mutational studies showed that changing two amino acids in FKBP51 to the corresponding

amino acids in FKBP52, A116V and L119P, led to GR stimulation by FKBP51 (Riggs et al., 2007). Rapamycin and SAFit2 bind in the same pocket and address the same key interactions, but their binding induces different conformational changes in the FK1 domain of FKBP51 (Gaali et al., 2015; Shi et al., 2018). The inhibitor binding modes reveal that the FK1 domain adopts a similar conformation to the apo state when Rapamycin is bound (Fig. 44A-D). In contrast, the binding of SAFit2 leads to changes in two loops above the enzymatic pocket. One loop involves the residue F67, which is flipped out of the pocket, and the other loop, which is normally positioned above Y113, involves residues A116 and L119 (Fig. 44E and F). The residues surrounding F67 are K58, K60, and K129 in FKBP51 and T58, W60, and V129 in FKBP52. Consequently, FKBP52 will undergo different conformational changes upon SAFit2 binding than FKBP51, which could explain the opposing effect in the hormone binding assay.

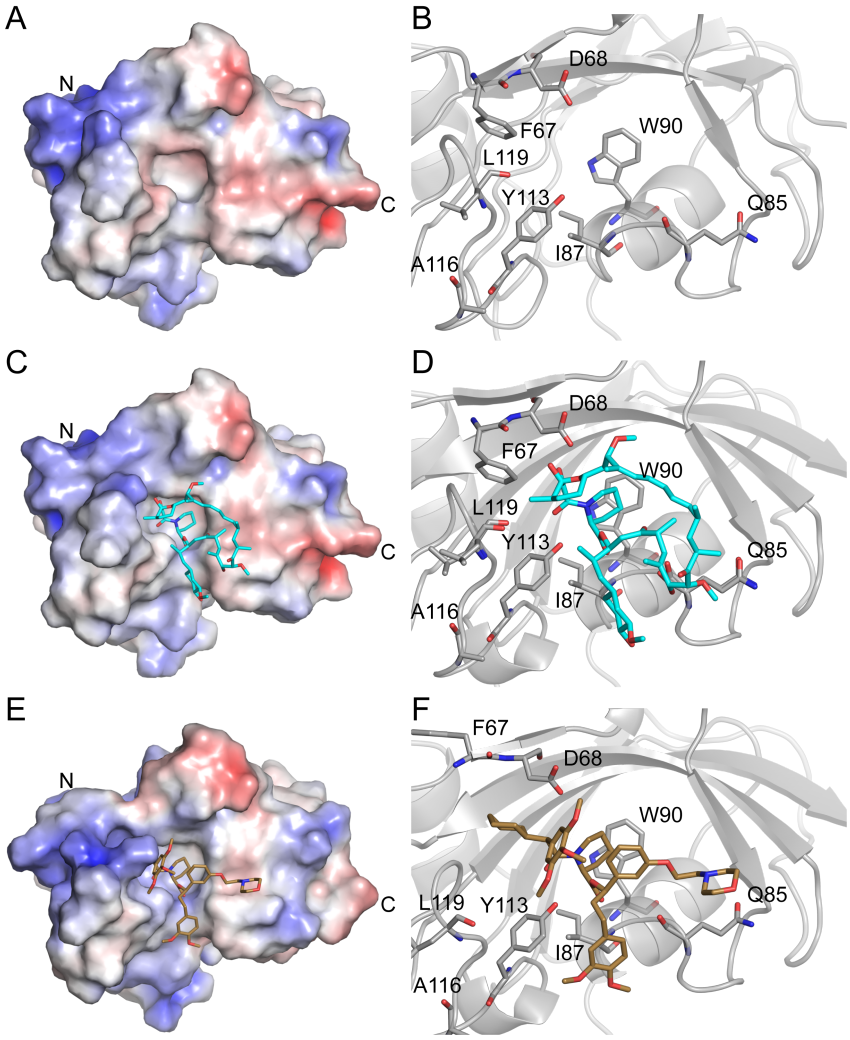

Figure 44: 3D structure of FKBP51 in the apo and ligand bound state. Surface representation and close-up of the binding pocket of FKBP51 in the apo state (A,B), with Rapamycin (cyan) (unpublished structure kindly provided by Dr. Dennis Fiegen) (C,D), and with SAFit2 (brown) (PDB ID 6TXX) (Draxler et al., 2020) (E,F). Key residues in the pocket are shown as sticks and labeled accordingly.

The binding of Rapamycin to the FK1 domain has almost the same effect on hormone association as deletion of the FK1 domain (Table 30). However, neither was able to completely restore hormone association to the same level as in GR or Hsp90:GR complexes. Hormone association would need to be accelerated by 2.4- or 8.5-fold in presence of FKBP51 and FKBP52, respectively, to reach the Hsp90:GR level. This is indicative of additional regulatory mechanisms next to the FK1 domain. Binding experiments with the C-terminal Hsp90α peptide further support this assumption since the peptide accelerated hormone association by 2.2- and 5.8-fold in the presence of FKBP51 and FKBP52, respectively. The FK2 domain of FKBP51 has been shown to be involved in the interaction with the PR (Sinars et al., 2003). While the same has not been shown for FKBP52, a similar mode of action for FKBP51/52 and GR is possible. Overall, conformational changes of the FK1 domain seem to alter the interaction surface and play a role in hormone regulation in case of FKBP51. The impact of the PPIase activity remains uncertain. However, the FK1 binding pocket could play a significant role in FKBP52-mediated effects on hormone association. Correlation of the *in vitro* and *in vivo* results propose that the overexpression of FKBP51 in cellular environments leads to an increase in complexes with reduced hormone binding, which results in less activated GR. As inhibition of the FK1 domain with Rapamycin had a more drastic impact on the FKBP52-mediated effects on hormone association, inhibitors targeting the FK1 domain might not mediate cellular effects by inhibiting FKBP51. Instead, inhibition of FKBP52 or other members of the PPIase family could be the cause of cellular effects. PPIase knock-out cells could help address this question at least with regard to GR signaling. Further steps to investigate GR regulation could include the design of FK1 mutants and chimeric constructs to elucidate how FKBP51 and FKBP52 modulate hormone association *in vitro*.

Table 30: Fold changes observed in hormone association to Hsp90α:GR complexes in presence of ΔN FKBP51/52 constructs or FK1 inhibitors in relation to full-length FKBP51/52.

	FKBP51	FKBP52
	Fold change	Fold change
ΔN	1.8	6.5
Rapamycin	1.4	6.3
SAFit2	0.7	3

In the context of depression and neuropsychiatric disorders that are caused by the overexpression of FKBP51 and subsequent GC resistance, the findings of this work might provide a new perspective on potential intervention opportunities. The opposing effects of FKBP51 and FKBP52 described in the literature led to the hypothesis that inhibitors need to be highly selective in order to be of therapeutic use (Gaali et al., 2015). However, the findings within this thesis revealed two different regulation mechanisms for FKBP51 and FKBP52. Therefore, it might not be necessary to achieve selectivity. This provides two possible paths for the development of therapeutic concepts addressing FKBP51 in depression

and neurodegenerative diseases: (1) the identification of chemical compounds that prevent FKBP51 from interacting with Hsp90:GR (Fig. 45A) or (2) targeted reduction of cellular FKBP51 protein levels (Fig. 45B). In recent years, the development of proteolysis targeting chimera (PROTAC) has been advanced to the generation of high affinity binders that are able to selectively induce protein degradation (Sakamoto et al., 2001; Zengerle et al., 2015). They have two binding moieties to bind a protein of interest and an E3 ligase. The formation of a target protein:PROTAC:E3 ligase complex leads to polyubiquitination of the target protein and its subsequent degradation by the proteasome (Fig. 45B) (Sakamoto et al., 2001; Ciechanover, 1994). The PROTAC approach could be feasible to reduce FKBP51 protein levels in overexpression cases.

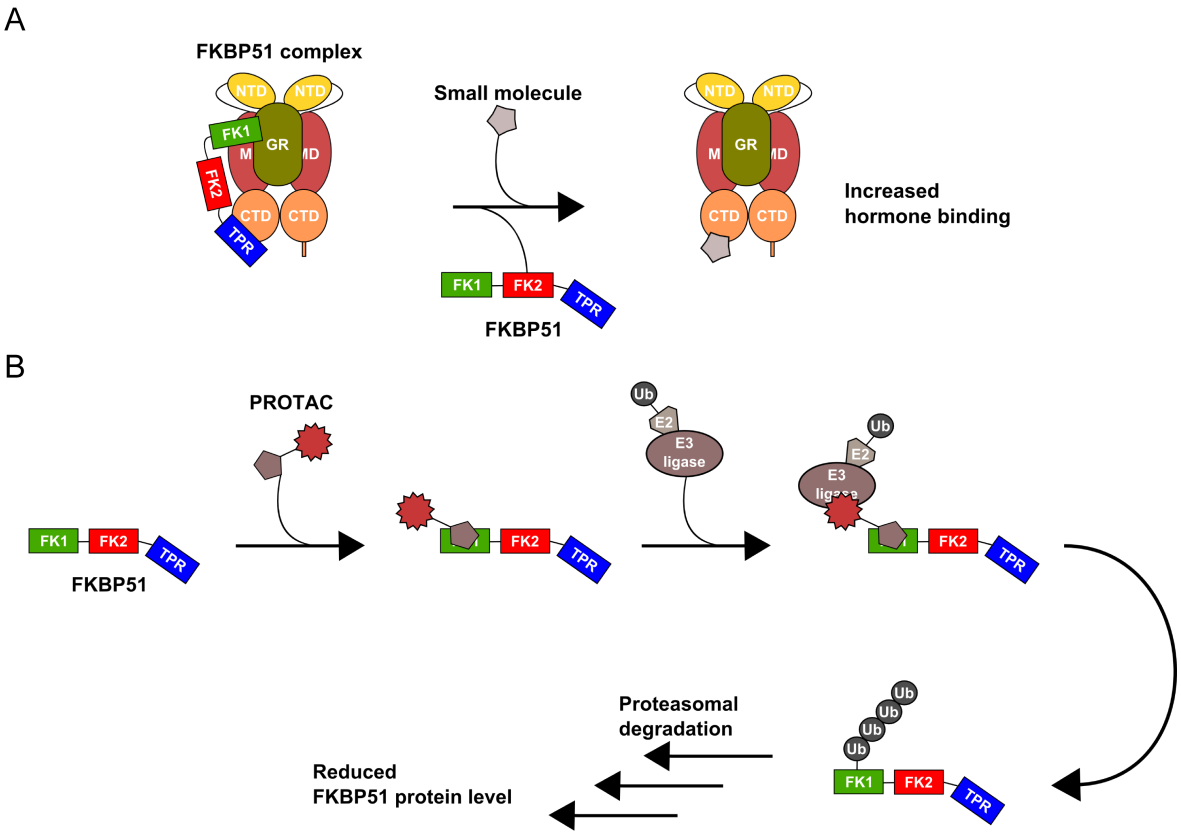

Figure 45: Therapeutic concepts for diseases related to FKBP51 overexpression. (A) Disruption of the interaction between FKBP51 and Hsp90:GR via a small molecule. Consequently, hormone binding to GR would increase. (B) Reduction of cellular FKBP51 levels by PROTACs. A PROTAC molecule binds to FKBP51 and recruits an E3 ubiquitin ligase, which would lead to polyubiquitination of FKBP51 and its subsequent degradation by the proteasome (Sakamoto et al., 2001).

The following screening strategy can be proposed to identify chemical compounds that restore glucocorticoid signaling (Fig. 46). While the TPR domain of FKBP51 is flat, polar, and thus presents a case of low druggability, the hormone binding assay considers the complex interaction profile and provides the necessary detection system to identify chemical compounds that modulate hormone binding to GR. In addition, the assay allows high-throughput screening (HTS), which makes a thorough drug discovery campaign feasible. The aim of the compound

screening on the Hsp90:GR:FKBP51 complex would be to identify hits that increase hormone association to a level comparable to the Hsp90:GR complex. The advantage of this setup is that not only FKBP51 binders would be identified but in addition compounds that bind to Hsp90 or GR and modulate hormone binding. Hits that accelerate hormone association in Hsp90:GR:FKBP51 complexes would then be further characterized biophysically (nanoDSF, SPR) in order to identify their target within the complex. After successful target identification, the binding mode of selected compounds could be structurally investigated using X-ray crystallography and NMR to enable structure-based drug design (SBDD).

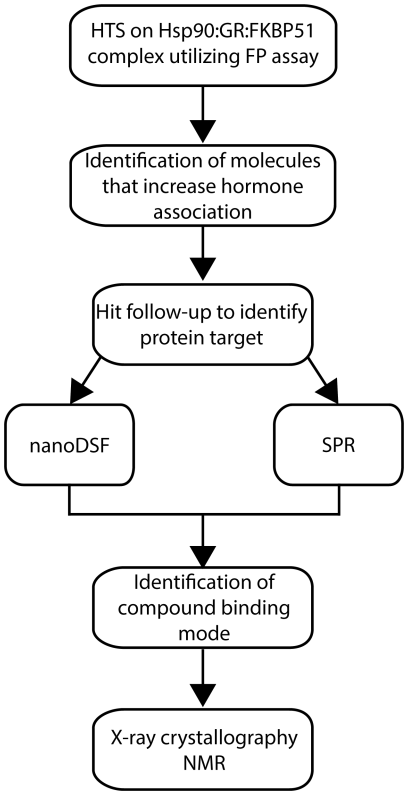

Figure 46: Proposed screening strategy to identify chemical compounds that modulate hormone binding to GR. Identification of FKBP51 binders and modulators of Hsp90:GR through a HTS campaign followed by biophysical characterization could enable the development of a chemical compound that restores GR hormone binding.

Altogether, the new data on Hsp90:GR:FKBP51/52 complexes provide a better understanding of a sophisticated system, which remains an important target for drug discovery.

5.7 Mechanistic insight into the role of FKBP51/52 in the Hsp90 chaperone cycle

The thesis provides intriguing insights into the role of FKBP51/52 in the Hsp90 chaperone cycle and during GR activation. Biophysical measurements and SAXS revealed that FKBP51 and FKBP52 use two separate binding modes to interact with Hsp90. This is also reflected in their distinct functions. FKBP51 and FKBP52 significantly slowed down hormone association to GR. This insight into the molecular mechanism on GR regulation by FKBP51 provides an explanation why overexpression of FKBP51 has such a drastic impact on GR activity *in vivo*. In contrast, previous publications proposed that FKBP52 binding leads to the formation of complexes with high affinity states for hormone binding (Davies et al., 2002). The results of this thesis indicate that FKBP52 inhibits GR activation in an even stronger manner compared to FKBP51. It is clear that the role of FKBP52 is not yet completely understood and further studies are necessary. A sequential model in which FKBP52 replaces FKBP51 is feasible in terms of binding affinities to Hsp90 but not in respect to their function and cellular availability since FKBP51 and FKBP52 are present in substoichiometric ratios (Finka and Goloubinoff, 2013). Hsp90 is one of the most abundant proteins in the cell and the likelihood of FKBP51 and FKBP52 being in the vicinity of every Hsp90:GR complex is low. Furthermore, the existence of a specific mechanism that coordinates and facilitates an exchange would be required. Consequently, it is more likely that different Hsp90:GR:co-chaperone complexes and several pathways exist in parallel. As mentioned previously, it is possible that FKBP52 facilitates the transfer of GR from Hsp40:Hsp70 to Hsp90 by accelerating the ATPase activity in such a complex. It would be intriguing to see if FKBP51 and FKBP52 in fact modulate this transfer and if they have distinct effects from each other in this context.

Overall, the *in vitro* results lead to the following Hsp90:GR chaperone cycle (Fig. 47): The binding of GR and ATP induces conformational changes in Hsp90. These changes inhibit the ATPase activity while hormone binding remains unaffected. Next, either FKBP51 or FKBP52 enters the cycle which leads to an increase in ATPase activity and a reduction in hormone binding. This could be mediated by direct or indirect interaction with GR. During this step, Hsp90 could undergo additional conformational changes and GR could fold. The entry of p23 moves the cycle forward. A tetrameric complex is formed and p23 either competes with FKBP51 and FKBP52 for interaction sites on Hsp90 or induces conformational changes in Hsp90. Thereby, p23 reduces the influence of PPIases on GR and enables hormone binding, which leads to a fully activated GR.

Nonetheless, structural studies are needed to visualize the tetrameric complex, the interaction between the components and to elucidate the effect of co-chaperones on each other. As challenging as it would be for cryo-EM and X-ray crystallography, SAXS experiments have been able to deliver structural information on Hsp90:FKBP51/52 complexes and might further provide a first glance at Hsp90:GR:PPIase and Hsp90:GR:PPIase:p23 complexes.

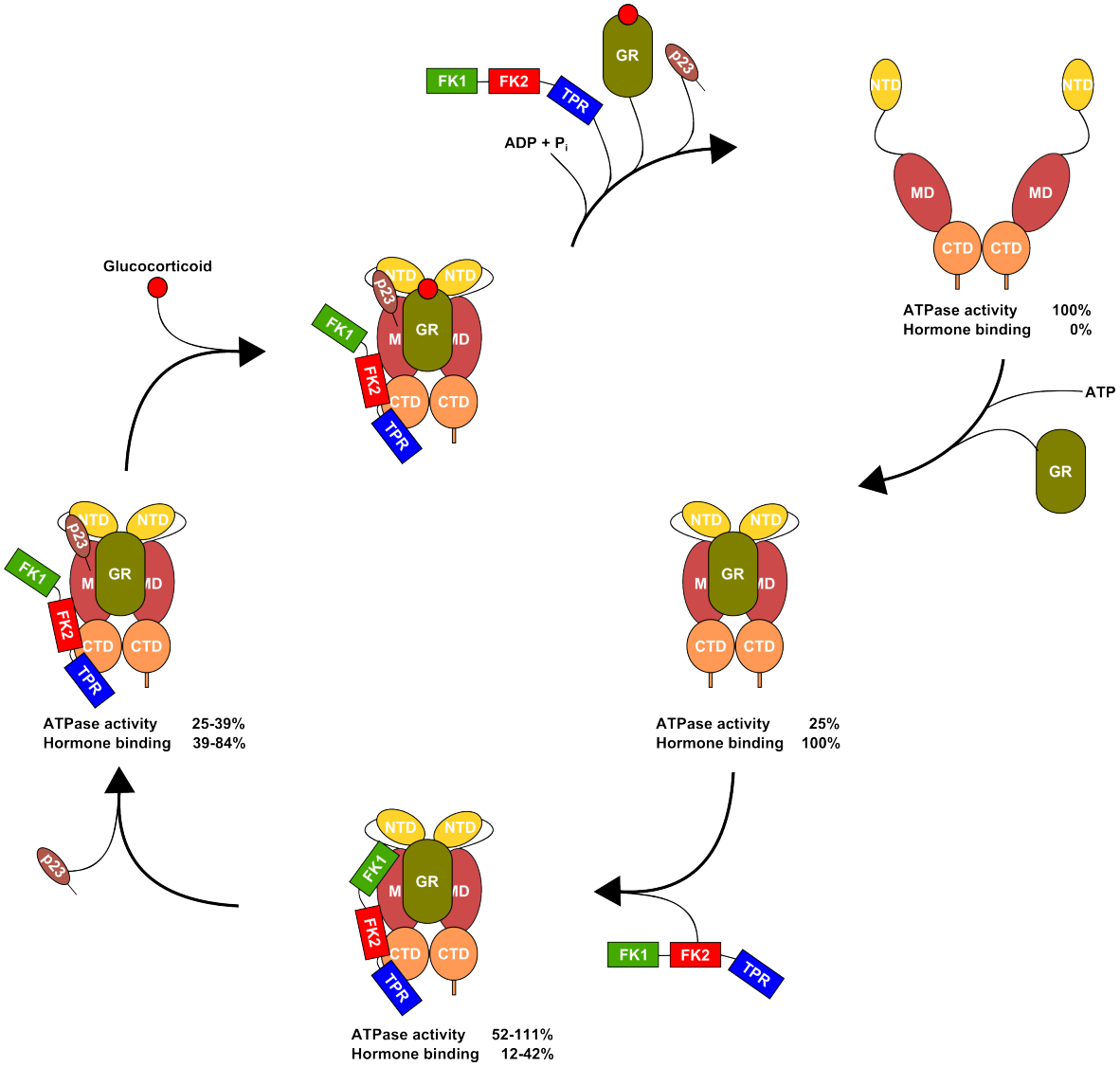

Figure 47: Hsp90:GR chaperone cycle based on *in vitro* experiments. The binding of GR reduces the ATPase activity of Hsp90 to 25 %, but does not affect hormone binding. Either FKBP51 or FKBP52 bind to Hsp90:GR and lead to 2- or 4.4-fold acceleration of ATPase activity, respectively. In parallel, hormone association is decelerated to 42 and 12 % by direct or indirect interaction with GR. The fully closed-state of Hsp90 is induced by p23, which facilitates hormone binding to GR and reduces the ATPase activity again.

Ebong et al. (2016) characterized the interconversion and intermediates in the Hsp90:GR chaperone cycle by mass spectrometry. Interestingly, their findings do not completely match the observed complexes in this work. One of the fundamental differences is the composition of Hsp90 complexes after p23 addition. Hsp70 and Hop are expelled from the transfer-client complex (Hsp90:GR:Hop:Hsp70:FKBP51/52) and complexes with the following composition were detected by Ebong et al. (2016): $(\text{Hsp90})_2$:$(\text{GR})_1$:$(\text{FKBP51})_1$:$(\text{p23})_2$ and $(\text{Hsp90})_2$:$(\text{GR})_1$:$(\text{FKBP52})_1$. Strikingly, their experiments suggest that p23 is released from complexes that contain FKBP52, which is in contrast to the findings of this dissertation. Here, functional characterization showed a clear impact of p23 on FKBP51/52 regulation and the presence of tetrameric complexes containing FKBP51/52 and p23 was confirmed

by AUC experiments. The latter also provided valuable information about binding affinities and concentrations. Not all Hsp90α:GR complexes were saturated with p23 even with a three-fold molar excess of p23 in relation to Hsp90α. An important aspect that could explain the observed compositions of Ebong et al. (2016) who used equimolar concentrations. Those conditions might not identify the major and biological prevalent complex species but instead side products caused by the affinity of the components to each other. Thus, the mass spectrometry results have to be carefully analyzed and taken with a grain of salt. However, the overall conclusions point into the same direction. Parallel pathways exist that allow different co-chaperone compositions until GR has been activated and can be transported into the nucleus. The establishment of a human Hsp90 FRET system similar to the yeast Hsp90 FRET system would allow further studies on the cycle progression with FKBP51 and FKBP52. Ultimately, FRET experiments could show if p23 induces conformational changes that alter the interaction of FKBP51/52 and Hsp90. As SAXS showed that Hsp90:PPIase complexes retained pronounced flexibility, additional SAXS experiments to incorporate the GR and further biophysical experiments with full-length GR are required to completely understand the roles of FKBP51 and FKBP52 in client maturation.

Appendix

Primary sequences of protein constructs

The primary sequences of all protein constructs covered in this thesis are shown in the following section.

Hsp90α 1-732 (FL)

```
  1 MGHHHHHHHH HHSSGHIEGR HMPEETQTQD QPMEEEEVET FAFQAEIAQL MSLIINTFYS
 61 NKEIFLRELI SNSSDALDKI RYESLTDPSK LDSGKELHIN LIPNKQDRTL TIVDTGIGMT
121 KADLINNLGT IAKSGTKAFM EALQAGADIS MIGQFGVGFY SAYLVAEKVT VITKHNDDEQ
181 YAWESSAGGS FTVRTDTGEP MGRGTKVILH LKEDQTEYLE ERRIKEIVKK HSQFIGYPIT
241 LFVEKERDKE VSDDEAEEKE DKEEEKEKEE KESEDKPEIE DVGSDEEEEK KDGDKKKKKK
301 IKEKYIDQEE LNKTKPIWTR NPDDITNEEY GEFYKSLTND WEDHLAVKHF SVEGQLEFRA
361 LLFVPRRAPF DLFENRKKKN NIKLYVRRVF IMDNCEELIP EYLNFIRGVV DSEDLPLNIS
421 REMLQQSKIL KVIRKNLVKK CLELFTELAE DKENYKKFYE QFSKNIKLGI HEDSQNRKKL
481 SELLRYYTSA SGDEMVSLKD YCTRMKENQK HIYYITGETK DQVANSAFVE RLRKHGLEVI
541 YMIEPIDEYC VQQLKEFEGK TLVSVTKEGL ELPEDEEEKK KQEEKKTKFE NLCKIMKDIL
601 EKKVEKVVVS NRLVTSPCCI VTSTYGWTAN MERIMKAQAL RDNSTMGYMA AKKHLEINPD
661 HSIIETLRQK AEADKNDKSV KDLVILLYET ALLSSGFSLE DPQTHANRIY RMIKLGLGID
721 EDDPTADDTS AAVTEEMPPL EGDDDTSRME EVD
```

Hsp90α 279-732 (ΔN)

```
  1 MGSSHHHHHH SSGENLYFQG KIKEKYIDQE ELNKTKPIWT RNPDDITNEE YGEFYKSLTN
 61 DWEDHLAVKH FSVEGQLEFR ALLFVPRRAP FDLFENRKKK NNIKLYVRRV FIMDNCEELI
121 PEYLNFIRGV VDSEDLPLNI SREMLQQSKI LKVIRKNLVK KCLELFTELA EDKENYKKFY
181 EQFSKNIKLG IHEDSQNRKK LSELLRYYTS ASGDEMVSLK DYCTRMKENQ KHIYYITGET
241 KDQVANSAFV ERLRKHGLEV IYMIEPIDEY CVQQLKEFEG KTLVSVTKEG LELPEDEEEK
301 KKQEEKKTKF ENLCKIMKDI LEKKVEKVVV SNRLVTSPCC IVTSTYGWTA NMERIMKAQA
361 LRDNSTMGYM AAKKHLEINP DHSIIETLRQ KAEADKNDKS VKDLVILLYE TALLSSGFSL
421 EDPQTHANRI YRMIKLGLGI DEDDPTADDT SAAVTEEMPP LEGDDDTSRM EEVD
```

Hsp90α 473-732 (ΔNM)

```
  1 MGSSHHHHHH SSGENLYFQG EMVSLKDYCT RMKENQKHIY YITGETKDQV ANSAFVERLR
 61 KHGLEVIYMI EPIDEYCVQQ LKEFEGKTLV SVTKEGLELP EDEEEKKKQE EKKTKFENLC
121 KIMKDILEKK VEKVVVSNRL VTSPCCIVTS TYGWTANMER IMKAQALRDN STMGYMAAKK
181 HLEINPDHSI IETLRQKAEA DKNDKSVKDL VILLYETALL SSGFSLEDPQ THANRIYRMI
241 KLGLGIDEDD PTADDTSAAV TEEMPPLEGD DDTSRMEEVD
```

Hsp90α 549-732 (ΔNM2)

```
  1 MGSSHHHHHH SSGENLYFQG LELPEDEEEK KKQEEKKTKF ENLCKIMKDI LEKKVEKVVV
 61 SNRLVTSPCC IVTSTYGWTA NMERIMKAQA LRDNSTMGYM AAKKHLEINP DHSIIETLRQ
121 KAEADKNDKS VKDLVILLYE TALLSSGFSL EDPQTHANRI YRMIKLGLGI DEDDPTADDT
181 SAAVTEEMPP LEGDDDTSRM EEVD
```

Hsp90β 1-724 (FL)

```
  1 MGHHHHHHHH HHSSGHENLY FQGHMPEEVH HGEEEVETFA FQAEIAQLMS LIINTFYSNK
 61 EIFLRELISN ASDALDKIRY ESLTDPSKLD SGKELKIDII PNPQERTLTL VDTGIGMTKA
121 DLINNLGTIA KSGTKAFMEA LQAGADISMI GQFGVGFYSA YLVAEKVVVI TKHNDDEQYA
181 WESSAGGSFT VRADHGEPIG RGTKVILHLK EDQTEYLEER RVKEVVKKHS QFIGYPITLY
241 LEKEREKEIS DDEAEEEKGE KEEEDKDDEE KPKIEDVGSD EEDDSGKDKK KKTKKIKEKY
301 IDQEELNKTK PIWTRNPDDI TQEEYGEFYK SLTNDWEDHL AVKHFSVEGQ LEFRALLFIP
361 RRAPFDLFEN KKKKNNIKLY VRRVFIMDSC DELIPEYLNF IRGVVDSEDL PLNISREMLQ
421 QSKILKVIRK NIVKKCLELF SELAEDKENY KKFYEAFSKN LKLGIHEDST NRRRLSELLR
481 YHTSQSGDEM TSLSEYVSRM KETQKSIYYI TGESKEQVAN SAFVERVRKR GFEVVYMTEP
541 IDEYCVQQLK EFDGKSLVSV TKEGLELPED EEEKKKMEES KAKFENLCKL MKEILDKKVE
601 KVTISNRLVS SPCCIVTSTY GWTANMERIM KAQALRDNST MGYMMAKKHL EINPDHPIVE
661 TLRQKAEADK NDKAVKDLVV LLFETALLSS GFSLEDPQTH SNRIYRMIKL GLGIDEDEVA
721 AEEPNAAVPD EIPPLEGDED ASRMEEVD
```

Hsp90β 271-724 (ΔN)

```
  1 MGSSHHHHHH SSGENLYFQG GGKIKEKYID QEELNKTKPI WTRNPDDITQ EEYGEFYKSL
 61 TNDWEDHLAV KHFSVEGQLE FRALLFIPRR APFDLFENKK KKNNIKLYVR RVFIMDSCDE
121 LIPEYLNFIR GVVDSEDLPL NISREMLQQS KILKVIRKNI VKKCLELFSE LAEDKENYKK
181 FYEAFSKNLK LGIHEDSTNR RRLSELLRYH TSQSGDEMTS LSEYVSRMKE TQKSIYYITG
241 ESKEQVANSA FVERVRKRGF EVVYMTEPID EYCVQQLKEF DGKSLVSVTK EGLELPEDEE
301 EKKKMEESKA KFENLCKLMK EILDKKVEKV TISNRLVSSP CCIVTSTYGW TANMERIMKA
361 QALRDNSTMG YMMAKKHLEI NPDHPIVETL RQKAEADKND KAVKDLVVLL FETALLSSGF
421 SLEDPQTHSN RIYRMIKLGL GIDEDEVAAE EPNAAVPDEI PPLEGDEDAS RMEEVD
```

Hsp90β 465-724 (ΔNM)

```
  1 MGSSHHHHHH SSGENLYFQG GGEMTSLSEY VSRMKETQKS IYYITGESKE QVANSAFVER
 61 VRKRGFEVVY MTEPIDEYCV QQLKEFDGKS LVSVTKEGLE LPEDEEEKKK MEESKAKFEN
121 LCKLMKEILD KKVEKVTISN RLVSSPCCIV TSTYGWTANM ERIMKAQALR DNSTMGYMMA
181 KKHLEINPDH PIVETLRQKA EADKNDKAVK DLVVLLFETA LLSSGFSLED PQTHSNRIYR
241 MIKLGLGIDE DEVAAEEPNA AVPDEIPPLE GDEDASRMEE VD
```

Hsp90β 542-724 (ΔNM2)

```
  1 MGSSHHHHHH SSGENLYFQG GGELPEDEEE KKKMEESKAK FENLCKLMKE ILDKKVEKVT
 61 ISNRLVSSPC CIVTSTYGWT ANMERIMKAQ ALRDNSTMGY MMAKKHLEIN PDHPIVETLR
121 QKAEADKNDK AVKDLVVLLF ETALLSSGFS LEDPQTHSNR IYRMIKLGLG IDEDEVAAEE
181 PNAAVPDEIP PLEGDEDASR MEEVD
```

FKBP51 1-457 (FL)

```
  1 MHHHHHHHHH HENLYFQSGM TTDEGAKNNE ESPTATVAEQ GEDITSKKDR GVLKIVKRVG
 61 NGEETPMIGD KVYVHYKGKL SNGKKFDSSH DRNEPFVFSL GKGQVIKAWD IGVATMKKGE
121 ICHLLCKPEY AYGSAGSLPK IPSNATLFFE IELLDFKGED LFEDGGIIRR TKRKGEGYSN
181 PNEGATVEIH LEGRCGGRMF DCRDVAFTVG EGEDHDIPIG IDKALEKMQR EEQCILYLGP
241 RYGFGEAGKP KFGIEPNAEL IYEVTLKSFE KAKESWEMDT KEKLEQAAIV KEKGTVYFKG
301 GKYMQAVIQY GKIVSWLEME YGLSEKESKA SESFLLAAFL NLAMCYLKLR EYTKAVECCD
361 KALGLDSANE KGLYRRGEAQ LLMNEFESAK GDFEKVLEVN PQNKAARLQI SMCQKKAKEH
421 NERDRRIYAN MFKKFAEQDA KEEANKAMGK KTSEGVTNEK GTDSQAMEEE KPEGHV
```

FKBP51 1-140 (ΔMC)

```
  1 MSYYHHHHHH DYDIPTTENL YFQGAMAMTT DEGAKNNEES PTATVAEQGE DITSKKDRGV
 61 LKIVKRVGNG EETPMIGDKV YVHYKGKLSN GKKFDSSHDR NEPFVFSLGK GQVIKAWDIG
121 VATMKKGEIC HLLCKPEYAY GSAGSLPKIP SNATLFFEIE LLDFKGE
```

FKBP51 16-260 (ΔC)

```
  1 MSYYHHHHHH DYDIPTTENL YFQGAMATVA EQGEDITSKK DRGVLKIVKR VGNGEETPMI
 61 GDKVYVHYKG KLSNGKKFDS SHDRNEPFVF SLGKGQVIKA WDIGVATMKK GEICHLLCKP
121 EYAYGSAGSL PKIPSNATLF FEIELLDFKG EDLFEDGGII RRTKRKGEGY SNPNEGATVE
181 IHLEGRCGGR MFDCRDVAFT VGEGEDHDIP IGIDKALEKM QREEQCILYL GPRYGFGEAG
241 KPKFGIEPNA ELIYEVTLKS FEKAKESWEM D
```

FKBP51 139-457 (ΔN)

```
  1 MHHHHHHHHH HENLYFQSGG EDLFEDGGII RRTKRKGEGY SNPNEGATVE IHLEGRCGGR
 61 MFDCRDVAFT VGEGEDHDIP IGIDKALEKM QREEQCILYL GPRYGFGEAG KPKFGIEPNA
121 ELIYEVTLKS FEKAKESWEM DTKEKLEQAA IVKEKGTVYF KGGKYMQAVI QYGKIVSWLE
181 MEYGLSEKES KASESFLLAA FLNLAMCYLK LREYTKAVEC CDKALGLDSA NEKGLYRRGE
241 AQLLMNEFES AKGDFEKVLE VNPQNKAARL QISMCQKKAK EHNERDRRIY ANMFKKFAEQ
301 DAKEEANKAM GKKTSEGVTN EKGTDSQAME EEKPEGHV
```

FKBP51 139-414 (ΔN2)

```
  1 MHHHHHHHHH HENLYFQSGG EDLFEDGGII RRTKRKGEGY SNPNEGATVE IHLEGRCGGR
 61 MFDCRDVAFT VGEGEDHDIP IGIDKALEKM QREEQCILYL GPRYGFGEAG KPKFGIEPNA
121 ELIYEVTLKS FEKAKESWEM DTKEKLEQAA IVKEKGTVYF KGGKYMQAVI QYGKIVSWLE
181 MEYGLSEKES KASESFLLAA FLNLAMCYLK LREYTKAVEC CDKALGLDSA NEKGLYRRGE
241 AQLLMNEFES AKGDFEKVLE VNPQNKAARL QISMCQKKAK EHNERDRRIY ANMFK
```

FKBP52 1-459 (FL)

```
  1 MHHHHHHHHH HGGENLYFQG ATAEEMKATE SGAQSAPLPM EGVDISPKQD EGVLKVIKRE
 61 GTGTEMPMIG DRVFVHYTGW LLDGTKFDSS LDRKDKFSFD LGKGEVIKAW DIAIATMKVG
121 EVCHITCKPE YAYGSAGSPP KIPPNATLVF EVELFEFKGE DLTEEEDGGI IRRIQTRGEG
181 YAKPNEGAIV EVALEGYYKD KLFDQRELRF EIGEGENLDL PYGLERAIQR MEKGEHSIVY
241 LKPSYAFGSV GKEKFQIPPN AELKYELHLK SFEKAKESWE MNSEEKLEQS TIVKERGTVY
301 FKEGKYKQAL LQYKKIVSWL EYESSFSNEE AQKAQALRLA SHLNLAMCHL KLQAFSAAIE
361 SCNKALELDS NNEKGLFRRG EAHLAVNDFE LARADFQKVL QLYPNNKAAK TQLAVCQQRI
421 RRQLAREKKL YANMFERLAE EENKAKAEAS SGDHPTDTEM KEEQKSNTAG SQSQVETEA
```

FKBP52 1-140 (ΔMC)

```
  1 MSYYHHHHHH DYDIPTTENL YFQGAMAMTA EEMKATESGA QSAPLPMEGV DISPKQDEGV
 61 LKVIKREGTG TEMPMIGDRV FVHYTGWLLD GTKFDSSLDR KDKFSFDLGK GEVIKAWDIA
121 IATMKVGEVC HITCKPEYAY GSAGSPPKIP PNATLVFEVE LFEFKGE
```

FKBP52 16-260 (ΔC)

```
  1 MSYYHHHHHH DYDIPTTENL YFQGAMAAPL PMEGVDISPK QDEGVLKVIK REGTGTEMPM
 61 IGDRVFVHYT GWLLDGTKFD SSLDRKDKFS FDLGKGEVIK AWDIAIATMK VGEVCHITCK
121 PEYAYGSAGS PPKIPPNATL VFEVELFEFK GEDLTEEEDG GIIRRIQTRG EGYAKPNEGA
181 IVEVALEGYY KDKLFDQREL RFEIGEGENL DLPYGLERAI QRMEKGEHSI VYLKPSYAFG
241 SVGKEKFQIP PNAELKYELH LKSFEKAKES WE
```

FKBP52 139-459 (ΔN)

```
  1 MSYYHHHHHH DYDIPTTENL YFQGAMAGED LTEEEDGGII RRIQTRGEGY AKPNEGAIVE
 61 VALEGYYKDK LFDQRELRFE IGEGENLDLP YGLERAIQRM EKGEHSIVYL KPSYAFGSVG
121 KEKFQIPPNA ELKYELHLKS FEKAKESWEM NSEEKLEQST IVKERGTVYF KEGKYKQALL
181 QYKKIVSWLE YESSFSNEEA QKAQALRLAS HLNLAMCHLK LQAFSAAIES CNKALELDSN
241 NEKGLFRRGE AHLAVNDFEL ARADFQKVLQ LYPNNKAAKT QLAVCQQRIR RQLAREKKLY
301 ANMFERLAEE ENKAKAEASS GDHPTDTEMK EEQKSNTAGS QSQVETEA
```

FKBP52 139-416 (ΔN2)

```
  1 MSYYHHHHHH DYDIPTTENL YFQGAMAGED LTEEEDGGII RRIQTRGEGY AKPNEGAIVE
 61 VALEGYYKDK LFDQRELRFE IGEGENLDLP YGLERAIQRM EKGEHSIVYL KPSYAFGSVG
121 KEKFQIPPNA ELKYELHLKS FEKAKESWEM NSEEKLEQST IVKERGTVYF KEGKYKQALL
181 QYKKIVSWLE YESSFSNEEA QKAQALRLAS HLNLAMCHLK LQAFSAAIES CNKALELDSN
241 NEKGLFRRGE AHLAVNDFEL ARADFQKVLQ LYPNNKAAKT QLAVCQQRIR RQLAREKKLY
301 ANMFE
```

GR-LBD 521-777 F602S/A605V/V702A/E705G/M752T (GR-LBDm)

```
  1 GSPGIRHHHH HHHHGGVPAT LPQLTPTLVS LLEVIEPEVL YAGYDSSVPD STWRIMTTLN
 61 MLGGRQVIAA VKWAKAIPGF RNLHLDDQMT LLQYSWMSLM VFALGWRSYR QSSANLLCFA
121 PDLIINEQRM TLPCMYDQCK HMLYVSSELH RLQVSYEEYL CMKTLLLLSS VPKDGLKSQE
181 LFDEIRMTYI KELGKAIAKR GGNSSQNWQR FYQLTKLLDS MHEVVENLLN YCFQTFLDKT
241 MSIEFPETLA EIITNQIPKY SNGNIKKLLF HQK
```

Comparison of Hsp90α/β ATPase assay

Table 31: Catalytic activities (k_{cat}) of Hsp90α/β in ATPase assay experiments. R: Replicate. SD: Standard deviation.

Protein	R 1 [min^{-1}]	R 2 [min^{-1}]	R 3 [min^{-1}]	Mean [min^{-1}]	SD [min^{-1}]
Hsp90α	0.299	0.282	0.252	0.278	0.024
Hsp90β	0.056	0.053	0.050	0.053	0.003

Determined affinities of Rapamycin and SAFit2

Surface plasmon resonance (SPR) is based on a change in the refractive index of the medium in close proximity of a metal surface that can be used to monitor the binding of analyte molecules to ligand molecules, which are immobilized on a metal surface (Patching, 2014). An oscillating electromagnetic wave is generated on the surface of metal with an excitation laser. The refractive index of the medium, which is in contact with the metal surface, changes during binding events. This change can be detected by the reflection angle. The measured signal can be used to calculate the dissociation constant, binding stoichiometries as well as kinetic association and dissociation rates.

SPR binding studies with SAFit2 and Rapamycin were carried out on a Biacore T200 instrument using complex buffer (Table 9) supplement with 0.05 % Tween-20 and 5 % DMSO.

Purified avi-tagged and biotinylated full-length FKBP51 and FKBP52 were provided by Viktor Beke and immobilized on a SA chip. The chip is covered with pre-immobilized

Streptavidin which binds with high affinity to biotin. Thus, enabling a gentle and directed immobilization. The SA chip was pre-conditioned with three 60 s injections of 1 M NaCl dissolved in 50 mM NaOH. To capture biotinylated proteins, FKBP51/52 FL were diluted to 30 $\frac{\mu g}{mL}$ in SPR buffer and immobilized on the surface for up to 40 s.

Analytes were prepared in a 1:3 dilution series in running buffer with a starting concentration of 10 μM. Binding experiments were performed in multi cycle mode at a flow rate of 30 $\frac{\mu L}{min}$ with 120 s association time and 300 s dissociation time. Experiments were evaluated with the Biacore T200 Evaluation Software. Samples were referenced against a blank cell and corrected for an inaccurate DMSO concentration (solvent correction).

Table 32: Determined K_D values of FK1 binder Rapamycin (n=2) and SAFit2 (n=3) by SPR (±SD).

	Rapamycin	SAFit2
FKBP51	74±48 nM	65±23 nM
FKBP52	78±52 nM	> 10 µM

Table 33: Statistical analysis of hormone binding to different GR containing complexes. Statistical significance was assessed using a two-sample t-test and a significance level of 0.05.

Figure	Sample	k_{obs} [min^{-1}]	p-value
Fig. 30C	GR-LBDm:Hsp90α	0.03377±0.00542	< 0.0001
	GR-LBDm:Hsp90α:FKBP51	0.01408±0.00088	
Fig. 30C	GR-LBDm:Hsp90α:FKBP51	0.01408±0.00088	< 0.0001
	GR-LBDm:Hsp90α:FKBP51ΔN	0.02475±0.00162	
Fig. 30C	GR-LBDm:Hsp90α	0.03377±0.00542	< 0.0001
	GR-LBDm:Hsp90α:FKBP52	0.00432±0.00085	
Fig. 30D	GR-LBDm:Hsp90α:FKBP51	0.01408±0.00088	< 0.0001
	GR-LBDm:Hsp90α:FKBP51:peptide	0.03078±0.00304	
Fig. 30D	GR-LBDm:Hsp90α:FKBP51ΔN	0.02475±0.00162	0.0041
	GR-LBDm:Hsp90α:FKBP51ΔN:peptide	0.03268±0.00460	
Fig. 30D	GR-LBDm:Hsp90α:FKBP52	0.00432±0.00085	< 0.0001
	GR-LBDm:Hsp90α:FKBP52:peptide	0.02333±0.00064	
Fig. 30D	GR-LBDm:Hsp90α:FKBP52ΔN	0.02607±0.00171	0.0126
	GR-LBDm:Hsp90α:FKBP52ΔN:peptide	0.03360±0.00447	
Fig. 31A	GR-LBDm:Hsp90α:p23	0.03430±0.00290	0.0045
	GR-LBDm:Hsp90α:FKBP51:p23	0.02790±0.00318	
Fig. 31A	GR-LBDm:Hsp90α:FKBP51	0.01408±0.00088	< 0.0001
	GR-LBDm:Hsp90α:FKBP51:p23	0.02790±0.00318	
Fig. 31A	GR-LBDm:Hsp90α:FKBP51ΔN	0.02475±0.00162	0.0004
	GR-LBDm:Hsp90α:FKBP51ΔN:p23	0.03057±0.00198	
Fig. 31A	GR-LBDm:Hsp90α:p23	0.03430±0.00290	< 0.0001
	GR-LBDm:Hsp90α:FKBP52:p23	0.01309±0.00079	
Fig. 31A	GR-LBDm:Hsp90α:FKBP52	0.00432±0.00085	< 0.0001
	GR-LBDm:Hsp90α:FKBP52:p23	0.01309±0.00079	
Fig. 32	GR-LBDm:Hsp90α:FKBP51:ATP	0.01408±0.00088	< 0.0001
	GR-LBDm:Hsp90α:FKBP51:no nucleotide	0.00718±0.00063	
Fig. 32	GR-LBDm:Hsp90α:FKBP51:ATP	0.01408±0.00088	< 0.0001
	GR-LBDm:Hsp90α:FKBP51:ATPγS	0.00616±0.00054	
Fig. 32	GR-LBDm:Hsp90α:FKBP51:p23:ATP	0.02790±0.00318	< 0.0001
	GR-LBDm:Hsp90α:FKBP51:p23:no nucleotide	0.00504±0.00188	
Fig. 32	GR-LBDm:Hsp90α:FKBP51ΔN:ATP	0.02475±0.00162	< 0.0001
	GR-LBDm:Hsp90α:FKBP51ΔN:no nucleotide	0.01442±0.00234	
Fig. 32	GR-LBDm:Hsp90α:FKBP51ΔN:p23:ATP	0.03057±0.00198	< 0.0001
	GR-LBDm:Hsp90α:FKBP51ΔN:p23:no nucleotide	0.01447±0.00262	

Fig. 32	GR-LBDm:Hsp90α:FKBP52:ATP	0.00432±0.00085	< 0.0001
	GR-LBDm:Hsp90α:FKBP52:no nucleotide	0.00010±0.00013	
Fig. 32	GR-LBDm:Hsp90α:FKBP52:p23:ATP	0.01309±0.00079	< 0.0001
	GR-LBDm:Hsp90α:FKBP52:p23:no nucleotide	0.00054±0.00084	
Fig. 32	GR-LBDm:Hsp90α:FKBP52ΔN:ATP	0.02607±0.00171	0.0230
	GR-LBDm:Hsp90α:FKBP52ΔN:no nucleotide	0.02055±0.00386	
Fig. 32	GR-LBDm:Hsp90α:FKBP52ΔN:p23:ATP	0.02466±0.00191	< 0.001
	GR-LBDm:Hsp90α:FKBP52ΔN:p23:no nucleotide	0.01629±0.00185	
Fig. 33A	GR-LBDm:Hsp90β	0.03090±0.00237	< 0.0001
	GR-LBDm:Hsp90β:FKBP51	0.00827±0.00096	
Fig. 33A	GR-LBDm:Hsp90β:FKBP51	0.00827±0.00096	< 0.0001
	GR-LBDm:Hsp90β:FKBP51ΔN	0.01834±0.00067	
Fig. 33A	GR-LBDm:Hsp90β	0.03090±0.00237	< 0.0001
	GR-LBDm:Hsp90β:FKBP52	0.00083±0.00074	
Fig. 33A	GR-LBDm:Hsp90β:FKBP52	0.00083±0.00074	< 0.0001
	GR-LBDm:Hsp90β:FKBP52ΔN	0.01809±0.00270	
Fig. 33B	GR-LBDm:Hsp90β:FKBP51	0.00827±0.00096	< 0.0001
	GR-LBDm:Hsp90β:FKBP51:p23	0.01834±0.00067	
Fig. 33B	GR-LBDm:Hsp90β:FKBP51ΔN	0.01834±0.00067	0.0004
	GR-LBDm:Hsp90β:FKBP51ΔN:p23	0.02348±0.00152	
Fig. 33B	GR-LBDm:Hsp90β:FKBP52	0.00083±0.00074	0.0068
	GR-LBDm:Hsp90β:FKBP52:p23	0.00396±0.00136	
Fig. 33B	GR-LBDm:Hsp90β:FKBP52ΔN	0.01809±0.00270	0.0436
	GR-LBDm:Hsp90β:FKBP52ΔN:p23	0.02238±0.00156	
Fig. 33C	GR-LBDm:Hsp90α:FKBP51	0.01408±0.00088	< 0.0001
	GR-LBDm:Hsp90β:FKBP51	0.00827±0.00096	
Fig. 33C	GR-LBDm:Hsp90α:FKBP51ΔN	0.02475±0.00162	< 0.0001
	GR-LBDm:Hsp90β:FKBP51ΔN	0.01834±0.00067	
Fig. 33C	GR-LBDm:Hsp90α:FKBP51:p23	0.02790±0.00318	< 0.0001
	GR-LBDm:Hsp90β:FKBP51:p23	0.01834±0.00067	
Fig. 33C	GR-LBDm:Hsp90α:FKBP51ΔN:p23	0.03057±0.00198	0.0006
	GR-LBDm:Hsp90β:FKBP51ΔN:p23	0.02348±0.00152	
Fig. 33C	GR-LBDm:Hsp90α:FKBP52	0.00432±0.00085	0.0002
	GR-LBDm:Hsp90β:FKBP52	0.00083±0.00074	
Fig. 33C	GR-LBDm:Hsp90α:FKBP52ΔN	0.02607±0.00171	0.0020
	GR-LBDm:Hsp90β:FKBP52ΔN	0.01809±0.00270	
Fig. 33C	GR-LBDm:Hsp90α:FKBP52:p23	0.01309±0.00079	< 0.0001
	GR-LBDm:Hsp90β:FKBP52:p23	0.00396±0.00136	

Fig. 33C	GR-LBDm:Hsp90α:FKBP52ΔN:p23	0.02466±0.00191	0.0835
	GR-LBDm:Hsp90β:FKBP52ΔN:p23	0.02238±0.00156	
Fig. 34A	GR-LBDm:Hsp90α:FKBP51	0.01408±0.00088	0.0079
	GR-LBDm:Hsp90α:FKBP51:Rapamycin	0.01852±0.00299	
Fig. 34A	GR-LBDm:Hsp90α:FKBP51:p23	0.02790±0.00318	0.5063
	GR-LBDm:Hsp90α:FKBP51:p23:Rapamycin	0.02966±0.00491	
Fig. 34A	GR-LBDm:Hsp90α:FKBP52	0.00432±0.00085	<0.0001
	GR-LBDm:Hsp90α:FKBP52:Rapamycin	0.02492±0.00194	
Fig. 34A	GR-LBDm:Hsp90α:FKBP52:p23	0.01309±0.00079	0.0002
	GR-LBDm:Hsp90α:FKBP52:p23:Rapamycin	0.02897±0.00593	
Fig. 34B	GR-LBDm:Hsp90α:FKBP51	0.01408±0.00088	<0.0001
	GR-LBDm:Hsp90α:FKBP51:SAFit2	0.00996±0.00050	
Fig. 34B	GR-LBDm:Hsp90α:FKBP51:p23	0.02790±0.00318	0.5913
	GR-LBDm:Hsp90α:FKBP51:p23:SAFit2	0.02696±0.00111	
Fig. 34B	GR-LBDm:Hsp90α:FKBP52	0.00432±0.00085	<0.0001
	GR-LBDm:Hsp90α:FKBP52:SAFit2	0.01183±0.00044	
Fig. 34B	GR-LBDm:Hsp90α:FKBP52:p23	0.01309±0.00079	<0.0001
	GR-LBDm:Hsp90α:FKBP52:p23:SAFit2	0.02314±0.00190	
Fig. 34C	GR-LBDm:Hsp90α:FKBP51	0.01408±0.00088	0.0259
	GR-LBDm:Hsp90α:FKBP51:Benztropine	0.01615±0.00173	
Fig. 34C	GR-LBDm:Hsp90α:FKBP51:p23	0.02790±0.00318	0.2684
	GR-LBDm:Hsp90α:FKBP51:p23:Benztropine	0.02951±0.00110	
Fig. 34C	GR-LBDm:Hsp90α:FKBP52	0.00432±0.00085	0.0773
	GR-LBDm:Hsp90α:FKBP52:Benztropine	0.00521±0.00071	
Fig. 34C	GR-LBDm:Hsp90α:FKBP52:p23	0.01309±0.00079	0.0119
	GR-LBDm:Hsp90α:FKBP52:p23:Benztropine	0.01517±0.00146	
Fig. 34D	GR-LBDm:Hsp90α:FKBP51	0.01408±0.00088	0.0011
	GR-LBDm:Hsp90α:FKBP51:Radicicol	0.01032±0.00155	
Fig. 34D	GR-LBDm:Hsp90α:FKBP51:p23	0.02790±0.00318	<0.0001
	GR-LBDm:Hsp90α:FKBP51:p23:Radicicol	0.01074±0.00185	
Fig. 34D	GR-LBDm:Hsp90α:FKBP52	0.00432±0.00085	0.5683
	GR-LBDm:Hsp90α:FKBP52:Radicicol	0.00392±0.00130	
Fig. 34D	GR-LBDm:Hsp90α:FKBP52:p23	0.01309±0.00079	<0.0001
	GR-LBDm:Hsp90α:FKBP52:p23:Radicicol	0.00346±0.00049	

Table 35: Statistical analysis of the ATPase activity of different Hsp90 complexes. Statistical significance was assessed using a two-sample *t*-test and a significance level of 0.05.

Figure	Sample	k_{cat} [min^{-1}]	p-value
Fig. 35A	Hsp90α	0.27769±0.02380	0.0004
	Hsp90α:GR-LBDm	0.07457±0.02192	
Fig. 35A	Hsp90α	0.27769±0.02380	0.1764
	Hsp90α:FKBP51	0.24134±0.03013	
Fig. 35A	Hsp90α:GR-LBDm	0.07457±0.02192	0.0174
	Hsp90α:GR-LBDm:FKBP51	0.15554±0.02838	
Fig. 35A	Hsp90α:GR-LBDm	0.07457±0.02192	< 0.0001
	Hsp90α:GR-LBDm:FKBP52	0.30941±0.00816	
Fig. 35B	Hsp90α	0.27769±0.02380	0.0010
	Hsp90α:p23	0.11048±0.02346	
Fig. 35B	Hsp90α	0.27769±0.02380	0.0001
	Hsp90α:GR-LBDm:p23	0.05538±0.00835	
Fig. 35B	Hsp90α:p23	0.11048±0.02346	0.1248
	Hsp90α:GR-LBDm:p23	0.05538±0.00835	
Fig. 35B	Hsp90α:GR-LBDm:p23	0.05538±0.00835	0.0013
	Hsp90α:GR-LBDm:p23:FKBP52	0.11296±0.00919	
Fig. 37A	Hsp90α:GR-LBDm:FKBP52	0.30941±0.00816	0.0003
	Hsp90α:GR-LBDm:FKBP52:Rapamycin	0.13995±0.02248	
Fig. 37A	Hsp90α:GR-LBDm	0.07457±0.02192	0.2293
	Hsp90α:GR-LBDm:SAFit2	0.09414±0.00956	
Fig. 37A	Hsp90α:GR-LBDm:SAFit2	0.09414±0.00956	0.0044
	Hsp90α:GR-LBDm:FKBP51:SAFit2	0.18785±0.02632	
Fig. 37A	Hsp90α:GR-LBDm:SAFit2	0.09414±0.00956	0.0012
	Hsp90α:GR-LBDm:FKBP52:SAFit2	0.26032±0.03346	

References

Albers, M. W., Walsh, C. T., and Schreiber, S. L. (1990). Substrate specificity for the human rotamase FKBP: a view of FK506 and rapamycin as leucine-(twisted amide)-proline mimics. *The Journal of Organic Chemistry*, 55:4984–4986.

Alessi, D. R., James, S. R., Downes, C. P., Holmes, A. B., Gaffney, P. R. J., Reese, C. B., and Cohen, P. (1997). Characterization of a 3-phosphoinositide-dependent protein kinase which phosphorylates and activates protein kinase bα. *Current Biology*, 7:261–269.

Ali, M. M., Roe, S. M., Vaughan, C. K., Meyer, P., Panaretou, B., Piper, P. W., Prodromou, C., and Pearl, L. H. (2006). Crystal structure of an Hsp90-nucleotide-p23/Sba1 closed chaperone complex. *Nature*, 440:1013–1017.

Avellino, R., Romano, S., Parasole, R., Bisogni, R., Lamberti, A., Poggi, V., Venuta, S., and Romano, M. F. (2005). Rapamycin stimulates apoptosis of childhood acute lymphoblastic leukemia cells. *Blood*, 106:1400–1406.

Balchin, D., Hayer-Hartl, M., and Hartl, F. U. (2016). In vivo aspects of protein folding and quality control. *Science*, 353:aac4354.

Banumathy, G., Singh, V., Pavithra, S. R., and Tatu, U. (2003). Heat shock protein 90 function is essential for *Plasmodium falciparum* growth in human erythrocytes. *Journal of Biological Chemistry*, 278:18336–18345.

Barik, S. (2006). Immunophilins: for the love of proteins. *Cellular and Molecular Life Sciences*, 63:2889–2900.

Baughman, G., Harrigan, M. T., Campbell, N. F., Nurrish, S. J., and Bourgeois, S. (1991). Genes newly identified as regulated by glucocorticoids in murine thymocytes. *Molecular Endocrinology*, 5:637–644.

Biebl, M. M. and Buchner, J. (2019). Structure, function, and regulation of the hsp90 machinery. *Cold Spring Harbor Perspectives in Biology*, 11:a034017.

Bierer, B. E., Mattila, P. S., Standaert, R. F., Herzenberg, L. A., Burakoff, S. J., Crabtree, G., and Schreiber, S. L. (1990). Two distinct signal transmission pathways in T lymphocytes are inhibited by complexes formed between an immunophilin and either FK506 or rapamycin. *Proceedings of the National Academy of Sciences*, 87:9231–9235.

Binder, E. B. (2009). The role of FKBP5, a co-chaperone of the glucocorticoid receptor in the pathogenesis and therapy of affective and anxiety disorders. *Psychoneuroendocrinology*, 34:S186–S195.

Binder, E. B., Bradley, R. G., Liu, W., Epstein, M. P., Deveau, T. C., Mercer, K. B., Tang, Y., Gillespie, C. F., Heim, C. M., Nemeroff, C. B., Schwartz, A. C., Cubells, J. F., and Ressler, K. J. (2008). Association of FKBP5 polymorphisms and childhood abuse with risk of posttraumatic stress disorder symptoms in adults. *JAMA*, 299:1291–1305.

Binder, E. B., Salyakina, D., Lichtner, P., Wochnik, G. M., Ising, M., Putz, B., Papiol, S., Seaman, S., Lucae, S., Kohli, M. A., Nickel, T., Kunzel, H. E., Fuchs, B., Majer, M., Pfennig, A., Kern, N., Brunner, J., Modell, S., Baghai, T., Deiml, T., Zill, P., Bondy, B., Rupprecht, R., Messer, T., Kohnlein, O., Dabitz, H., Bruckl, T., Muller, N., Pfister, H., Lieb, R., Mueller, J. C., Lohmussaar, E., Strom, T. M., Bettecken, T., Meitinger, T., Uhr, M., Rein, T., Holsboer, F., and Muller-Myhsok, B. (2004). Polymorphisms in FKBP5 are associated with increased recurrence of depressive episodes and rapid response to antidepressant treatment. *Nature Genetics*, 36:1319–1325.

Black, B. E., Holaska, J. M., Rastinejad, F., and Paschal, B. M. (2001). DNA binding domains in diverse nuclear receptors function as nuclear export signals. *Current Biology*, 11:1749–1758.

Bledsoe, R. K., Montana, V. G., Stanley, T. B., Delves, C. J., Apolito, C. J., McKee, D. D., Consler, T. G., Parks, D. J., Stewart, E. L., Willson, T. M., Lambert, M. H., Moore, J. T., Pearce, K. H., and Xu, H. E. (2002). Crystal structure of the glucocorticoid receptor ligand binding domain reveals a novel mode of receptor dimerization and coactivator recognition. *Cell*, 110:93–105.

Blundell, K. L., Pal, M., Roe, S. M., Pearl, L. H., and Prodromou, C. (2017). The structure of FKBP38 in complex with the MEEVD tetratricopeptide binding-motif of Hsp90. *PLoS One*, 12:e0173543.

Boczek, E. E., Reefschlager, L. G., Dehling, M., Struller, T. J., Hausler, E., Seidl, A., Kaila, V. R., and Buchner, J. (2015). Conformational processing of oncogenic v-Src kinase by the molecular chaperone Hsp90. *Proceedings of the National Academy of Sciences*, 112:E3189–E3198.

Bortsov, A. V., Smith, J. E., Diatchenko, L., Soward, A. C., Ulirsch, J. C., Rossi, C., Swor, R. A., Hauda, W. E., Peak, D. A., Jones, J. S., Holbrook, D., Rathlev, N. K., Foley, K. A., Lee, D. C., Collette, R., Domeier, R. M., Hendry, P. L., and McLean, S. A. (2013). Polymorphisms in the glucocorticoid receptor co-chaperone FKBP5 predict persistent musculoskeletal pain after traumatic stress exposure. *Pain*, 154:1419 – 1426.

Bouwmeester, T., Bauch, A., Ruffner, H., Angrand, P.-O., Bergamini, G., Croughton, K., Cruciat, C., Eberhard, D., Gagneur, J., Ghidelli, S., Hopf, C., Huhse, B., Mangano, R., Michon, A.-M., Schirle, M., Schlegl, J., Schwab, M., Stein, M. A., Bauer, A., Casari, G., Drewes, G., Gavin, A.-C., Jackson, D. B., Joberty, G., Neubauer, G., Rick, J., Kuster, B.,

and Superti-Furga, G. (2004). A physical and functional map of the human TNF-α/NF-κB signal transduction pathway. *Nature Cell Biology*, 6:97–105.

Bracher, A., Kozany, C., Thost, A.-K., and Hausch, F. (2011). Structural characterization of the PPIase domain of FKBP51, a cochaperone of human Hsp90. *Acta Crystallographica Section D*, 67:549–559.

Brinker, A., Scheufler, C., von der Mülbe, F., Fleckenstein, B., Herrmann, C., Jung, G., Moarefi, I., and Hartl, F. U. (2002). Ligand discrimination by TPR domains: Relevance and selectivity of EEVD-recognition in Hsp70·Hop·Hsp90 complexes. *Journal of Biological Chemistry*, 277:19265–19275.

Campanella, C., Pace, A., Caruso Bavisotto, C., Marzullo, P., Marino Gammazza, A., Buscemi, S., and Palumbo Piccionello, A. (2018). Heat shock proteins in Alzheimer's disease: Role and targeting. *International Journal of Molecular Sciences*, 19:2603.

Carrigan, A., Walther, R. F., Salem, H. A., Wu, D., Atlas, E., Lefebvre, Y. A., and Haché, R. J. G. (2007). An active nuclear retention signal in the glucocorticoid receptor functions as a strong inducer of transcriptional activation. *Journal of Biological Chemistry*, 282:10963–10971.

Chadli, A., Bouhouche, I., Sullivan, W., Stensgard, B., McMahon, N., Catelli, M. G., and Toft, D. O. (2000). Dimerization and N-terminal domain proximity underlie the function of the molecular chaperone heat shock protein 90. *Proceedings of the National Academy of Sciences*, 97:12524–12529.

Chadli, A., Felts, S. J., and Toft, D. O. (2008). GCUNC45 is the first Hsp90 co-chaperone to show α/β isoform specificity. *Journal of Biological Chemistry*, 283:9509–9512.

Cheung-Flynn, J., Roberts, P. J., Riggs, D. L., and Smith, D. F. (2003). C-terminal sequences outside the tetratricopeptide repeat domain of FKBP51 and FKBP52 cause differential binding to Hsp90. *Journal of Biological Chemistry*, 278:17388–17394.

Ciechanover, A. (1994). The ubiquitin-proteasome proteolytic pathway. *Cell*, 79:13–21.

Cruz-Topete, D. and Cidlowski, J. A. (2015). One hormone, two actions: Anti- and pro-inflammatory effects of glucocorticoids. *Neuroimmunomodulation*, 22:20–32.

Cunningham, C. N., Krukenberg, K. A., and Agard, D. A. (2008). Intra- and intermonomer interactions are required to synergistically facilitate ATP hydrolysis in Hsp90. *Journal of Biological Chemistry*, 283:21170–21178.

Dahiya, V. and Buchner, J. (2019). Functional principles and regulation of molecular chaperones. *Advances in Protein Chemistry and Structural Biology*, 114:1–60.

D'Andrea, L. D. and Regan, L. (2003). TPR proteins: the versatile helix. *Trends in Biochemical Sciences*, 28:655–662.

Davies, T. H., Ning, Y. M., and Sanchez, E. R. (2002). A new first step in activation of steroid receptors: hormone-induced switching of FKBP51 and FKBP52 immunophilins. *Journal of Biological Chemistry*, 277:4597–4600.

Davies, T. H., Ning, Y. M., and Sanchez, E. R. (2005). Differential control of glucocorticoid receptor hormone-binding function by tetratricopeptide repeat (TPR) proteins and the immunosuppressive ligand FK506. *Biochemistry*, 44:2030–2038.

Denny, W. B., Prapapanich, V., Smith, D. F., and Scammell, J. G. (2005). Structure-function analysis of squirrel monkey FK506-binding protein 51, a potent inhibitor of glucocorticoid receptor activity. *Endocrinology*, 146:3194–3201.

Denny, W. B., Valentine, D. L., Reynolds, P. D., Smith, D. F., and Scammell, J. G. (2000). Squirrel monkey immunophilin FKBP51 is a potent inhibitor of glucocorticoid receptor binding. *Endocrinology*, 141:4107–4113.

Ding, G., Chen, P., Zhang, H., Huang, X., Zang, Y., Li, J., Li, J., and Wong, J. (2016). Regulation of Ubiquitin-like with plant homeodomain and RING finger domain 1 (UHRF1) protein stability by heat shock protein 90 chaperone machinery. *Journal of Biological Chemistry*, 291:20125–20135.

Dittmar, K. D., Banach, M., Galigniana, M. D., and Pratt, W. B. (1998). The role of DnaJ-like proteins in glucocorticoid receptor·hsp90 heterocomplex assembly by the reconstituted hsp90·p60·hsp70 foldosome complex. *Journal of Biological Chemistry*, 273:7358–7366.

Dittmar, K. D. and Pratt, W. B. (1997). Folding of the glucocorticoid receptor by the reconstituted Hsp90-based chaperone machinery. the initial hsp90.p60.hsp70-dependent step is sufficient for creating the steroid binding conformation. *Journal of Biological Chemistry*, 272:13047–13054.

Dollins, D. E., Warren, J. J., Immormino, R. M., and Gewirth, D. T. (2007). Structures of GRP94-nucleotide complexes reveal mechanistic differences between the hsp90 chaperones. *Molecular Cell*, 28:41–56.

Draxler, S. W. (2016). Fragment-based screening on a cochaperone target protein. Master's thesis, University of Würzburg.

Draxler, S. W., Bauer, M., Eickmeier, C., Nadal, S., Nar, H., Rangel Rojas, D., Seeliger, D., Zeeb, M., and Fiegen, D. (2020). Hybrid screening approach for very small fragments: X-ray and computational screening on FKBP51. *Journal of Medicinal Chemistry*, 63:5856–5864.

Dutta, R. and Inouye, M. (2000). GHKL, an emergent ATPase/kinase superfamily. *Trends in Biochemical Sciences*, 25:24–28.

Ebong, I. O., Beilsten-Edmands, V., Patel, N. A., Morgner, N., and Robinson, C. V. (2016). The interchange of immunophilins leads to parallel pathways and different intermediates in the assembly of Hsp90 glucocorticoid receptor complexes. *Cell Discovery*, 2:16002.

Echeverria, P. C., Bernthaler, A., Dupuis, P., Mayer, B., and Picard, D. (2011). An interaction network predicted from public data as a discovery tool: application to the Hsp90 molecular chaperone machine. *PLoS One*, 6:e26044.

Echeverria, P. C. and Picard, D. (2010). Molecular chaperones, essential partners of steroid hormone receptors for activity and mobility. *Biochimica et Biophysica Acta (BBA) - Molecular Cell Research*, 1803:641–649.

Edman, K., Hosseini, A., Bjursell, M. K., Aagaard, A., Wissler, L., Gunnarsson, A., Kaminski, T., Köhler, C., Bäckström, S., Jensen, T. J., Cavallin, A., Karlsson, U., Nilsson, E., Lecina, D., Takahashi, R., Grebner, C., Geschwindner, S., Lepistö, M., Hogner, A. C., and Guallar, V. (2015). Ligand binding mechanism in steroid receptors: From conserved plasticity to differential evolutionary constraints. *Structure*, 23:2280–2290.

Eustace, B. K., Sakurai, T., Stewart, J. K., Yimlamai, D., Unger, C., Zehetmeier, C., Lain, B., Torella, C., Henning, S. W., Beste, G., Scroggins, B. T., Neckers, L., Ilag, L. L., and Jay, D. G. (2004). Functional proteomic screens reveal an essential extracellular role for hsp90α in cancer cell invasiveness. *Nature Cell Biology*, 6:507–514.

Evans, C. G., Wisén, S., and Gestwicki, J. E. (2006). Heat shock proteins 70 and 90 inhibit early stages of amyloid β-(1–42) aggregation *in Vitro*. *Journal of Biological Chemistry*, 281:33182–33191.

Farrell, C. and O'Keane, V. (2016). Epigenetics and the glucocorticoid receptor: A review of the implications in depression. *Psychiatry Research*, 242:349–356.

Felts, S. J., Owen, B. A., Nguyen, P., Trepel, J., Donner, D. B., and Toft, D. O. (2000). The hsp90-related protein TRAP1 is a mitochondrial protein with distinct functional properties. *Journal of Biological Chemistry*, 275:3305–3312.

Fingar, D. C., Salama, S., Tsou, C., Harlow, E., and Blenis, J. (2002). Mammalian cell size is controlled by mTOR and its downstream targets S6K1 and 4EBP1/eIF4E. *Genes & Development*, 16:1472–1487.

Finka, A. and Goloubinoff, P. (2013). Proteomic data from human cell cultures refine mechanisms of chaperone-mediated protein homeostasis. *Cell Stress and Chaperones*, 18:591–605.

Fischer, G. (1994). Peptidyl-prolyl cis/trans isomerases and their effectors. *Angewandte Chemie International Edition in English*, 33:1415–1436.

Franke, D., Petoukhov, M. V., Konarev, P. V., Panjkovich, A., Tuukkanen, A., Mertens, H. D. T., Kikhney, A. G., Hajizadeh, N. R., Franklin, J. M., Jeffries, C. M., and Svergun, D. I. (2017). ATSAS 2.8: a comprehensive data analysis suite for small-angle scattering from macromolecular solutions. *Journal of Applied Crystallography*, 50:1212–1225.

Freedman, N. D. and Yamamoto, K. R. (2004). Importin 7 and importin α/importin β are nuclear import receptors for the glucocorticoid receptor. *Molecular Biology of the Cell*, 15:2276–2286.

Fries, G. R., Gassen, N. C., and Rein, T. (2017). The FKBP51 glucocorticoid receptor co-chaperone: Regulation, function, and implications in health and disease. *International Journal of Molecular Sciences*, 18:2614.

Fujita, T., Shibuya, H., Ohashi, T., Yamanishi, K., and Taniguchi, T. (1986). Regulation of human interleukin-2 gene: Functional DNA sequences in the 5' flanking region for the gene expression in activated T lymphocytes. *Cell*, 46:401–407.

Gaali, S., Kirschner, A., Cuboni, S., Hartmann, J., Kozany, C., Balsevich, G., Namendorf, C., Fernandez-Vizarra, P., Sippel, C., Zannas, A. S., Draenert, R., Binder, E. B., Almeida, O. F., Ruhter, G., Uhr, M., Schmidt, M. V., Touma, C., Bracher, A., and Hausch, F. (2015). Selective inhibitors of the FK506-binding protein 51 by induced fit. *Nature Chemical Biology*, 11:33–37.

Galat, A. (2003). Peptidylprolyl cis / trans isomerases (immunophilins): Biological diversity - targets - functions. *Current Topics in Medicinal Chemistry*, 3:1315–1347.

Galat, A., Lane, W. S., Standaert, R. F., and Schreiber, S. L. (1992). A rapamycin-selective 25-kda immunophilin. *Biochemistry*, 31:2427–2434.

Galigniana, M. D., Radanyi, C., Renoir, J.-M., Housley, P. R., and Pratt, W. B. (2001). Evidence that the peptidylprolyl isomerase domain of the hsp90-binding immunophilin FKBP52 is involved in both dynein interaction and glucocorticoid receptor movement to the nucleus. *Journal of Biological Chemistry*, 276:14884–14889.

Gao, T., Furnari, F., and Newton, A. C. (2005). PHLPP: A phosphatase that directly dephosphorylates Akt, promotes apoptosis, and suppresses tumor growth. *Molecular Cell*, 18:13–24.

Garnier, C., Barbier, P., Gilli, R., Lopez, C., Peyrot, V., and Briand, C. (1998). Heat-shock protein 90 (hsp90) binds *in Vitro* to tubulin dimer and inhibits microtubule formation. *Biochemical and Biophysical Research Communications*, 250:414–419.

Geiger, T., Wehner, A., Schaab, C., Cox, J., and Mann, M. (2012). Comparative proteomic analysis of eleven common cell lines reveals ubiquitous but varying expression of most proteins. *Molecular & Cellular Proteomics*, 11:M111.014050.

Geller, R., Andino, R., and Frydman, J. (2013). Hsp90 inhibitors exhibit resistance-free antiviral activity against respiratory syncytial virus. *PLoS One*, 8:e56762.

Georgopoulos, C. and Welch, W. J. (1993). Role of the major heat shock proteins as molecular chaperones. *Annual Review of Cell Biology*, 9:601–634.

Girstmair, H., Tippel, F., Lopez, A., Tych, K., Stein, F., Haberkant, P., Schmid, P. W. N., Helm, D., Rief, M., Sattler, M., and Buchner, J. (2019). The hsp90 isoforms from *S. cerevisiae* differ in structure, function and client range. *Nature Communications*, 10:3626.

Gralen, N. and Svedberg, T. (1940). Soluble reserve-carbohydrates in the liliifloreae. *Biochemical Journal*, 34:234–248.

Grenert, J. P., Johnson, B. D., and Toft, D. O. (1999). The importance of ATP binding and hydrolysis by Hsp90 in formation and function of protein heterocomplexes. *Journal of Biological Chemistry*, 274:17525–17533.

Hahle, A., Merz, S., Meyners, C., and Hausch, F. (2019). The many faces of FKBP51. *Biomolecules*, 9:35.

Hainzl, O., Lapina, M. C., Buchner, J., and Richter, K. (2009). The charged linker region is an important regulator of Hsp90 function. *Journal of Biological Chemistry*, 284:22559–22567.

Hartl, F. U. and Hayer-Hartl, M. (2009). Converging concepts of protein folding *in vitro* and *in vivo*. *Nature Structural & Molecular Biology*, 16:574–581.

Haslbeck, M., Franzmann, T., Weinfurtner, D., and Buchner, J. (2005). Some like it hot: the structure and function of small heat-shock proteins. *Nature Structural & Molecular Biology*, 12:842–846.

Hawkins, U. A., Gomez-Sanchez, E. P., Gomez-Sanchez, C. M., and Gomez-Sanchez, C. E. (2012). The ubiquitous mineralocorticoid receptor: Clinical implications. *Current Hypertension Reports*, 14:573–580.

Heitzer, M. D., Wolf, I. M., Sanchez, E. R., Witchel, S. F., and DeFranco, D. B. (2007). Glucocorticoid receptor physiology. *Reviews in Endocrine and Metabolic Disorders*, 8:321–330.

Hellenkamp, B., Wortmann, P., Kandzia, F., Zacharias, M., and Hugel, T. (2017). Multidomain structure and correlated dynamics determined by self-consistent FRET networks. *Nature Methods*, 14:174–180.

Hernández, M. P., Chadli, A., and Toft, D. O. (2002). HSP40 binding is the first step in the HSP90 chaperoning pathway for the progesterone receptor. *Journal of Biological Chemistry*, 277:11873–11881.

Hessling, M., Richter, K., and Buchner, J. (2009). Dissection of the ATP-induced conformational cycle of the molecular chaperone Hsp90. *Nature Structural & Molecular Biology*, 16:287–293.

Höfeld, J., Minami, Y., and Hartl, F.-U. (1995). Hip, a novel cochaperone involved in the eukaryotic hsc70/hsp40 reaction cycle. *Cell*, 83:589–598.

Hickey, E., Brandon, S. E., Smale, G., Lloyd, D., and Weber, L. A. (1989). Sequence and regulation of a gene encoding a human 89-kilodalton heat shock protein. *Molecular and Cellular Biology*, 9:2615–2626.

Hofmann, L. (2018). Fkbp51 dependent signaling mechanisms during stress response. Master's thesis, Ulm University.

Holsboer, F. (2000). The corticosteroid receptor hypothesis of depression. *Neuropsychopharmacology*, 23:477–501.

Hou, J. and Wang, L. (2012). FKBP5 as a selection biomarker for gemcitabine and Akt inhibitors in treatment of pancreatic cancer. *PLoS One*, 7:e36252.

Howard, K. J., Holley, S. J., Yamamoto, K. R., and Distelhorst, C. W. (1990). Mapping the HSP90 binding region of the glucocorticoid receptor. *Journal of Biological Chemistry*, 265:11928–11935.

Jacqueline, D., Paul, T., and Malcolm, D. W. (2003). Structures of immunophilins and their ligand complexes. *Current Topics in Medicinal Chemistry*, 3:1392–1409.

Jahn, M., Rehn, A., Pelz, B., Hellenkamp, B., Richter, K., Rief, M., Buchner, J., and Hugel, T. (2014). The charged linker of the molecular chaperone Hsp90 modulates domain contacts and biological function. *Proceedings of the National Academy of Sciences*, 111:17881–17886.

Jiang, W., Cazacu, S., Xiang, C., Zenklusen, J. C., Fine, H. A., Berens, M., Armstrong, B., Brodie, C., and Mikkelsen, T. (2008). FK506 binding protein mediates glioma cell growth and sensitivity to rapamycin treatment by regulating NF-κB signaling pathway. *Neoplasia*, 10:235–243.

Johnson, J., Corbisier, R., Stensgard, B., and Toft, D. (1996). The involvement of p23, hsp90, and immunophilins in the assembly of progesterone receptor complexes. *The Journal of Steroid Biochemistry and Molecular Biology*, 56:31–37.

Johnson, J. L. (2012). Evolution and function of diverse Hsp90 homologs and cochaperone proteins. *Biochimica et Biophysica Acta (BBA) - Molecular Cell Research*, 1823:607–613.

Johnson, J. L. and Toft, D. O. (1994). A novel chaperone complex for steroid receptors involving heat shock proteins, immunophilins, and p23. *Journal of Biological Chemistry*, 269:24989–24993.

Joëls, M. (2011). Impact of glucocorticoids on brain function: Relevance for mood disorders. *Psychoneuroendocrinology*, 36:406–414.

Jääskeläinen, T., Makkonen, H., and Palvimo, J. J. (2011). Steroid up-regulation of FKBP51 and its role in hormone signaling. *Current Opinion in Pharmacology*, 11:326–331.

Khan, S. H., Awasthi, S., Guo, C., Goswami, D., Ling, J., Griffin, P. R., Simons, S. S., and Kumar, R. (2012). Binding of the N-terminal region of coactivator TIF2 to the intrinsically disordered AF1 domain of the glucocorticoid receptor is accompanied by conformational reorganizations. *Journal of Biological Chemistry*, 287:44546–44560.

Kikhney, A. G. and Svergun, D. I. (2015). A practical guide to small angle X-ray scattering (SAXS) of flexible and intrinsically disordered proteins. *FEBS Letters*, 589:2570–2577.

Kirschke, E., Goswami, D., Southworth, D., Griffin, P. R., and Agard, D. A. (2014). Glucocorticoid receptor function regulated by coordinated action of the Hsp90 and Hsp70 chaperone cycles. *Cell*, 157:1685–1697.

Kissinger, C. R., Parge, H. E., Knighton, D. R., Lewis, C. T., Pelletier, L. A., Tempczyk, A., Kalish, V. J., Tucker, K. D., Showalter, R. E., Moomaw, E. W., Gastinel, L. N., Habuka, N., Chen, X., Maldonado, F., Barker, J. E., Bacquet, R., and Villafranca, J. E. (1995). Crystal structures of human calcineurin and the human FKBP12–FK506–calcineurin complex. *Nature*, 378:641–644.

Kozany, C., Marz, A., Kress, C., and Hausch, F. (2009). Fluorescent probes to characterise FK506-binding proteins. *Chembiochem*, 10:1402–1410.

Krukenberg, K. A., Bottcher, U. M., Southworth, D. R., and Agard, D. A. (2009). Grp94, the endoplasmic reticulum Hsp90, has a similar solution conformation to cytosolic Hsp90 in the absence of nucleotide. *Protein Science*, 18:1815–1827.

Kullmann, M., Schneikert, J., Moll, J., Heck, S., Zeiner, M., Gehring, U., and Cato, A. C. B. (1998). RAP46 is a negative regulator of glucocorticoid receptor action and hormone-induced apoptosis. *Journal of Biological Chemistry*, 273:14620–14625.

Kumar, R., Moche, M., Winblad, B., and Pavlov, P. F. (2017). Combined x-ray crystallography and computational modeling approach to investigate the Hsp90 c-terminal peptide binding to FKBP51. *Scientific Reports*, 7:14288.

Kumar, R. and Thompson, E. B. (1999). The structure of the nuclear hormone receptors. *Steroids*, 64:310–319.

Kumar, R. and Thompson, E. B. (2012). Folding of the glucocorticoid receptor N-terminal transactivation function: Dynamics and regulation. *Molecular and Cellular Endocrinology*, 348:450–456.

Laemmli, U. K. (1970). Cleavage of structural proteins during the assembly of the head of bacteriophage T4. *Nature*, 227:680–685.

Lai, B. T., Chin, N. W., Stanek, A. E., Keh, W., and Lanks, K. W. (1984). Quantitation and intracellular localization of the 85k heat shock protein by using monoclonal and polyclonal antibodies. *Molecular and Cellular Biology*, 4:2802–2810.

Lang, K., Schmid, F. X., and Fischer, G. (1987). Catalysis of protein folding by prolyl isomerase. *Nature*, 329:268–270.

Langer, T., Rosmus, S., and Fasold, H. (2003). Intracellular localization of the 90 kda heat shock protein (HSP90alpha) determined by expression of a EGFP-HSP90alpha-fusion protein in unstressed and heat stressed 3T3 cells. *Cell Biology International*, 27:47–52.

Laue, T. M. (1995). Sedimentation equilibrium as thermodynamic tool. *Methods in Enzymology*, 259:427–452.

Laue, T. M. and Stafford, W. F., r. (1999). Modern applications of analytical ultracentrifugation. *Annual Review of Biophysics and Biomolecular Structure*, 28:75–100.

Lea, W. A. and Simeonov, A. (2011). Fluorescence polarization assays in small molecule screening. *Expert Opinion on Drug Discovery*, 6:17–32.

Lee, C.-C., Lin, T.-W., Ko, T.-P., and Wang, A. H. J. (2011). The hexameric structures of human heat shock protein 90. *PLoS One*, 6:e19961.

Li, J., Richter, K., and Buchner, J. (2011). Mixed Hsp90-cochaperone complexes are important for the progression of the reaction cycle. *Nature Structural & Molecular Biology*, 18:61–66.

Li, J., Richter, K., Reinstein, J., and Buchner, J. (2013). Integration of the accelerator Aha1 in the Hsp90 co-chaperone cycle. *Nature Structural & Molecular Biology*, 20:326–331.

Li, L., Fridley, B., Kalari, K., Jenkins, G., Batzler, A., Safgren, S., Hildebrandt, M., Ames, M., Schaid, D., and Wang, L. (2008). Gemcitabine and cytosine arabinoside cytotoxicity: Association with lymphoblastoid cell expression. *Cancer Research*, 68:7050–7058.

Linnstaedt, S. D., Riker, K. D., Rueckeis, C. A., Kutchko, K. M., Lackey, L., McCarthy, K. R., Tsai, Y.-H., Parker, J. S., Kurz, M. C., Hendry, P. L., Lewandowski, C., Datner, E., Pearson, C., Neil, B., Domeier, R., Kaushik, S., Laederach, A., and McLean, S. A. (2018). A functional riboSNitch in the 3' UTR of *FKBP5* alters microRNA-320a binding efficiency and mediates vulnerability to chronic post-traumatic pain. *The Journal of Neuroscience*, 38:8407–8420.

Liu, B., Zhang, T.-N., Knight, K. J., and Goodwin, E. J. (2019). The glucocorticoid receptor in cardiovascular health and disease. *Cells*, 8(10):1227.

Liu, J., Farmer, Jesse D., J., Lane, W. S., Friedman, J., Weissman, I., and Schreiber, S. L. (1991). Calcineurin is a common target of cyclophilin-cyclosporin a and FKBP-FK506 complexes. *Cell*, 66:807–815.

Lorenz, O. R., Freiburger, L., Rutz, D. A., Krause, M., Zierer, B. K., Alvira, S., Cuellar, J., Valpuesta, J. M., Madl, T., Sattler, M., and Buchner, J. (2014). Modulation of the Hsp90 chaperone cycle by a stringent client protein. *Molecular Cell*, 53:941–953.

Lüders, J., Demand, J., and Höhfeld, J. (2000). The ubiquitin-related BAG-1 provides a link between the molecular chaperones Hsc70/Hsp70 and the proteasome. *Journal of Biological Chemistry*, 275:4613–4617.

Makkonen, H., Kauhanen, M., Paakinaho, V., Jääskeläinen, T., and Palvimo, J. J. (2009). Long-range activation of FKBP51 transcription by the androgen receptor via distal intronic enhancers. *Nucleic Acids Research*, 37:4135–4148.

Mayer, M. P. and Le Breton, L. (2015). Hsp90: Breaking the symmetry. *Molecular Cell*, 58:8–20.

McCaffrey, P. G., Perrino, B. A., Soderling, T. R., and Rao, A. (1993). NF-AT$_p$, a T lymphocyte DNA-binding protein that is a target for calcineurin and immunosuppressive drugs. *Journal of Biological Chemistry*, 268:3747–3752.

McClellan, A. J., Tam, S., Kaganovich, D., and Frydman, J. (2005). Protein quality control: chaperones culling corrupt conformations. *Nature Cell Biology*, 7:736–741.

McDonough, H. and Patterson, C. (2003). CHIP: a link between the chaperone and proteasome systems. *Cell stress & chaperones*, 8:303–308.

McEwan, I. J., Wright, A. P., Dahlman-Wright, K., Carlstedt-Duke, J., and Gustafsson, J. A. (1993). Direct interaction of the tau 1 transactivation domain of the human glucocorticoid receptor with the basal transcriptional machinery. *Molecular and Cellular Biology*, 13:399–407.

Meyer, P., Prodromou, C., Liao, C., Hu, B., Roe, S., Vaughan, C., Vlasic, I., Panaretou, B., Piper, P., and Pearl, L. (2004). Structural basis for recruitment of the ATpase activator Aha1 to the Hsp90 chaperone machinery. *The The EMBO Journalournal*, 23:1402–1410.

Minami, Y., Kimura, Y., Kawasaki, H., Suzuki, K., and Yahara, I. (1994). The carboxy-terminal region of mammalian HSP90 is required for its dimerization and function in vivo. *Molecular and Cellular Biology*, 14:1459–1464.

Morgan, A. A. and Rubenstein, E. (2013). Proline: The distribution, frequency, positioning, and common functional roles of proline and polyproline sequences in the human proteome. *PLoS One*, 8:e53785.

Ni, L., Yang, C.-S., Gioeli, D., Frierson, H., Toft, D. O., and Paschal, B. M. (2010). FKBP51 promotes assembly of the Hsp90 chaperone complex and regulates androgen receptor signaling in prostate cancer cells. *Molecular and Cellular Biology*, 30:1243–1253.

Oroz, J., Chang, B. J., Wysoczanski, P., Lee, C. T., Perez-Lara, A., Chakraborty, P., Hofele, R. V., Baker, J. D., Blair, L. J., Biernat, J., Urlaub, H., Mandelkow, E., Dickey, C. A., and Zweckstetter, M. (2018). Structure and pro-toxic mechanism of the human Hsp90/PPIase/Tau complex. *Nature Communications*, 9:4532.

Padmanabhan, S., Mukhopadhyay, A., Narasimhan, S. D., Tesz, G., Czech, M. P., and Tissenbaum, H. A. (2009). A PP2A regulatory subunit regulates *C. elegans* insulin/IGF-1 signaling by modulating AKT-1 phosphorylation. *Cell*, 136:939–951.

Panaretou, B., Prodromou, C., Roe, S. M., O'Brien, R., Ladbury, J. E., Piper, P. W., and Pearl, L. H. (1998). ATP binding and hydrolysis are essential to the function of the Hsp90 molecular chaperone in vivo. *The EMBO Journal*, 17:4829–4836.

Panaretou, B., Siligardi, G., Meyer, P., Maloney, A., Sullivan, J. K., Singh, S., Millson, S. H., Clarke, P. A., Naaby-Hansen, S., Stein, R., Cramer, R., Mollapour, M., Workman, P., Piper, P. W., Pearl, L. H., and Prodromou, C. (2002). Activation of the ATPase activity of hsp90 by the stress-regulated cochaperone aha1. *Molecular Cell*, 10:1307–1318.

Patching, S. G. (2014). Surface plasmon resonance spectroscopy for characterisation of membrane protein-ligand interactions and its potential for drug discovery. *Biochim. Biophys. Acta*, 1838:43–55.

Pearl, L. H. and Prodromou, C. (2000). Structure and *in vivo* function of Hsp90. *Current Opinion in Structural Biology*, 10:46–51.

Peattie, D. A., Harding, M. W., Fleming, M. A., DeCenzo, M. T., Lippke, J. A., Livingston, D. J., and Benasutti, M. (1992). Expression and characterization of human FKBP52, an immunophilin that associates with the 90-kda heat shock protein and is a component of steroid receptor complexes. *Proceedings of the National Academy of Sciences*, 89:10974–10978.

Pei, H., Li, L., Fridley, B. L., Jenkins, G. D., Kalari, K. R., Lingle, W., Petersen, G., Lou, Z., and Wang, L. (2009). FKBP51 affects cancer cell response to chemotherapy by negatively regulating Akt. *Cancer Cell*, 16:259–266.

Pereira, M. J., Palming, J., Svensson, M. K., Rizell, M., Dalenbäck, J., Hammar, M., Fall, T., Sidibeh, C. O., Svensson, P.-A., and Eriksson, J. W. (2014). FKBP5 expression in human adipose tissue increases following dexamethasone exposure and is associated with insulin resistance. *Metabolism - Clinical and Experimental*, 63:1198–1208.

Pettersen, E. F., Goddard, T. D., Huang, C. C., Couch, G. S., Greenblatt, D. M., Meng, E. C., and Ferrin, T. E. (2004). UCSF Chimera—a visualization system for exploratory research and analysis. *Journal of Computational Chemistry*, 25:1605–1612.

Picard, D., Khursheed, B., Garabedian, M. J., Fortin, M. G., Lindquist, S., and Yamamoto, K. R. (1990). Reduced levels of hsp90 compromise steroid receptor action *in vivo*. *Nature*, 348:166–168.

Pick, E., Kluger, Y., Giltnane, J. M., Moeder, C., Camp, R. L., Rimm, D. L., and Kluger, H. M. (2007). High HSP90 expression is associated with decreased survival in breast cancer. *Cancer Research*, 67:2932–2937.

Pierce, M. M., Raman, C. S., and Nall, B. T. (1999). Isothermal titration calorimetry of protein-protein interactions. *Methods*, 19:213–221.

Pirkl, F. and Buchner, J. (2001). Functional analysis of the Hsp90-associated human peptidyl prolyl cis/trans isomerases FKBP51, FKBP52 and Cyp40. *Journal of Molecular Biology*, 308:795–806.

Pratt, W. B., Galigniana, M. D., Morishima, Y., and Murphy, P. J. (2004). Role of molecular chaperones in steroid receptor action. *Essays in Biochemistry*, 40:41–58.

Pratt, W. B. and Toft, D. O. (1997). Steroid receptor interactions with heat shock protein and immunophilin chaperones. *Endocrine Reviews*, 18:306–360.

Prodromou, C. (2012). The 'active life' of Hsp90 complexes. *Biochimica et Biophysica Acta (BBA) - Molecular Cell Research*, 1823:614–623.

Prodromou, C., Roe, S. M., Piper, P. W., and Pearl, L. H. (1997). A molecular clamp in the crystal structure of the N-terminal domain of the yeast Hsp90 chaperone. *Nature Structural & Molecular Biology*, 4:477–482.

Prodromou, C., Siligardi, G., O'Brien, R., Woolfson, D. N., Regan, L., Panaretou, B., Ladbury, J. E., Piper, P. W., and Pearl, L. H. (1999). Regulation of Hsp90 ATPase activity by tetratricopeptide repeat (TPR)-domain co-chaperones. *The EMBO Journal*, 18:754–762.

Putcha, P., Danzer, K. M., Kranich, L. R., Scott, A., Silinski, M., Mabbett, S., Hicks, C. D., Veal, J. M., Steed, P. M., Hyman, B. T., and McLean, P. J. (2010). Brain-permeable small-molecule inhibitors of Hsp90 prevent α-synuclein oligomer formation and rescue α-synuclein-induced toxicity. *Journal of Pharmacology and Experimental Therapeutics*, 332:849–857.

Ramachandran, G. N. and Sasisekharan, V. (1968). Conformation of polypeptides and proteins. *Advances in Protein Chemistry*, 23:283–437.

Rambo, R. (2019). ScÅtter. Version: 3.1.

Retzlaff, M., Hagn, F., Mitschke, L., Hessling, M., Gugel, F., Kessler, H., Richter, K., and Buchner, J. (2010). Asymmetric activation of the hsp90 dimer by its cochaperone aha1. *Molecular Cell*, 37:344–354.

Richter, K., Soroka, J., Skalniak, L., Leskovar, A., Hessling, M., Reinstein, J., and Buchner, J. (2008). Conserved conformational changes in the ATPase cycle of human Hsp90. *Journal of Biological Chemistry*, 283:17757–17765.

Richter, K., Walter, S., and Buchner, J. (2004). The co-chaperone Sba1 connects the ATPase reaction of Hsp90 to the progression of the chaperone cycle. *Journal of Molecular Biology*, 342:1403–1413.

Riggs, D. L., Cox, M. B., Tardif, H. L., Hessling, M., Buchner, J., and Smith, D. F. (2007). Noncatalytic role of the FKBP52 peptidyl-prolyl isomerase domain in the regulation of steroid hormone signaling. *Molecular Cell Biology*, 27:8658–8669.

Riggs, D. L., Roberts, P. J., Chirillo, S. C., Cheung-Flynn, J., Prapapanich, V., Ratajczak, T., Gaber, R., Picard, D., and Smith, D. F. (2003). The Hsp90-binding peptidylprolyl isomerase FKBP52 potentiates glucocorticoid signaling *in vivo*. *The EMBO Journal*, 22:1158–1167.

Rodina, A., Wang, T., Yan, P., Gomes, E. D., Dunphy, M. P. S., Pillarsetty, N., Koren, J., Gerecitano, J. F., Taldone, T., Zong, H., Caldas-Lopes, E., Alpaugh, M., Corben, A., Riolo, M., Beattie, B., Pressl, C., Peter, R. I., Xu, C., Trondl, R., Patel, H. J., Shimizu, F., Bolaender, A., Yang, C., Panchal, P., Farooq, M. F., Kishinevsky, S., Modi, S., Lin, O., Chu, F., Patil, S., Erdjument-Bromage, H., Zanzonico, P., Hudis, C., Studer, L., Roboz, G. J., Cesarman, E., Cerchietti, L., Levine, R., Melnick, A., Larson, S. M., Lewis, J. S., Guzman, M. L., and Chiosis, G. (2016). The epichaperome is an integrated chaperome network that facilitates tumour survival. *Nature*, 538:397–401.

Roe, S. M., Ali, M. M., Meyer, P., Vaughan, C. K., Panaretou, B., Piper, P. W., Prodromou, C., and Pearl, L. H. (2004). The mechanism of Hsp90 regulation by the protein kinase-specific cochaperone p50(cdc37). *Cell*, 116:87–98.

Romano, S., D'Angelillo, A., Pacelli, R., Staibano, S., De Luna, E., Bisogni, R., Eskelinen, E. L., Mascolo, M., Calì, G., Arra, C., and Romano, M. F. (2010). Role of FK506-binding protein 51 in the control of apoptosis of irradiated melanoma cells. *Cell Death & Differentiation*, 17:145–157.

Rutz, D. A., Luo, Q., Freiburger, L., Madl, T., Kaila, V. R. I., Sattler, M., and Buchner, J. (2018). A switch point in the molecular chaperone Hsp90 responding to client interaction. *Nature Communications*, 9:1472.

Sabbagh, J. J., Cordova, R. A., Zheng, D., Criado-Marrero, M., Lemus, A., Li, P., Baker, J. D., Nordhues, B. A., Darling, A. L., Martinez-Licha, C., Rutz, D. A., Patel, S., Buchner,

J., Leahy, J. W., Koren, J., r., Dickey, C. A., and Blair, L. J. (2018). Targeting the FKBP51/GR/Hsp90 complex to identify functionally relevant treatments for depression and PTSD. *ACS Chemical Biology*, 13:2288–2299.

Sahasrabudhe, P., Rohrberg, J., Biebl, M. M., Rutz, D. A., and Buchner, J. (2017). The plasticity of the Hsp90 co-chaperone system. *Molecular Cell*, 67:947–961.e5.

Sakamoto, K. M., Kim, K. B., Kumagai, A., Mercurio, F., Crews, C. M., and Deshaies, R. J. (2001). Protacs: Chimeric molecules that target proteins to the Skp1–Cullin–F box complex for ubiquitination and degradation. *Proceedings of the National Academy of Sciences*, 98:8554–8559.

Sarbassov, D. D., Guertin, D. A., Ali, S. M., and Sabatini, D. M. (2005). Phosphorylation and regulation of Akt/PKB by the rictor-mTOR complex. *Science*, 307:1098–1101.

Sawada, S., Suzuki, G., Kawase, Y., and Takaku, F. (1987). Novel immunosuppressive agent, FK506. In vitro effects on the cloned T cell activation. *The Journal of Immunology*, 139:1797–1803.

Schalm, S. S., Fingar, D. C., Sabatini, D. M., and Blenis, J. (2003). TOS motif-mediated raptor binding regulates 4E-BP1 multisite phosphorylation and function. *Current Biology*, 13:797–806.

Scheufler, C., Brinker, A., Bourenkov, G., Pegoraro, S., Moroder, L., Bartunik, H., Hartl, F. U., and Moarefi, I. (2000). Structure of TPR domain-peptide complexes: critical elements in the assembly of the Hsp70-Hsp90 multichaperone machine. *Cell*, 101:199–210.

Schmid, A. B., Lagleder, S., Grawert, M. A., Rohl, A., Hagn, F., Wandinger, S. K., Cox, M. B., Demmer, O., Richter, K., Groll, M., Kessler, H., and Buchner, J. (2012). The architecture of functional modules in the Hsp90 co-chaperone Sti1/Hop. *The EMBO Journal*, 31:1506–1517.

Schmidt, M. V., Paez-Pereda, M., Holsboer, F., and Hausch, F. (2012). The prospect of FKBP51 as a drug target. *ChemMedChem*, 7:1351–1359.

Schoch, G. A., D'Arcy, B., Stihle, M., Burger, D., Bär, D., Benz, J., Thoma, R., and Ruf, A. (2010). Molecular switch in the glucocorticoid receptor: Active and passive antagonist conformations. *Journal of Molecular Biology*, 395:568–577.

Schopf, F. H., Biebl, M. M., and Buchner, J. (2017). The HSP90 chaperone machinery. *Nature Reviews Molecular Cell Biology*, 18:345–360.

Schuck, P. (2000). Size-distribution analysis of macromolecules by sedimentation velocity ultracentrifugation and lamm equation modeling. *Biophysical Journal*, 78:1606–1619.

Schülke, J.-P., Wochnik, G. M., Lang-Rollin, I., Gassen, N. C., Knapp, R. T., Berning, B., Yassouridis, A., and Rein, T. (2010). Differential impact of tetratricopeptide repeat proteins on the steroid hormone receptors. *PLoS One*, 5:e11717.

Schulte, T. W., Akinaga, S., Soga, S., Sullivan, W., Stensgard, B., Toft, D., and Neckers, L. M. (1998). Antibiotic radicicol binds to the N-terminal domain of Hsp90 and shares important biologic activities with geldanamycin. *Cell Stress Chaperones*, 3:100–108.

Seitz, T., Thoma, R., Schoch, G. A., Stihle, M., Benz, J., D'Arcy, B., Wiget, A., Ruf, A., Hennig, M., and Sterner, R. (2010). Enhancing the stability and solubility of the glucocorticoid receptor ligand-binding domain by high-throughput library screening. *Journal of Molecular Biology*, 403:562–577.

Shaw, J. P., Utz, P. J., Durand, D. B., Toole, J. J., Emmel, E. A., and Crabtree, G. R. (1988). Identification of a putative regulator of early t cell activation genes. *Science*, 241:202–205.

Shaw, K. T., Ho, A. M., Raghavan, A., Kim, J., Jain, J., Park, J., Sharma, S., Rao, A., and Hogan, P. G. (1995). Immunosuppressive drugs prevent a rapid dephosphorylation of transcription factor NFAT1 in stimulated immune cells. *Proceedings of the National Academy of Sciences*, 92:11205–11209.

Shi, D., Bai, Q., Zhou, S., Liu, X., Liu, H., and Yao, X. (2018). Molecular dynamics simulation, binding free energy calculation and unbinding pathway analysis on selectivity difference between FKBP51 and FKBP52: Insight into the molecular mechanism of isoform selectivity. *Proteins: Structure, Function, and Bioinformatics*, 86:43–56.

Shiau, A. K., Harris, S. F., Southworth, D. R., and Agard, D. A. (2006). Structural analysis of *E. coli* hsp90 reveals dramatic nucleotide-dependent conformational rearrangements. *Cell*, 127:329–340.

Siekierka, J. J., Hung, S. H. Y., Poe, M., Lin, C. S., and Sigal, N. H. (1989). A cytosolic binding protein for the immunosuppressant FK506 has peptidyl-prolyl isomerase activity but is distinct from cyclophilin. *Nature*, 341:755–757.

Sikorski, R. S., Boguski, M. S., Goebl, M., and Hieter, P. (1990). A repeating amino acid motif in CDC23 defines a family of proteins and a new relationship among genes required for mitosis and RNA synthesis. *Cell*, 60:307–317.

Silverstein, A. M., Galigniana, M. D., Kanelakis, K. C., Radanyi, C., Renoir, J. M., and Pratt, W. B. (1999). Different regions of the immunophilin FKBP52 determine its association with the glucocorticoid receptor, hsp90, and cytoplasmic dynein. *Journal of Biological Chemistry*, 274:36980–36986.

Sinars, C. R., Cheung-Flynn, J., Rimerman, R. A., Scammell, J. G., Smith, D. F., and Clardy, J. (2003). Structure of the large FK506-binding protein FKBP51, an Hsp90-binding protein

and a component of steroid receptor complexes. *Proceedings of the National Academy of Sciences*, 100:868–873.

Smith, S. M. and Vale, W. W. (2006). The role of the hypothalamic-pituitary-adrenal axis in neuroendocrine responses to stress. *Dialogues in clinical neuroscience*, 8:383–395.

Solassol, J., Mange, A., and Maudelonde, T. (2011). FKBP family proteins as promising new biomarkers for cancer. *Current Opinion in Pharmacology*, 11:320–325.

Southworth, D. R. and Agard, D. A. (2008). Species-dependent ensembles of conserved conformational states define the Hsp90 chaperone ATPase cycle. *Molecular Cell*, 32:631–640.

Stebbins, C. E., Russo, A. A., Schneider, C., Rosen, N., Hartl, F. U., and Pavletich, N. P. (1997). Crystal structure of an Hsp90-geldanamycin complex: Targeting of a protein chaperone by an antitumor agent. *Cell*, 89:239–250.

Suren, T., Rutz, D., Mossmer, P., Merkel, U., Buchner, J., and Rief, M. (2018). Single-molecule force spectroscopy reveals folding steps associated with hormone binding and activation of the glucocorticoid receptor. *Proceedings of the National Academy of Sciences*, 115:11688–11693.

Svergun, D. I. (1999). Restoring low resolution structure of biological macromolecules from solution scattering using simulated annealing. *Biophysical Journal*, 76:2879–2886.

Tang, Y., Getzenberg, R. H., Vietmeier, B. N., Stallcup, M. R., Eggert, M., Renkawitz, R., and DeFranco, D. B. (1998). The DNA-binding and $\tau 2$ transactivation domains of the rat glucocorticoid receptor constitute a nuclear matrix-targeting signal. *Molecular Endocrinology*, 12:1420–1431.

Timmermans, S., Souffriau, J., and Libert, C. (2019). A general introduction to glucocorticoid biology. *Frontiers in Immunology*, 10:1545.

Tsutsumi, S., Mollapour, M., Prodromou, C., Lee, C.-T., Panaretou, B., Yoshida, S., Mayer, M. P., and Neckers, L. M. (2012). Charged linker sequence modulates eukaryotic heat shock protein 90 (Hsp90) chaperone activity. *Proceedings of the National Academy of Sciences*, 109:2937–2942.

Udi, N., Jozelio Freire de, C., Rosa Maria, R. P., and Yehuda, S. (2010). Glucocorticoids and the cardiovascular system: State of the art. *Current Pharmaceutical Design*, 16:3574–3585.

Van Duyne, G. D., Standaert, R. F., Karplus, P. A., Schreiber, S. L., and Clardy, J. (1991). Atomic structure of FKBP-FK506, an immunophilin-immunosuppressant complex. *Science*, 252:839–842.

Vandevyver, S., Dejager, L., and Libert, C. (2014). Comprehensive overview of the structure and regulation of the glucocorticoid receptor. *Endocrine Reviews*, 35:671–693.

Verba, K. A., Wang, R. Y., Arakawa, A., Liu, Y., Shirouzu, M., Yokoyama, S., and Agard, D. A. (2016). Atomic structure of Hsp90-Cdc37-Cdk4 reveals that Hsp90 traps and stabilizes an unfolded kinase. *Science*, 352:1542–1547.

Volkov, V. V. and Svergun, D. I. (2003). Uniqueness of *ab initio* shape determination in small-angle scattering. *Journal of Applied Crystallography*, 36:860–864.

Wayne, N. and Bolon, D. N. (2007). Dimerization of Hsp90 is required for *in Vivo* function: Design and analysis of monomers and dimers. *Journal of Biological Chemistry*, 282:35386–35395.

Wedemeyer, W. J., Welker, E., and Scheraga, H. A. (2002). Proline cis-trans isomerization and protein folding. *Biochemistry*, 41:14637–14644.

Weikum, E. R., Knuesel, M. T., Ortlund, E. A., and Yamamoto, K. R. (2017). Glucocorticoid receptor control of transcription: precision and plasticity via allostery. *Nature Reviews Molecular Cell Biology*, 18:159–174.

Weiwad, M., Edlich, F., Kilka, S., Erdmann, F., Jarczowski, F., Dorn, M., Moutty, M.-C., and Fischer, G. (2006). Comparative analysis of calcineurin inhibition by complexes of immunosuppressive drugs with human FK506 binding proteins. *Biochemistry*, 45:15776–15784.

Whitesell, L., Mimnaugh, E. G., De Costa, B., Myers, C. E., and Neckers, L. M. (1994). Inhibition of heat shock protein HSP90-pp60v-src heteroprotein complex formation by benzoquinone ansamycins: essential role for stress proteins in oncogenic transformation. *Proceedings of the National Academy of Sciences*, 91:8324–8328.

Willmund, F. and Schroda, M. (2005). HEAT SHOCK PROTEIN 90C is a bona fide Hsp90 that interacts with plastidic HSP70B in *Chlamydomonas reinhardtii*. *Plant Physiology*, 138:2310–2322.

Wochnik, G. M., Ruegg, J., Abel, G. A., Schmidt, U., Holsboer, F., and Rein, T. (2005). FK506-binding proteins 51 and 52 differentially regulate dynein interaction and nuclear translocation of the glucocorticoid receptor in mammalian cells. *Journal of Biological Chemistry*, 280:4609–4616.

Wu, B., Li, P., Liu, Y., Lou, Z., Ding, Y., Shu, C., Ye, S., Bartlam, M., Shen, B., and Rao, Z. (2004). 3d structure of human FK506-binding protein 52: implications for the assembly of the glucocorticoid receptor/Hsp90/immunophilin heterocomplex. *Proceedings of the National Academy of Sciences*, 101:8348–8353.

Xu, W., Mollapour, M., Prodromou, C., Wang, S., Scroggins, B. T., Palchick, Z., Beebe, K., Siderius, M., Lee, M.-J., Couvillon, A., Trepel, J. B., Miyata, Y., Matts, R., and Neckers, L. (2012). Dynamic tyrosine phosphorylation modulates cycling of the HSP90-P50^{CDC37}-AHA1 chaperone machine. *Molecular Cell*, 47:434–443.

Young, J. C., Obermann, W. M. J., and Hartl, F. U. (1998). Specific binding of tetratricopeptide repeat proteins to the C-terminal 12-kDa domain of hsp90. *Journal of Biological Chemistry*, 273:18007–18010.

Zengerle, M., Chan, K.-H., and Ciulli, A. (2015). Selective small molecule induced degradation of the BET bromodomain protein BRD4. *ACS Chemical Biology*, 10:1770–1777.

Zhao, R., Kakihara, Y., Gribun, A., Huen, J., Yang, G., Khanna, M., Costanzo, M., Brost, R. L., Boone, C., Hughes, T. R., Yip, C. M., and Houry, W. A. (2008). Molecular chaperone Hsp90 stabilizes Pih1/Nop17 to maintain R2TP complex activity that regulates snoRNA accumulation. *Journal of Cell Biology*, 180:563–578.

Zhou, J. and Cidlowski, J. A. (2005). The human glucocorticoid receptor: One gene, multiple proteins and diverse responses. *Steroids*, 70:407–417.

Zuehlke, A. and Johnson, J. L. (2010). Hsp90 and co-chaperones twist the functions of diverse client proteins. *Biopolymers*, 93:211–217.

Zuehlke, A. D., Beebe, K., Neckers, L., and Prince, T. (2015). Regulation and function of the human HSP90AA1 gene. *Gene*, 570:8–16.

Zuehlke, A. D. and Johnson, J. L. (2012). Chaperoning the chaperone: a role for the co-chaperone Cpr7 in modulating Hsp90 function in *Saccharomyces cerevisiae*. *Genetics*, 191:805–814.

Acknowledgments

I want to start by thanking Prof. Dr. Johannes Buchner from the Chair of Biotechnology at the TU München for accepting the supervision of my external Ph.D. thesis. His open-mindedness and ideas tremendously impacted the projects and lead to fruitful discussions.
Thanks to Prof. Dr. Michael Sattler from the Chair of Biomolecular NMR Spectroscopy at the TU München for being second examiner of my Ph.D. thesis.
Furthermore, I want to thank Maximilian Biebl for supervising the practical course with me and introducing me to the fluorescence polarization assay. Thanks also to Jannis Lawatscheck for doing the AUC experiments when time was short.
I am very grateful to Dr. Dennis Fiegen for supporting and supervising my Ph.D. project at Boehringer Ingelheim in Biberach. His scientific input and discussions were helpful to finish the project. Thank you for letting me work on my own to develop myself further as a scientist.
At this point, I would also like to thank Dr. Herbert Nar for giving me the opportunity to do my Ph.D. in the Structural Research Group at Boehringer Ingelheim and for the scientific discussions around my project. Thank you for your input on our manuscripts and your help in revising them.
A big shout-out to Viktor Beke who was an excellent student and helped push the project forward during the last year. I enjoyed our time working together and the hour-long discussions we had in the lab, not only about work. I also want to thank you for proof-reading my dissertation.
Being a Ph.D. student in industry can be lonesome. Thank you Rebecca Ebenhoch for sharing and understanding the troubles and the life of a Ph.D. student. I would also like to thank Waldemar Eberhard, Julian Friedl, and Heike Kölle for all the fun breaks im Süßigkeitenbüro.
Thank you to the whole X-ray team for supporting the many crystallization campaigns Viktor and I did. Although it was mostly late in the afternoon, we could always count on your support, your help and an extensive stock of prepared crystallization plates.
Thanks to the biophysics team, Katja Mück, Yvette Hoevels, and Franziska Moser for introducing me to SPR, ITC, DSF, and MST and helping with troubleshooting. And in case of Katja for also almost everything else lab-related!
For introducing me to SAXS, answering my many SAXS-related questions and also proof-reading my thesis, I would like to thank Dr. Sophia Reindl.
Thank you Stefanie Braig for being a fantastic co-worker in the PK IV group and for helping me organize the shipment of my samples and also proof-reading my thesis.
I further want to thank the whole Structural Research group at Boehringer Ingelheim. You all had a great impact on me and made my thesis enjoyable.
I want to thank my family for all their support, their understanding, and that I could always count on them. Finally, I cannot thank Natascha Piede enough. Your support during my thesis and life has been invaluable. Thank you for being by my side, your countless suggestions on my thesis and patiently listening to all the talks I had to give more than once!